Preparation of nickel phyllosilicate catalysts by one-step modified spherical silica
synthesis in carbon dioxide hydrogenation and selective hydrogenation of furfural to
furfuryl alcohol

Miss Sasithorn Kuhaudomlap

จุฬาลงกรณ์มหาวิทยาลัย
CHULALONGKORN UNIVERSITY

A Dissertation Submitted in Partial Fulfillment of the Requirements
for the Degree of Doctor of Engineering in Chemical Engineering
Department of Chemical Engineering
FACULTY OF ENGINEERING
Chulalongkorn University
Academic Year 2021
Copyright of Chulalongkorn University

การเตรียมตัวเร่งปฏิกิริยานิกเกิลฟิลโลซิลิเกตโดยการปรับปรุงการสังเคราะห์ซิลิกาทรงกลมในขั้นตอนเดียวในคาร์บอนไดออกไซด์ไฮโดรจิเนชันและไฮโดรจิเนชันแบบเลือกเกิดของเฟอร์ฟิวรัลไปเป็นเฟอร์ฟิวริลแอลกอฮอล์

น.ส.ศศิธร คูหาอุดมลาภ

จุฬาลงกรณ์มหาวิทยาลัย
CHULALONGKORN UNIVERSITY

วิทยานิพนธ์นี้เป็นส่วนหนึ่งของการศึกษาตามหลักสูตรปริญญาวิศวกรรมศาสตรดุษฎีบัณฑิต
สาขาวิชาวิศวกรรมเคมี ภาควิชาวิศวกรรมเคมี
คณะวิศวกรรมศาสตร์ จุฬาลงกรณ์มหาวิทยาลัย
ปีการศึกษา 2564

Thesis Title   Preparation of nickel phyllosilicate catalysts by one-step
                       modified spherical silica synthesis in carbon dioxide
                       hydrogenation and selective hydrogenation of furfural
                       to furfuryl alcohol
By   Miss Sasithorn Kuhaudomlap
Field of Study   Chemical Engineering
Thesis Advisor   Professor JOONGJAI PANPRANOT, Ph.D.

Accepted by the FACULTY OF ENGINEERING, Chulalongkorn University in Partial Fulfillment of the Requirement for the Doctor of Engineering

            .... Dean of the FACULTY OF
                                                         ENGINEERING
            (Professor SUPOT TEACHAVORASINSKUN, D.Eng.)

DISSERTATION COMMITTEE
            .... Chairman
            (Associate Professor Okorn Mekasuwandumrong, D.Eng.)
            .... Thesis Advisor
            (Professor JOONGJAI PANPRANOT, Ph.D.)
            .... Examiner
            (Professor ANONGNAT SOMWANGTHANAROJ, Ph.D.)
            .... Examiner
            (Chutimon Satirapipathkul, D.Eng.)
            .... Examiner
            (Assistant Professor SUPHOT PHATANASRI, D.Eng.)

ศศิธร คูหาอุดมลาภ : การเตรียมตัวเร่งปฏิกิริยานิกเกิลฟิลโลซิลิเกตโดยการปรับปรุงการ
สังเคราะห์ซิลิกาทรงกลมในขั้นตอนเดียวในคาร์บอนไดออกไซด์ไฮโดรจิเนชันและไฮโดร
จิเนชันแบบเลือกเกิดของเฟอร์ฟิวรัลไปเป็นเฟอร์ฟิวริลแอลกอฮอล์. (Preparation of
nickel phyllosilicate catalysts by one-step modified spherical silica
synthesis in carbon dioxide hydrogenation and selective hydrogenation of
furfural to furfuryl alcohol) อ.ที่ปรึกษาหลัก : ศ. ดร.จูงใจ ปั้นประณต

เตรียมตัวเร่งปฏิกิริยานิกเกิลฟิลโลซิลลิเกตบนซิลิกาทรงกลมโดยการปรับปรุงวิธีการ
สังเคราะห์ซิลิกาทรงกลมในขั้นตอนเดียวภายใต้อุณหภูมิห้อง สำหรับ ๑๐ เปอร์เซ็นต์โดยน้ำหนัก
ของนิกเกิล พบว่าลำดับในการโหลดแหล่งกำเนิดของนิกเกิลและซิลิคอนระหว่างการสังเคราะห์ซิลิ
กาทรงกลมมีผลต่อคุณลักษณะและสมบัติในการเร่งปฏิกิริยาในปฏิกิริยาคาร์บอนไดออกไซด์เมเท
เนชัน อันตรกิริยาระหว่างนิกเกิลและซิลิกาที่แข็งแรงกว่า ในรูปของนิกเกิลฟิลโลซิลิเกต แสดงให้
เห็นถึงประสิทธิภาพการเร่งปฏิกิริยาที่ดีกว่าวิธีการแบบเคลือบฝัง ตัวเร่งปฏิกิริยาที่เตรียมโดยการ
โหลดพร้อมกันระหว่างนิกเกิลและซิลิกา(Ni_Alt_Si) แสดงความว่องไวในการเกิดปฏิกิริยา
คาร์บอนไดออกไซด์เมเทเนชันและค่าการเลือกเกิดของมีเทนที่สูงที่สุด ซึ่งสัมพันธ์กับความหนาแน่น
ของอิเล็กตรอนที่สูงของนิกเกิลบนพื้นผิว การกระจายของโลหะที่สูง และความสามารถในการดูด
ซับคาร์บอนไดออกไซด์ที่สูง นอกจากนี้ศึกษาการสังเคราะห์แบบขั้นตอนเดียวโดยการโหลดพร้อม
กันระหว่างแหล่งกำเนิดของนิกเกิลและซิลิคอนโดยที่ปริมาณการโหลดนิกเกิลแตกต่างกันในช่วง ๒-
๓๐ เปอร์เซนต์โดยน้ำหนัก ในปฏิกิริยาไฮโดรจิเนชันแบบเลือกเกิดของเฟอร์ฟิวรัลไปเป็นเฟอร์ฟิว
ริลแอลกอฮอล์ คุณสมบัติเฉพาะของนิกเกิลฟิลโลซิลิเกตที่เหลือหลังจากการรีดิวซ์สามารถทำหน้าที่
เป็นตัวรองรับที่ดีสำหรับโลหะนิกเกิล ทำให้เกิดการกระจายตัวที่สูงของอนุภาคนิกเกิลขนาดเล็ก
และประสิทธิภาพการเร่งปฏิกิริยาที่เสถียรสำหรับการรีไซเคิลหลายครั้ง ค่าการเปลี่ยนของเฟอร์
ฟิวรัลบนตัวเร่งปฏิกิริยานิกเกิลฟิลโลซิลิเกตมีการเพิ่มขึ้นตามปริมาณการโหลดของนิกเกิลที่เพิ่มขึ้น
โดยไม่มีการลดลงของค่าการเลือกเกิดของเฟอร์ฟิวริลแอลกอฮอล์ จึงแสดงได้ว่าการมีทั้งโลหะ
นิกเกิลและนิกเกิลฟิลโลซิลิเกตทำให้เกิดการทำงานร่วมกันที่มีผลต่อการเกิดเฟอร์ฟิวริล
แอลกอฮอล์

สาขาวิชา	วิศวกรรมเคมี	ลายมือชื่อนิสิต ....
ปีการศึกษา	2564	ลายมือชื่อ อ.ที่ปรึกษาหลัก ....

5971444921 : MAJOR CHEMICAL ENGINEERING

KEYWORD: Nickel phyllosilicate, furfural, furfuryl alcohol, CO2 methanation

Sasithorn Kuhaudomlap : Preparation of nickel phyllosilicate catalysts by one-step modified spherical silica synthesis in carbon dioxide hydrogenation and selective hydrogenation of furfural to furfuryl alcohol. Advisor: Prof. JOONGJAI PANPRANOT, Ph.D.

Spherical silica derived nickel phyllosilicate catalysts were prepared via a one-step modified spherical silica synthesis under room temperature. For 10wt% Ni loading, the loading sequence of Ni and Si sources during spherical silica synthesis was found to affect the characteristics and catalytic properties in CO_2 methanation. The stronger interaction between Ni and silica in the form of nickel phyllosilicate revealed the better catalytic performances than the impregnation method. The highest CO_2 methanation activity and methane selectivity were obtained over the catalyst prepared by alternate loading between Ni and Si (Ni_Alt_Si) due to high electron density of nickel on the surface, high metal dispersion, and high CO_2 adsorption ability. Furthermore, one step synthesis by alternate addition of Ni and Si precursor (Ni_Si) with different Ni loadings in the range of 2-30 wt% were evaluated in the selective hydrogenation of furfural to furfuryl alcohol. The unique properties of the remaining nickel phyllosilicate after reduction could act as a good support for metallic nickel, yielding high dispersion of small nickel particles and stable catalytic performances for multiple recycle runs. Furfural conversion over the Ni_PS catalysts increased monotonically with increasing Ni loading without FA selectivity drop. It is suggested that the presence of both metallic Ni^0 and $Ni_{phyllosilicate}$ also produced a synergistic promotional effect for FA formation.

Field of Study:	Chemical Engineering	Student's Signature ....
Academic Year:	2021	Advisor's Signature ....

ACKNOWLEDGEMENTS

TABLE OF CONTENTS

จุฬาลงกรณ์มหาวิทยาลัย

CHULALONGKORN UNIVERSITY

LIST OF TABLES

LIST OF FIGURES

จุฬาลงกรณ์มหาวิทยาลัย
CHULALONGKORN UNIVERSITY

CHARPTER I

INTRODUCTION

1.1 Statement and significance of the problems

Recent research on catalyst development not only focuses on their excellent catalytic performances but also on the environmental friendly properties, low cost, good stability, and recyclability. Silica supported nickel catalysts (Ni/SiO_2) are versatile catalysts with interesting properties due to their low cost, high specific surface area, controllable morphology/adjustable pore structures, and high availability and easy functionalization [1-3]. In addition, silica support can be prepared with environmentally friendly silicon source by using biomass raw material such as distiller' grains [4], rice husk [5], equisetum fluviatile [6]. Thus, Ni/SiO_2 catalysts are widely used in various catalytic reactions in both gas phase and liquid phase reaction. However, Ni species obtained from the conventional impregnation method usually suffer from sintering/agglomeration of nickel particles at high temperature during the pretreatment/reaction process or leaching of nickel species in liquid phase reaction because of its relatively weak interaction between nickel species and silica supports. These issues have become major problems for conventional silica supported nickel catalysts, which usually cause deactivation of catalysts, low surface availability, large amount of waste resources, loss of catalytic activity, and poor stability/recyclability. Many efficient strategies have been applied to develop Ni/SiO_2 catalysts including the addition of various promoters such as La_2O_3 [7] and V_2O_5 [6], the improvement of the porous structure and morphology of support/catalysts [8], the modification of preparation method[9, 10], the formation perovskite and hydrotalcite structures [11, 12], and the formation of unique structure/compound with a strong metal-support interaction[13]. However, these methods have some limitations such as high cost, loss of surface availability, low loading, complicate preparation process, required multiple steps and unique instruments for preparation. Therefore, it is a great challenge to

design and synthesize high performance Ni/SiO_2 catalysts with a simple preparation method, low-cost process, high nickel dispersion, unique structure, a strong metal-support interaction for adsorption more active sites, as well as good anti-sintering and stability property for large scale reaction.

Nickel phyllosilicate is a stable material with a strong metal-support interaction due to unique layer structure which consists of tetrahedral layers of SiO_4 (Si-O-Si) and octahedral layers of Ni (II) (Ni coordinated to oxygen atoms or hydroxyl groups, Si-O-Ni-O(OH))[4, 14]. These nickel species offer outstanding properties such as strong metal-support interaction, small metal domain size and high dispersion of active metal species, high specific surface area, rich porous structures, excellent adsorption properties, high thermal stability, tunable pore structure and morphology, adjustable component and synthesizing parameter, very cheap raw material and simple preparation procedures[15]. The reduction treatment of nickel phyllosilicate in H_2 can provide fine nickel particles size with strong interaction between nickel and silica material at high nickel content and high metal dispersion[16]. The complete reduction of nickel phyllosilicate to nickel metal is difficult and above 700°C[14]. Interestingly, it has been reported that the remaining of nickel phyllosilicate layer after reduction process could act as a good/stable support for metallic nickel, which resulted in the highly dispersed nickel particles with small size of homogeneous nickel particle, preventing the sintering and enhancing the stability[17]. Due to the unique structure and special properties, Ni/SiO_2 catalysts derived from nickel phyllosilicate have received considerable attention in recent catalysis research and could be an efficient strategy to address the sintering and leaching problem, as well as good stability for a Ni/SiO_2 catalysts.

Generally, the importance factors for the formation of nickel phyllosilicate are a nickel precursor and a silica material or monomer silica source and a reaction

environment (an alkaline or acidic condition) [18]. Nickel phyllosilicates are commonly synthesized via various methods including hydrothermal methods [1, 5, 14, 19], the ammonia evaporation method [20-22], deposition-precipitation methods [23, 24] and sol-gel method [25] though the reaction between nickel precursor and silica materials. Among which, the hydrothermal method has been widely employed for preparation of nickel phyllosilicate catalysts due to high crystallinity and high nickel content (depend on the hydrothermal temperature), handy experimental operation, environmentally friendly, and uniform dispersed of nickel phyllosilicate [4]. However, conventional hydrothermal reaction is carried out in an autoclave under harsh hydrothermal conditions at high temperature (>180 °C) with long reaction time (> 24 h), resulting in the loss of surface silanol group, limited nickel loading (even though there are excess nickel and silica amount) [7, 19, 26, 27], and small amount of nickel phyllosilicate and large particles being formed at relatively low hydrothermal temperatures (e.g. 120 and 160 °C) [16]. Thus, how to improve and synthesize Ni phyllosilicates with high nickel contents under mild conditions that can remain the superiority properties of nickel phyllosilicate is a great challenge. Chen et al. [4] synthesized nickel phyllosilicate via the hydrothermal method assisted by NH_4F and urea, which optimal nickel phyllosilicate (N/D-120-12) exhibited high catalytic performance for CO_2 methanation and excellent anti-sintering property. They reported that ammonium fluoride and urea can be efficient accelerator of the formation of H_4SiO_4 and $Ni(OH)_2$, respectively which is essential intermediates for the formation of nickel phyllosilicate. Li et al. [1] found that nickel phyllosilicate could be formed under mild hydrothermal conditions at 100 °C for 12 h by double accelerators of ammonium fluoride and urea which has similar morphology and nickel content with conventional hydrothermal method at 220 °C for 48 h. Although, these modified hydrothermal method can improve hydrothermal condition, there are still some limitation of

complicated operation procedure and too low hydrothermal conditions still provides low nickel content and small amount of nickel phyllosilicate formation [4].

Moreover, the preparation of nickel phyllosilicate usually consists of two major steps: step (1) silica material synthesis and step (2) nickel phyllosilicate formation via the reaction of silica material and nickel precursor. Two step synthesis offer an efficient catalyst; however, it consumes large amounts of the reagent and energy, complicate preparation process and requires long operation time. Thus, a simple one step strategy is in need and achieved extensive attention due to their advantages such as low cost, high efficiency and convenience, and elimination of the separation, drying and calcination process. One-pot synthesis of Ni phyllosilicates has recently been reported, for example, Chen et al. [26] prepared 3D-SBA-15 derived Ni phyllosilicate via a one-pot and two-pot hydrothermal methods at 180 °C. Compared with two-pot, one-pot synthesis exhibited small size nickel particles, high nickel phyllosilicate content, fine nickel particle size, monolithic appearance and showed high anti-sintering due to strong metal-support interaction derived from nickel phyllosilicate. In addition, it was found that hydrothermal conditions were significant factor for the formation of nickel phyllosilicate via one-pot synthesis, which sectional hydrothermal at 100 °C, 24 h and 180 °C, 24 h affected to the formation of nickel phyllosilicate in their work. Therefore, a simple one-step strategy has attracted great interest to synthesize nickel phyllosilicate and modified/applied with the spherical silica synthesis under mild conditions. The spherical silica synthesis has a facial preparation process with tunable components in a wide range, which nickel species can uniformly dispersed during spherical silica synthesis with one-step method.

The Ni phyllosilicates show good performances in a number of reactions including CO_2 and CO methanation [16], hydrogenation of levulinic acid to γ-valerolactone [28], xylose hydrogenation to xylitol [24], hydrogenation of maleic

anhydride [15], hydrogenation of polycyclic aromatic hydrocarbons [29], and carbon dioxide reforming of methane [30]. To our knowledge, the nickel phyllosilicate derived catalysts have been widely explored in various gas phase reactions, there are few research focused on the catalytic properties of nickel phyllosilicate in liquid phase reaction, especially for hydrogenation reaction. Thus, it is very interesting to investigate the different parameter for the formation of nickel phyllosilicate for both gas phase and liquid phase reaction: hydrogenation of carbon dioxide as reaction model for gas phase, selective hydrogenation of furfural to furfuryl alcohol as reaction model for liquid phase.

At present, limitation of fossil fuel resource and global warming are important problems so that many researches have focused on sustainable production of chemicals and fuels from renewable biomass. There is also a growing interest in reducing carbon dioxide levels in the atmosphere because it is well known that carbon dioxide is the main greenhouse gas and increase of its concentration in the air causes global warming which are highly serious problem [31]. There are many routes to reduce CO_2 emission including reduction of the consumption of fossil fuels, carbon capture, separation and storage, and transformation of CO_2 to value added chemical or fuel synthesis [32, 33]. CO_2 methanation is a simple reaction widely used to produce the substitute natural gas. Production of biomethane from carbon dioxide is considered as significant process to increase the value of natural gas (natural gas upgrade) and biogas derived from the fermentation of biomass. This is not only utilize CO_2, but also reduce CO_2 emission. The CO_2 methanation is highly exothermic reaction and there are kinetic limitations [32, 34]. Therefore, the development of catalysts for this reaction is an important factor. Many researches studied the improvement of catalytic performance in this reaction by using various catalysts. CO_2 methanation has been studied using several metal catalysts like Ru, Rh, Pd, Ni, Co, Cu and Fe [31, 33, 35, 36] supported on

various oxide supports such as TiO_2, Al_2O_3, SiO_2, CeO_2 and ZrO_2 [31, 33-35, 37, 38]. Although, noble metal exhibited higher activity for CO_2 methanation, high stability and good resistant to sintering and coke deposition but its high cost and limited availability makes it less attractive as industrial catalysts. Therefore, non-noble metal is interested due to relatively low cost [37]. Ni-based catalyst is one of the non-noble metal based catalysts which favors this reaction and is widely used as the active metal in large scale but it is usually suffered from deactivation due to sintering of nickel particles and carbon deposition in high reaction temperature [39]. To suppress the carbon formation, the high metal dispersion and strong metal-support interaction were reported. Therefore, many attempts have been conducted to improve catalytic performance of Ni-based catalyst, in order to possess both high activity and resistance to coke deposition.

Lignocellulosic biomass is an economical and abundant renewable resource available from agricultural residues. Production of various platform chemicals such as sugar alcohols, organic acids, furfural, and 5-HMF from lignocellulosic biomass via biorefining technologies has been industrially developed [40, 41]. Furfural, synthesized via catalytic dehydration of xylose in hemicellulose, is a versatile platform molecule that can be further converted into many high value derivatives and downstream fine chemicals and biofuels. Around 65% of furfural produced in the world is converted into furfuryl alcohol (FA), which is widely utilized in the manufacturing of fibers, adhesives, resins, fuel additives and can also be employed as an intermediate for the production of plasticizers, vitamin C, farm chemicals and dispersing agents [42, 43]. Due to the presence of both C=O and C=C bonds in the furfural structure, catalytic hydrogenation of furfural is a relatively complex reaction and undesired products can occur with the use of unsuitable catalysts, resulting in low selectivity to the target products. In recent years, significant progress has been made in the development of

high-performance catalysts with high activities and selectivities for the selective furfural hydrogenation to FA. Although noble metal catalysts such as Pt and Ru show high activities/selectivities under mild conditions [44, 45], their relatively high cost may limit their use in industrial applications. Among the non-noble metal catalysts, nickel has been demonstrated to be a good furfural hydrogenation catalyst due to its excellent H_2 dissociation and relatively low cost. However, nickel-based catalysts without modification/addition of a promoter typically exhibit low selectivity to FA [46, 47] because furfural adsorbs on nickel through both $\eta^1(O)$-aldehyde and $\eta^2(C,O)$-aldehyde modes, and as a consequence, both the C=C bonds on the furan ring and the C=O group in furfural are hydrogenated [48, 49]. In addition, Ni catalysts also suffer from poor metal support interactions that can cause leaching of nickel during liquid phase reaction processes, along with agglomeration of nickel species under high reduction temperatures [30, 50]. Developing stable nickel-based catalysts with higher FA selectivity while maintaining high activity and good recyclability is still challenging.

Therefore, in the present study, spherical silica derived nickel phyllosilicate was successfully prepared via one-step modified spherical silica synthesis with cetyltrimethyl ammonium bromide (CTAB) as the structural-directing agent and tetraethoxysilane (TEOS) as the silica source under room temperature to develop catalysts with improved activity and stability. The effect of different loading sequence of Ni and Si source was investigated to study the morphology and the formation of nickel phyllosilicate in gas phase hydrogenation of carbon dioxide. Consequently, the one step synthesized catalysts with various nickel loadings (2 – 30 wt% Ni) by an alternate addition of the nickel and silica sources during the spherical silica synthesis were evaluated in the liquid phase selective hydrogenation of furfural to FA under mild reaction conditions in order to simultaneously obtain excellent anti-leaching property and improve catalytic activity. To highlight the excellence of nickel

phyllosilicate for this method, nickel was loaded on spherical silica for comparison by two step conventional impregnation. Important reaction parameters including reduction temperature and reaction temperature were investigated, seeking to optimize furfural conversion and FA yield. In addition, the characteristics and catalytic properties of prepared catalysts were investigated by several characterization techniques such as XRD, AAS, CO_2-TPD, N_2 physisorption, CO-chemisorption, H_2 chemisorption, SEM, TGA, H_2-TPR, STEM, EDS, and XPS and correlated with the catalyst performances in both reactions. Finally, the stability and recyclability of nickel phyllosilicate catalysts were studied in both reactions.

1.2 Objective of research

The objectives of this research are

1. To investigate the characteristics of nickel phyllosilicte catalysts compared with nickel oxide prepared by conventional impregnation method.

2. To study the preparation method and to synthesize the nickel phyllosilicate catalysts via one-step modified spherical silica synthesis under mild conditions (room temperature and short time)

3. To study the characteristics and catalytic properties of nickel phyllosilicate doped spherical silica with different loading sequences of Ni and Si sources via one-step modified spherical silica synthesis and compared with spherical silica supported NiO via impregnation method in the hydrogenation of carbon dioxide.

4. To study the effect of nickel loading over nickel phyllosilicate containing spherical silica catalysts prepared by one-step modified spherical silica synthesis and

compared with spherical silica supported NiO via impregnation method on the catalytic performance for the liquid phase selective hydrogenation of furfural to furfuryl alcohol.

5. To study the effect of reduction temperature (400-700 ^{o}C) and reaction temperature (50-100 ^{o}C) on the catalytic properties of spherical silica derived nickel phyllosilicate (Ni_PS) prepared by one-step modified spherical silica synthesis in the liquid phase selective hydrogenation of furfural to furfuryl alcohol.

1.3 Scope of study
Paper I

1. Preparation of spherical silica particles (SSP) under room temperature.

2. Incorporation of 10wt% Ni in SSP by a one-step modified spherical silica synthesis with three different loading sequences: before/alternately/after Si addition during SSP synthesis and calcination in air at 550 ^{o}C for 6 h with heating rate of 2 ^{o}C/min.

3. Preparation of 10wt% Ni/SiO$_2$ catalysts by incipient wetness impregnation method for comparison and calcination in air at 550 ^{o}C for 6 h with heating rate of 2 ^{o}C/min.

4. Pretreatment of the catalysts by reduction with H$_2$ flow at 500 ^{o}C for 3 h.

5. Reaction study of the catalysts in gas phase hydrogenation of carbon dioxide using a fixed-bed quartz reactor under atmospheric pressure at 350-500 ^{o}C in steps of 50 ^{o}C and kept constant for 1 h at each temperature using WHSV = 36,000 cm^3/g$_{cat}$h and H$_2$:CO$_2$ = 10:1.

6. Stability and recyclability of the alternate loading between Ni and Si (Ni_Alt_Si) prepared by a one-step modified spherical silica synthesis under reaction temperature 300 and 450 $^\circ$C using WHSV = 24,000 cm^3/g$_{cat}$h and H$_2$:CO$_2$ = 10:1.

7. Characterization of the catalysts using X-ray diffraction (XRD), N$_2$ physisorption, CO$_2$-temperature programmed desorption (CO$_2$ –TPD), H$_2$-temperature programmed reduction (H$_2$-TPR), X-ray photoelectron spectroscopy (XPS), atomic absorption spectrophotometer (AAS), scanning electron microscope (SEM), transmission electron microscopy (TEM), hydrogen chemisorption (H2-chem) and thermal gravimetric analysis (TGA).

Paper II

1. Preparation of spherical silica particles (SSP) under room temperature.

2. Preparation of spherical silica derived nickel phyllosilicate with nickel loading of 2-30wt% via a one-step modified spherical silica synthesis by an alternate addition of the nickel and silica sources during the spherical silica synthesis and calcination in air at 550 $^\circ$C for 6 h with heating rate of 2 $^\circ$C/min.

3. Preparation of 20wt% Ni/SiO$_2$ catalysts by incipient wetness impregnation method for comparison and calcination in air at 550 $^\circ$C for 6 h with heating rate of 2 $^\circ$C/min.

4. Pretreatment of the catalysts by reduction with H$_2$ flow at 500 $^\circ$C for 3 h.

5. The effect of reduction temperature in the range of 400-700 $^\circ$C were studied over 30wt% Ni prepared by a one-step modified spherical silica synthesis.

6. The effect of reaction temperature in the range of 50-100 $^{\circ}$C were studied over 30wt% Ni prepared by a one-step modified spherical silica synthesis.

7. Reaction study of the catalysts in liquid phase selective hydrogenation of furfural at 50 $^{\circ}$C, 2 MPa and reaction time of 60-300 min using a 160 mL stainless steel Parr autoclave reactor with a Teflon liner.

8. Recyclability study of the 30wt% Ni prepared by a one-step modified spherical silica synthesis (30Ni_PS) and 20wt% Ni prepared by impregnation method (20Ni_Imp) for three cycles run under identical condition at 50 $^{\circ}$C, 2 MPa hydrogen pressure for 300 min.

9. Characterization of the calcined, reduced and spent catalysts using X-ray diffraction (XRD), N_2 physisorption, H_2-temperature programmed reduction (H_2-TPR), X-ray photoelectron spectroscopy (XPS), transmission electron microscopy (TEM), and Carbon monoxide chemisorption (CO-Chem).

1.4 Research methodology

```
┌─────────────────────────────────────────────────────────┐
│           Preparation of Ni on SiO₂ catalysts            │
└─────────────────────────────────────────────────────────┘
```

One-step modified spherical silica synthesis with difference Ni loading sequence: -Ni1_Si2 -Si1_Ni2 -Ni_Alt_Si	Preparation of spherical silica	One-step modified spherical silica synthesis with difference Ni loading in the range of 2-30wt% (Ni_PS)

Incipient wetness impregnation method

10wt% (Ni/SSP (Imp))   20wt% (20Ni_Imp)

Calcined at 550 C for 6 h in air with a heating rate of 2 C/min   Calcined at 550 C for 6 h in air with a heating rate of 2 C/min

Reduced with H₂ at 500 C for 3 h   Reduced with H₂ at 500 C for 3 h

Reaction study in CO₂ hydrogenation
-Stability and recyclability study

- ✓ XRD
- ✓ BET
- ✓ XPS
- ✓ TEM
- ✓ H₂-TPR

- ✓ SEM
- ✓ CO₂-TPD
- ✓ TGA
- ✓ AAS

Reaction study selective hydrogenation of furfural to FA
-The effect of Ni loading
-The effect of reduction temp.
-The effect of reaction temp.
-Recyclability study

Discussion and conclusions

1.5 Expected outcome

1. To obtain suitable method for preparation of nickel phyllosilicate with unique structure under mild condition.

2. To understand the characteristic and role of nickel phyllosilicate on the catalytic performance of both liquid phase and gas phase reaction.

3. To obtain suitable nickel phyllosilicate catalysts for liquid phase selective hydrogenation of furfural to furfuryl alcohol and gas phase hydrogenation of carbon dioxide.

4. The results of this research can be the formation and reaction model in gas phase and liquid phase reaction for the future study.

CHARPTER II

LITERATURE REVIEWS

2.1 Nickel phyllosilicate catalysts

Table 2. 1 Review of the preparation of nickel phyllosilicate catalysts

Catalysts (silica source, nickel source, bimetallic source)	Ni content (wt %)	Preparation method	Calcination (°C, h)	Reduction (°C, h), % H$_2$	S$_{BET}$ (m^2/g)	V$_p$ (cm^3/g)	D$_p$ (nm)	Metal crystallite size (nm) (XRD)	Metal particle size (nm) (TEM)
Ni-L (sodium silicate, nickel chloride) *L = Lizardite (1:1 PS)	46	Conventional hydrothermal (200 °C, 96 h) 2SiO$_2$Na$_2$O + 3NiCl$_2$ + 2NaOH → Si$_2$Ni$_3$O$_7$ + 6NaCl		unreduced	147	0.0036 (micro pore)	5.4		
				700 °C, 1 h, 100%	86	0.0284 (micro pore)	5.8		
				700 °C, 1 h, 3%	120	0.0112 (micro pore)	7.8		11

Material	Ref	Synthesis method	Calcination	Reduction condition	Surface area	Pore volume			
Ni-T (sodium silicate, nickel chloride) *T = Talc (2:1 PS)	36	Conventional hydrothermal (200 °C, 96 h) $4SiO_2Na_2O + 3NiCl_2 + 2HCl \rightarrow Si_4Ni_3O_{11} + 8NaCl$		800 °C, 1 h, 3%	14	0.0549 (micro pore)	7.3		
				unreduced	291	0.0001 (micro pore)	4.0		
				700 °C, 1 h, 100%	250	0.0614 (micro pore)	3.8	9	7
				800 °C, 1 h, 3%	160	0.0260 (micro pore)	4.4		
10Niphy@SiO$_2$ (silica nanosphere were prepared by a classical stober method, nickel nitrate)	18	Conventional hydrothermal (140 °C, 24 h)	450 °C, 4 h	500 °C, 3 h, 25%	103	0.29	9.2	10.1	10.1

Description						
5Ni5Cuphy@SiO₂ 18wt% metal (Ni/Cu molar ratio = 10:0, 9:1, 7:3, 5:5, 0:10; Cu 7.4 wt %) (silica nanosphere were prepared by a classical stober method, nickel nitrate, copper nitrate)	8.8	111	0.19	6.4	4.4	5.6
7Ni3Cuphy@SiO₂ 18wt% metal (Ni/Cu molar ratio = 10:0, 9:1, 7:3, 5:5, 0:10; Cu 3.9 wt %) (silica nanosphere were prepared by a classical stober	13.8	113	0.27	6.7	7.7	6.5

method, nickel nitrate, copper nitrate)								
9Ni1Cuphy@SiO$_2$ 18wt% metal (Ni/Cu molar ratio = 10:0, 9:1, 7:3, 5:5, 0:10; Cu 1.3 wt %) (silica nanosphere were prepared by a classical stober method, nickel nitrate, copper nitrate)	16.5			115	0.3	9.5	9.5	8.8
Ni/SiO$_2$-AEM (commercial colloidal silica, nickel nitrate hexahydrate)	40	Ammonia-evaporation (room temp, 5 h and	450 °C, 4 h / 500 °C, 2 h	446.3	0.84			4.2

Sample	(wt%)	Synthesis method	Calcination	Reduction	Surface area	Pore volume			
FDU-12 (tetraethyl silicate)		evaporation 80 °C) hydrothermal method	400 °C, 4 h		722	1.59			
N/F-H$_{220}$-48 (FDU-12 support were prepared by a typical hydrothermal method, nickel nitrate)	25.6	Conventional hydrothermal (220°C, 48 h)	400 °C, 4 h	700°C	403	0.971		5.73	6.04
N/F-A$_{100}$-12 (FDU-12 support were prepared by a typical hydrothermal method, nickel nitrate)	24.1	Modified hydrothermal (double accelerators of ammonium fluoride and urea) (100°C, 12 h)	400 °C, 4 h	700°C	324	0.587		4.48	4.62

Sample		Method							
NiSiO₃(TEOS, nickel sulfate hexahydrate))		Stober method			195.4				
NiSiO₃/Pt-300 (TEOS, nickel sulfate hexahydrate; Pt 4.6 wt%)		Nickel phyllosilicate by hydrothermal method (180 °C, 12 h) and Pt were loaded by wet-chemistry reduction method		300 °C, 5 h, 50%	289.3		3.8		
NiSiO₃/Pt-400 (TEOS, nickel sulfate hexahydrate; Pt 4.6 wt%)				400 °C, 5 h, 50%	151.4				
NiSiO₃/Pt-500 (TEOS, nickel sulfate hexahydrate; Pt 4.6 wt%)				500 °C, 5 h, 50%	124.8				
SiO₂ (distill's grains)			500 °C, 4 h		244	0.5			
N/D-100-12 (distill's grains, nickel nitrate)	21.1	Modified hydrothermal (double accelerators	400 °C, 2 h	750 °C, 1 h, 100%	132	0.4		4.6	4.7

Sample		Method				
N/D-120-6 (distill's grains, nickel nitrate)	21.8	Modified hydrothermal (double accelerators (NH$_4$F, urea) method) (100°C, 12 h)	124	0.4	4.6	4.8
N/D-120-12 (distill's grains, nickel nitrate)	22.4	Modified hydrothermal (double accelerators (NH$_4$F, urea) method) (120°C, 6 h)	111	0.4	4.7	4.9
N/D-120-18 (distill's grains, nickel nitrate)	23.5	Modified hydrothermal (NH$_4$F, urea) method) (120°C, 12 h)	96	0.3	5.0	5.2

Page 34

	Method					
	(double accelerators (NH$_4$F, urea) method) (120°C, 18 h)					
N/D-140-12 (distill's grains, nickel nitrate)	Modified hydrothermal (double accelerators (NH$_4$F, urea) method) (140°C, 12 h)	24.2	91	0.3	5.2	5.4
N/D-220-48-H (distill's grains, nickel nitrate)	Conventional hydrothermal (220°C, 48 h)	10.4	136	0.5	4.2	4.5
N/D-80-AE (distill's grains, nickel nitrate)	Ammonia evaporation (evaporation 80 °C)	22.7	204	0.5	4.9	5.2

Sample		Method						
N/D-80-12 (distill's grains, nickel nitrate)	19.8	Modified hydrothermal (double accelerators (NH₄F, urea) method) (80°C, 12 h)		181	0.4		4.8	5.0
N/D-60-12 (distill's grains, nickel nitrate)	11.5	Modified hydrothermal (double accelerators (NH₄F, urea) method) (60°C, 12 h)		213	0.4		3.6	3.8
N/D-40-12 (distill's grains, nickel nitrate)	4.1	Modified hydrothermal (double accelerators (NH₄F, urea)		218	0.5		2.6	2.9

Sample	Synthesis condition	Calcination	Ni (wt%)	S_{BET} (m²/g)	V_{pore} (cm³/g)			
SR (rice husks)	method) (40°C, 12 h)	450°C, 4 h		287	0.39			
N_{180}/SR (nickel nitrate)	Conventional hydrothermal (180°C, 48 h)		4.2	146	0.50		3.93	4.13
N_{220}/SR (nickel nitrate)	Conventional hydrothermal (220°C, 48 h)	750°C	10.2	126	0.56		4.32	4.54
N_{180}/SR-U-24 (nickel nitrate)	Hydrothermal with urea (180°C, 24 h)	450°C, 2 h	22.6	241	0.47		5.21	5.25
M_S (MSN material with particle sizes of 99 nm)				969	1.12			
M_M (MSN material with particle sizes of 184 nm)				907	0.98			

M_L (MSN material with particle sizes of 725 nm)							
				852	0.99		
M_S/H-8 (nickel nitrate)	6.3	Hydrothermal (120°C, 8 h)		784	0.97	<5	1.4
M_S/H-16 (nickel nitrate)	13.8	Hydrothermal (120°C, 16 h)		645	0.95	<5	1.8
M_S/H-24 (nickel nitrate)	19.7	Hydrothermal (120°C, 24 h)	500°C, 2 h	593	1.03	<5	2.6
M_S/H-32 (nickel nitrate)	22.3	Hydrothermal (120°C, 32 h)	700 °C, 1 h, 100%	563	0.99	<5	3.1
M_M/H-24 (nickel nitrate)	12.6	Hydrothermal (120°C, 24 h)		633	0.87	<5	1.9
M_L/H-24 (nickel nitrate)	5.9	Hydrothermal (120°C, 24 h)		699	0.96	<5	1.5
SR (TEOS)		Sol gel		1428	1.17		
NPS-120 (nickel nitrate)	18.56	Hydrothermal (120°C, 24 h)	500°C, 2 h / 750°C	606	1.75	<5	3.3

Sample	wt%	Preparation method	Calcination				
NPS-160 (nickel nitrate)	23.88	Hydrothermal (160°C, 24 h)		482	1.54		<5	4.4
NPS-180 (nickel nitrate)	30.53	Hydrothermal (180°C, 24 h)		395	1.45		5.8	5.7
NPS-200 (nickel nitrate)	31.65	Hydrothermal (200°C, 24 h)		282	0.67		6.1	6.3
NPS-180-5C (nickel nitrate, Ce(NO$_3$)$_3$ 6H$_2$O = 5 wt%)	28.73	Incipient wetness impregnation, CeO$_2$- modified		352	0.90		5.2	5.7
SiO2 (Fumed silica)				301	1.50	18.2		
Ni-DP (nickel nitrate)	20.1	Deposition precipitation (Na$_2$CO$_3$ as precipitator)	650°C, 4 h 800°C, 2 h	341	0.75	7.4	7.2	6.4
Ni-EA (nickel nitrate)	20.9	Ammonia evaporation (90°C)		378	0.64	5.9	6.9	6.8

NiPS-12.8 (silica sol, nickel nitrate)	9			128	0.49	15.7	
NiPS-6.4 (silica sol, nickel nitrate)	15.8			146	0.45	11.6	
NiPS-3.2 (silica sol, nickel nitrate)	21.7	Hydrothermal (180°C, 48 h)	500°C, 2 h	149	0.29	8.2	
NiPS-1.6 (silica sol, nickel nitrate)	34.3			159	0.29	7.5	1.6
NiPS-0.8 (silica sol, nickel nitrate)	44.4		480°C, 2 h	163	0.26	6.5	
MCM-41 (Equisetum fluviatile=>sodium silicate)		Biomass-based sodium silicate extracted from equisetum fluviatile (85°C, 24 h)		606	0.2		
M/180 (nickel nitrate)	17.2	Hydrothermal (180°C, 24 h)	750°C / 500°C, 2 h	413	0.3	4.6	4.5

M/200 (nickel nitrate)	31.9	Hydrothermal (200°C, 24 h)		293	0.7	5.3	5.9
M/220 (nickel nitrate)	41.8	Hydrothermal (220°C, 24 h)		181	0.5	5.9	6.4
M/200-0.5V (nickel nitrate, vanadyl (IV) acetylacetonate ethylene glycol, V = 0.5wt %)	31.1			290	0.7	5.1	5.4
M/200-1V (nickel nitrate, vanadyl (IV) acetylacetonate ethylene glycol V = 1 wt %)	30.9	Impregnation (60°C, 48 h)		283	0.7	4.7	5.0
M/200-3V (nickel nitrate, vanadyl (IV) acetylacetonate ethylene glycol, V = 3 wt %)	30.2			279	0.7	4.5	4.7

NiPS-H2-600	35.3	Ammonia evaporation hydrothermal method		264	0.51		4.1	4.2
S₃@NiPS-600	28	A modified facile hydrothermal method: to graft sucrose or a sucrose-melamine	600°C, 2 h	365	0.57		6.7	5.7
S₃M₁.₅@NiPS-600	24.3	A modified facile hydrothermal method: to graft sucrose or a sucrose-melamine		357	0.59		6.1	7.6

Sample		Synthesis	Calcination					
MCF (TEOS)		P123 as a surfactant, TMB as an organic swelling agent	550°C, 5 h	436	2.77			
N/M-P-18 (nickel nitrate)	20.05	Hydrothermal (180°C, 18 h)	500°C, 2 h; 700°C	225.2	0.8		4.2	4.5
N/M-P-30 (nickel nitrate)	31.60	Hydrothermal (180°C, 30 h)		204.8	0.82		4.3	4.2
N/M-P-42 (nickel nitrate)	32.05	Hydrothermal (180°C, 42 h)		187	0.73		5.1	5.1
3D-SBA-15 (TMOS)			550°C, 5 h	511	0.61	5.60		
N/S-6-Hy (nickel nitrate hexahydrate)	24.22	Hydrothermal 180°C, 6 h	500°C, 2 h; 750°C, 1 h	395	0.88	3.81	4.7	4.6
N/S-12-Hy (nickel nitrate hexahydrate)	28.35	Hydrothermal 180°C, 12 h		380	0.84	3.81	3	3.4
N/S-18-Hy (nickel nitrate hexahydrate)	30.58	Hydrothermal 180°C, 18 h		304	0.61	3.82	4	4.0
N/S-24-Hy (nickel nitrate hexahydrate)	30.63	Hydrothermal 180°C, 24 h		286	0.66	3.83	3.9	3.5

N/S-36-Hy (nickel nitrate hexahydrate)	30.55	Hydrothermal 180°C, 36 h		269	0.67	3.81	5.2	4.9
N/S-48-Hy (nickel nitrate hexahydrate)	30.72	Hydrothermal 180°C, 48 h		245	0.59	3.81	5.5	5.5
MCF (TEOS)		Hydrothermal (P123 as a surfactant, TMB as an organic swelling agent) 130°C, 24 h	550°C, 5 h	434.3	2.69			
N/M-P-24 (nickel nitrate)	25.3	Hydrothermal (180°C, 24 h)	700°C, 1 h, 100%	239.4	0.9		4.3	4.7
N/M-P-32 (nickel nitrate)	31.8	Hydrothermal (180°C, 32 h)		200.6	0.84		4.4	5.1
N/M-P-40 (nickel nitrate)	32.2	Hydrothermal (180°C, 40 h)	500°C, 2 h	194.7	0.77		4.8	5.4
N/M-P-32-3L (nickel nitrate, $La(NO_3)_3 6H_2O$: 3 wt%)	30.4	Incipient wetness impregnation:		189.3	0.81		4.2	4.6

Sample (precursor)	wt%	Description / Method	Conditions						
N/M-P-32-5L (nickel nitrate, La(NO₃)₃6H₂O: 5 wt%))	30.1	La$_2$O$_3$-modified nickel phyllosilicate		184.2	0.74		3.9	4.0
N/M-P-32-7L (nickel nitrate, La(NO₃)₃6H₂O: 7 wt%)	29.5			173.6	0.71		3.7	4.4
Ni/SiO2-AEM (colloidal silica, nickel nitrate hexahydrate)	40	Ammonia evaporation (room temp, 5 h and evaporation 80 °C)	450°C, 4 h / 500°C, 2 h, 100% / 800°C, 2 h	446.3	0.84			4.2
SiO$_2$ (TEOS)		Hydrolysis of TEOS in basic media		17	0.03	79		6
5NiPS (nickel nitrate)	3.5	Hydrothermal		70	0.01	58		
10NiPS (nickel nitrate)	9.1	(120°C, 12 h)		95	0.14	60		

Catalyst		Synthesis method							
PS-10Ni (SiO$_2$ commercial, nickel nitrate)	10	Modified ammonia evaporation	400°C, 4 h	500°C, 1 h	264			-	2.1
PS-20Ni (SiO$_2$ commercial, nickel nitrate)	20				343			2.6	2.5
PS-36Ni (SiO$_2$ commercial, nickel nitrate)	36				403			3.4	3.0
SiO$_2$ (gas sol, commercial)					200				
Ni@PSi (nickel nitrate)		Ammonia evaporation (evaporation 80°C)	600°C, 2 h						3.7
3%Mo-Ni@Psi (nickel nitrate, (NH$_4$)$_6$Mo$_7$O$_{24}$4H$_2$O: 3 wt%)				500°C, 2 h	261.4	0.48	7.4		4.3
				550°C, 2 h	270.7	0.45	6.6		4.4
				600°C, 2 h	200.3	0.40	8.0		5.1
1%Mo-Ni@Psi (nickel nitrate,	33			500°C, 2 h					4.2

Sample	Ni loading (wt%)	Preparation method	Calcination	Surface area	Pore volume	Pore size		
$(NH_4)_6Mo_7O_{24}4H_2O$: 1 wt%								4.6
10%Mo-Ni@Psi (nickel nitrate, $(NH_4)_6Mo_7O_{24}4H_2O$: 10 wt%)								
SiO_2 (silica sol)				174	0.3	4.6		
PS-0.09 (nickel nitrate)	7.1	Ammonia evaporation (evaporation 80°C)	600°C, 4 h	227	0.5	7.6	2.7	
PS-0.19 (nickel nitrate)	13.7			270	0.6	7.1	2.9	
PS-0.32 (nickel nitrate)	22.0		550°C, 2 h, 100%	312	0.8	7.8	3.4	
PS-0.48 (nickel nitrate)	31.5			347	0.6	7.7	3.8	
PS-0.68 (nickel nitrate)	38.8			336	0.8	7.8	4.3	
PS-0.94 (nickel nitrate)	46.0			326	0.7	7.2	4.6	

Sample		Method						
PS-1.3 (nickel nitrate)	54.5				243	0.5	7.0	4.9
Ni-SiO2-AEH (silica sol, nickel nitrate)	18.1	Modified ammonia evaporation (evaporation 80°C)	700°C, 4 h	600°C, 2 h	275			4.8
Ni-SiO2-DP (silica sol, nickel nitrate)	15.2	Modified deposition-precipitation	500°C, 4 h		248			4.2
SiO2 (silica sol)					153.9	0.19	4.7	
NiSi-PS (nickel nitrate)	36.1	Modified ammonia evaporation (evaporation 80°C)	600°C	500°C, 2 h	352.5	0.76	7.0	3.3
Ph-NT (nickel nitrate, modified silane)		Sol gel						
SiO2 (TEOS)		Stober process			3.04		12.3 65	

Catalyst		Synthesis	Calcination	Reduction					
3%Ni@SiO2 (nickel nitrate hexahydrate)	3.66	Deposition-precipitation	700°C, 4 h	650°C, 1 h	17.8		9.179		
11%Ni@SiO2 (nickel nitrate hexahydrate)	11.03				68.07		6.005		
3D-SBA-15 (tetramethoxysilane)			550°C, 5 h		512	0.58			
Ni/S-T (nickel nitrate)	32.7	Two-pot hydrothermal 180°C, 24 h	400°C, 2 h	750°C, 1 h, 100%	228	0.63		3.8	4.1
Ni/S-O (nickel nitrate)	35.8	One-pot hydrothermal 100°C, 24 h +180°C, 24 h	550°C, 5 h		467	0.67		3.5	3.7
Ni/SiO2 (silica sol, nickel nitrate)	30	Ammonia evaporation (evaporation 80°C)	400°C, 4 h	600°C, 4 h	391.1	0.510	3.9		
			500°C, 4 h		346.7	0.641	3.7		
			600°C, 4 h		345.6	0.462	3.9		
			700°C, 4 h		296.1	0.486	5.0		
$Cu_{40}Ni_1PS$ (colloidal silica, nickel nitrate,	0.7	Ammonia evaporation	400°C, 4 h	350°C, 3 h, 10%	644.6	1.07			

Sample		Method	Calcination			
copper nitrate: 38.9 wt%)						
Cu$_{36}$Ni$_5$PS (colloidal silica, nickel nitrate, copper nitrate: 35.6 wt%)	3.9	hydrothermal (evaporation 80°C and heat to 150°C, 24 h)		601.6	1.09	
Cu$_{31}$Ni$_{10}$PS (colloidal silica, nickel nitrate, copper nitrate: 30.2 wt%)	8.8			598	1.09	
SBA-15 (TEOS)			550°C, 6 h	780	1.16	6.9
Ni/Co-1:3 (nickel nitrate, cobalt nitrate, Ni and Co loading = 20 wt%, Ni:Co = 1:3)		Deposition precipitation	500°C, 6 h	104	1.06	3.9-23
Ni/Co-2:2 (nickel nitrate, cobalt nitrate, Ni and Co loading = 20 wt%, Ni:Co = 2:2)			700°C	73	1.02	3.9-25

Catalyst		Preparation method	Calcination				
Ni/Co-3:1(nickel nitrate, cobalt nitrate, Ni and Co loading = 20 wt%, Ni:Co = 3:1)							
10Ni/SiO_2-H_2O (silica commercial, nickel nitrate)	10	Water impregnation		121	0.98	3.9-19	23.4
10Ni/SiO_2-NH_3 (silica commercial, nickel nitrate)	10	Ammonia impregnation					13.8
10Ni/SiO_2-NH_3-DBD (silica commercial, nickel nitrate)	10	Ammonia impregnation combined with dielectric-barrier discharge	500°C, 4 h — 700°C, 2 h				9.9
30Ni/SiO_2-H_2O (silica commercial, nickel nitrate)	30	Water impregnation		174	0.47		33.8

30Ni/SiO$_2$-NH$_3$ (silica commercial, nickel nitrate)	30	Ammonia impregnation	176	0.54	16.4
30Ni/SiO$_2$-NH$_3$-DBD (silica commercial, nickel nitrate)	30	Ammonia impregnation combined with dielectric-barrier discharge	222	0.43	13
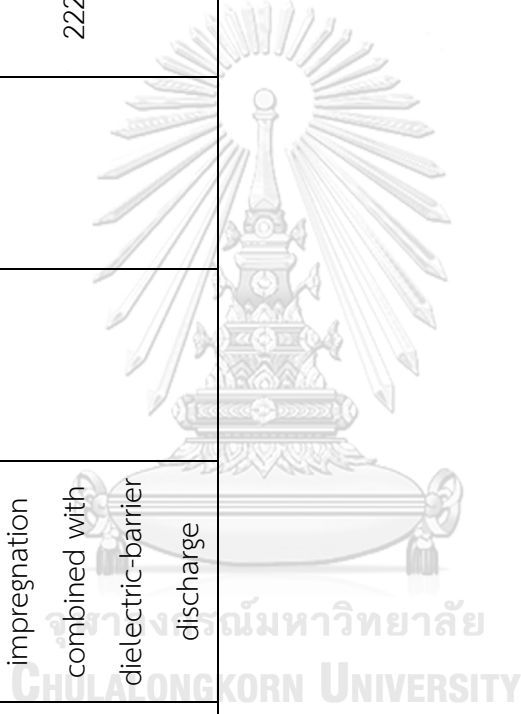
2.2 Furfural hydrogenation

Table 2. 2 Review of catalytic performances of Ni-based catalysts in furfural hydrogenation

Catalysts	Reaction condition	Solvent	Reaction time (min)	Furfural conversion (%)	FA selectivity (%)	Ref./(year)
NiB/Al$_2$O$_3$	Temp = 80°C, P$_{H2}$ = 50 bar	Methanol	180	19.38	87.19	[51]/(2011)
NiCeB/Al$_2$O$_3$				7.7	95.87	
NiCuB/Al$_2$O$_3$				14.75	100	
NiFeB/Al$_2$O$_3$				14.81	91.56	
NiCoB/Al$_2$O$_3$				19.88	89.44	
NiMoB/Al$_2$O$_3$ (Mo/Ni atom=1:7)				99.13	90.98	
Cu$_{11.2}$Ni$_{4.7}$-MgAlO	Temp = 200°C, P$_{H2}$ = 10 bar	Ethanol	120	93.2	89.2	[52]/(2011)
Ni-Pt/SiO$_2$	Temp = 250°C, P$_{H2}$ = 6.9 bar	2-propanol	90	44.1	466.4	[53]/(2014)
Ni-Pd(5:1)/ TiO$_2$-ZrO$_2$ (Ni load: 5 wt %)	Temp = 130°C, P$_{H2}$ = 50 bar	Ethanol	480	100	2.1	[54]/(2015)
Cu-Ni/CNT	Temp = 130°C	Ethanol	600	100	0.2	

Catalyst	Condition	Solvent	Time (min)			Reference
Cu-Ni/MgO	P_{H2} = 40 bar	Ethanol	60	30.6	27.4	[55]/(2016)
Cu-Ni /γ-Al$_2$O$_3$	Temp = 100℃, P_{H2} = 30 bar			63.2	67.3	
Cu-Ni/TiO$_2$				58.7	42.7	
Cu-Ni/ZrO$_2$				57.8	41.2	
Cu-Ni/CNT				29.2	77.2	
Fe(NiFe)O$_4$–SiO$_2$	Temp = 90℃, P_{H2} = 20 bar	Heptane	240	100	94.3	[55]/(2016)
Ni/Al$_2$O$_3$	Temp = 140℃, P_{H2} = 40 bar	Water	240		>99	[56]/(2016)
Ni/Mg-Al$_2$O$_3$ (Ni load: 10 Wt %)	Temp = 140℃, P_{H2} = 40 bar	Water	240		>99	
Ni/Ca-Al$_2$O$_3$					>99	
Ni/Sr-Al$_2$O$_3$					>99	
Ni/Ba-Al$_2$O$_3$					>99	

Catalyst	Conditions	Solvent				Ref/Year
Ni-Cu sol-gel	Temp = 130°C, P$_{H2}$ = 60 bar	i-propanol	-	100	92	[57]/(2016)
5%Ni/CN	Temp = 200°C, P$_{H2}$ = 10 bar	2-propanol	240	96	95	[43]/(2016)
MAN-2	Gas phase: 180°C, 1 atm, LHSV=1.8h^{-1}, GHSV=1800h^{-1}	300	97.6	94.5	3.9	
1.1Ni-0.8Co-Al	Gas phase: 150°C, 1 atm, H$_2$/furfural=25	60	98	71.8	9.9	
1.4Ni-1.4Mg-Al			94	68.6	10.2	
Ni-Pt/SiO$_2$	Temp = 250°C, P$_{H2}$ = 6.9 bar	2-propanol	90	44.1	466.4	[53]/(2017)
CuNi/MgAlO	Temp = 150°C, P$_{H2}$ = 40 bar	Ethanol	180	>99		[58]/(2017)
Cu7Ni1/MgAlO				>99	80	

Catalyst	Conditions	Solvent	Time			Ref./Year
NiCo/MgAlO				90	91	
CuNi/Al$_2$O$_3$				90	67	
CuNi/SiO$_2$				>99	70	
CuNi/MgO				54	>99	[47]/(2017)
Ni/NAC (N-doped AC)	Temp = 80°C, P$_{H2}$ = 40 bar	2-propanol	180	100		[47]/(2017)
Ni/NAC (N-doped AC)	Temp = 140°C, P$_{H2}$ = 40 bar	2-propanol	300	100	100	
Cu-Ni/γ-Al$_2$O$_3$ (Cu/Ni=1, Cu=10 wt %)	Temp = 130°C, P$_{H2}$ = 40 bar	2-propanol	240	92.6	93.6	[59]/(2017)
Ni-Fe(2)HT-573	Temp = 150°C, P$_{H2}$ = 10 bar	Iso-PrOH	45	96	95	[60]/(2017)
Ni$_1$Co$_1$B-K	Temp = 100°C, P$_{H2}$ = 30 bar	Ethanol	180	93.1	77.7	
Ni$_1$Co$_3$B-Na				99.8		[61]/(2017)

Catalyst	Conditions	Solvent				Reference
Co-10%Ni/MCF-41	Temp = 130°C P$_{H2}$ = 45 bar	Ethanol	180	100	0	[62]/(2018)
Co-10%Ni/MCM-48				100	6.7	
Co-10%Ni/MCF-2				100	12.6	
Co-10%Ni/SBA-15				100	0.7	
Co-10%Ni/ SC-SBA-15				100	1.5	
Ni$_1$Co$_1$B/H$^+$-ATP	Temp = 140°C P$_{H2}$ = 30 bar	Ethanol	120	91.3	82	[63]/ (2018)
R-Ni/AlOH	Temp = 180°C P$_{H2}$ = 30 bar	Iso-propanol	75	>99	1	[64]/ (2018)
Ni-Sn/AlOH				95	96	
Ni-Ga/AlOH				12.8	0	
Ni-Ag/AlOH				44.9	16	
Ni-Nb/AlOH				47.3	13	

57

Catalyst	Conditions	Solvent	Time			Reference
Ni-Zr/AlOH				>99	0	
Ni-In/AlOH	Temp = 180°C, P_{H2} = 30 bar	Iso-propanol	180	96	96	
Ni-In/amorphous alumina	Temp = 180°C, P_{H2} = 30 bar	Iso-propanol	75	>99	99.9	
Ni_2Co_1/SiO_2	Temp = 80°C, P_{H2} = 34 bar	2-propanol	300	9.3	49.5	[42]/(2018)
Ni_4Cu_1/SiO_2				9.1	50.4	
Ni_3Fe_1/SiO_2				25.8	59.8	
Ni_3Fe_1/SiO_2	Temp = 140°C, P_{H2} = 34 bar	Methanol	300	100	96.5	
Pt–Ni/MWNT	Temp = 100°C, P_{H2} = 30 bar	ethanol	300	95.9	84.1	[65]/(2018)
Pd–Ni/MWNT				92.7	2.1	
Ni/AC-SO_3H	Temp = 60°C, P_{H2} = 40 bar	2-propanol	480	>99	>99	[66]/(2018)

Catalyst	Conditions	Solvent	Time (min)	Conversion (%)	Yield (%)	Reference
Ni/AC-SO$_3$H	Temp = 140°C, P_{H2} = 40 bar	2-propanol	300	>99		[67]/(2018)
69wt%Ni/Al$_2$O$_3$	Temp = 120°C, P_{H2} = 50 bar	Diisopropyl ether	60	100		
66wt%Ni/SiO$_2$				100		
Ni$_6$MoC-SiO$_2$	Temp = 150°C, P_{H2} = 60 bar	Isopropanol	80	94	85	[68]/(2018)
Ni$_3$Fe$_1$/SiO$_2$	Temp = 140°C, P_{H2} = 34 bar	methanol	-	100	96.5	[42]/(2018)
Ni-LN650	Temp = 120°C, P_{H2} = 10 bar	H$_2$O	180	98.8	12.7	[69]/(2018)
Ni/MMO-NO$_3$	Temp = 110°C, P_{H2} = 30 bar	Iso-PrOH	180	100	97	[70]/(2019)
Ni/MMO-CO$_3$			180	100		
		Ethanol	360	98.7	92	[71]/

59

Catalyst	Conditions	Solvent				Reference
Ni$_{0.15}$/Al$_2$O$_3$-C	Temp = 160°C, P$_{H2}$ = 40 bar					(2019)
Ni$_6$MoC-SiO$_2$	Temp = 150°C, P$_{H2}$ = 60 bar	Isopropanol	180	94	85	[72]/ (2019)
Ni-Fe(3:1)-LDH	Temp = 140°C, P$_{H2}$ = bar	2-propanol	300	97	93	[73]/ (2019)
2.5Ni-Sep-u	Gas phase: WHSV= 1.5h^{-1}	300	42	28	5 (MF) 10 (F)	[74]/ (2019)
2.5Ni-Sep-i			20	11	1 (MF) 5 (F)	
2.5Ni-Sep-c			59	28	8 (MF) 16 (F)	
2.5Ni-Sep-a			85	8	26 (MF) 53 (F)	
Ni$_3$Sn$_2$-Al$_2$O$_3$	Gas phase: Cat 1 g, H$_2$/furfural	180	65	61.2		[75]/ (2019)

Catalyst	Condition	Solvent	Time	Yield (%)	Conversion (%)	Year/[Ref]
	= 5:1, WHSV = 0.5 h⁻¹, temp = 280°C, P = 1 atm					
Ni/AC	80°C, 4 MPa	2-propanol	3	86.4	23.3	2017/[47]
Ni/NAC-1-1073				100	0	
Ni–Fe(2)HT-573	150°C, 1 MPa	iso-PrOH	30 min	90	92	2017/[60]
5% Ni/Ac	200°C, 3 MPa	CPME	5		7	2018/[76]
Cu$_2$Ni$_1$AlO$_y$	120°C, 1.6 MPa	isopropanol	1.5	98	99	2021/[77]
Ni@NC	180°C, 0.1 MPa (N$_2$)	isopropanol	6	63	66	2021/[78]
Ni1Co1@NGC				99.4	88.6	
Ni-SAs/NC	130°C, 2 MPa (N$_2$)	2-ProOH	2	85.1	97.1	2021/[79]
PtNi HNFs	100°C, 2 MPa	isopropyl alcohol	1	99	99	2021/[80]
Ni/MgAlO	150 °C, 4 MPa		3	99	25	2017/[58]
40NCB/H$^+$-ATP-A	100 °C, 3 MPa		2	81.9	78.1	2018/[63]

Ni/SiO2	140 °C, 3.4 MPa		5	67.3	50.1	2018/[42]
MgAl-0.5-NiO$_x$	90 °C, 2 MPa			100	64	2021/[81]
Ni/TiO2-350	80 °C, 3 MPa		8	92.5	96.8	2021/[82]
MANR2-HT	150 °C, 1 MPa		6	100	86	2022/[83]
Ni/TiO$_2$-A2	50°C, 20 bar		2	65.7	66.7	2022/[84]
5Ni–10Re/C500	90 °C, 20 bar,		2	79	91	2022/[85]
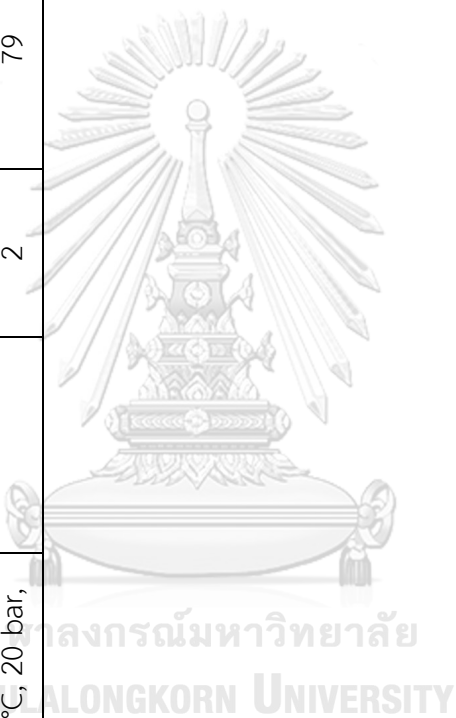
2.3 CO$_2$ hydrogenation

Table 2. 3 Review of catalytic performances of Ni-based catalysts in CO$_2$ hydrogenation

Catalysts	Preparation method	Reaction temp (°C)	Reaction condition	CO$_2$ conv. (%)	CH$_4$ selec. (%)	Ref.
10%Ni/SiO$_2$ (Ni_Alt_Si)	Modified sol-gel	350	H$_2$:CO$_2$ = 10:1, WHSV = 36000 cm^3/(g$_{cat}$h), Cat. = 50 mg	51	95	This work
15%Ni/SiC	Impregnation	360	H$_2$:CO$_2$ = 4:1, space velocity = 12000 h^{-1}, Cat. = 200 mg	79	100	[86]
15%Ni-La/SiC	Co-impregnation	360	H$_2$:CO$_2$ = 4:1, space velocity = 12000 h^{-1}, Cat. = 200 mg	85	100	
5%Ni-CZ$_{sol-gel}$	Pseudo sol-gel	350	H$_2$:CO$_2$ = 4:1, space velocity = 43000 h^{-1}, Cat. = 150 mg, Total flow = 55 cm^3/min	67.9	98.4	[87]
5%Ni-CZ$_{imp}$	Wet impregnation			25.4	84.7	

Catalyst	Synthesis method	Temperature (°C)	Conditions	Conversion (%)	Selectivity (%)	Ref.
5%Ni-SiO$_2$	Wet impregnation	350	H$_2$:CO$_2$ = 4:1, space velocity = 11000 h^{-1}, Cat. = 150 mg, total flow = 55 cm^3/min	27.6	85.5	
15%Ni/Al$_2$O$_3$	Impregnation	350	H$_2$:CO$_2$ = 4:1, GHSV = 15000 cm^3/(g$_{cat}$h), Cat. = 200 mg,	78.5	99	[32]
15%Ni-2CeO$_2$/Al$_2$O$_3$	Co-impregnation	350		85	99	
10%Ni/CeO$_2$	Wet impregnation	350	H$_2$:CO$_2$ = 4:1, space velocity = 10000 h^{-1}, Cat. = 300 mg,	90	100	[88]
10%Ni/MgO		450		70	97	
10%Ni/TiO$_2$		450		76	98	
10%Ni/α-Al$_2$O$_3$		450		80	99	
35Ni5Fe0.6Ru/ alumina xerogel	sol–gel	220 (10 bar)	H$_2$:CO$_2$ = 4:1, WHSV = 9600 cm^3/(g$_{cat}$h), Cat. = 50 mg	68.2	98.9	[89]
5NiC4Z	impregnation	350	H$_2$:CO$_2$ = 4:1, GHSV = 35,400 h^{-1}, Cat. = 500 mg	68.9	90.2	[90]

Catalyst	Method	Temperature	Conditions			Ref.
30Ni/Al$_2$O$_3$.0.5SiO$_2$	sol–gel	350	H$_2$:CO$_2$ = 3.5:1, GHSV = 9000 cm^3/(g$_{cat}$ h), Cat. = 200 mg	82.38	98.19	[91]
10%Ni/ZSM-5	impregnation	400	H$_2$:CO$_2$ = 4:1, GHSV = 2400 h^{-1}, total flow = 40 cm^3/min	76	75	[92]
10%Ni/SiO2				66	65	
10%Ni/SBA-15				71	69	
10%Ni/MCM-41				64	63	
10%Ni–1Mg/Si	co-impregnation	400	H$_2$:CO$_2$ = 4:1, GHSV = 15,000 cm^3 h^{-1} g^{-1}, Cat. = 200 mg,	73	97	[93]
15%Ni/SiC	Impregnation	360	4:1	79	100	[86]
15%Ni-5%La/SiC	Impregnation	360	4:1	85	100	[86]
10%Ni/CeO$_2$	Impregnation	350	4:1	90	100	[88]
10%Ni/MgO	Impregnation	450	4:1	70	97	[88]
10%Ni/TiO$_2$	Impregnation	450	4:1	76	98	[88]
10%Ni/**α**-Al$_2$O$_3$	Impregnation	450	4:1	82	99	[88]
35%Ni5%Fe0.6%Ru/Al$_2$O$_3$	Sol-gel	220	4:1	68.2	98.9	[89]

Catalyst	Method	Temperature	Ratio			Ref.
14%Ni/USY	Impregnation	400	4:1	65.5	94.2	[94]
14%Ni7%Ce/USY	Impregnation	400	4:1	68.3	95.5	[94]
5%Ni/CZ (Ce/Zr=4)	Impregnation	420	4:1	68.9	90.2	[90]
5%Ni/CZ	Impregnation	350	4:1	25.4	84.7	[87]
5%Ni/CZ	Sol-gel	350	4:1	67.9	98.4	[87]
5%Ni/SiO$_2$	Impregnation	350	4:1	27.6	85.5	[87]
3%Ni/MCM-41	C16 alkyl template	300	18:7	5.6	96	[95]
10%Ni/La$_2$O$_3$	Impregnation	380	4:1	100	100	[96]
20%Ni/Al$_2$O$_3$	Impregnation	350	3.5:1	77.2	100	[97]
2%Ce-20%Ni/Al$_2$O$_3$	Impregnation	350	3.5:1	80.3	100	[97]
2%Mn-20%Ni/Al$_2$O$_3$	Impregnation	350	3.5:1	78	100	[97]
2%La-20%Ni/Al$_2$O$_3$	Impregnation	350	3.5:1	75.4	97.6	[97]
2%Zr-20%Ni/Al$_2$O$_3$	Impregnation	350	3.5:1	74.4	99.1	[97]
10%Ni/Al$_2$O$_3$	Impregnation	350	3.5:1	69	92	[98]
15%Ni/Al$_2$O$_3$	Impregnation	350	3.5:1	71	100	[98]
20%Ni/Al$_2$O$_3$	Impregnation	350	3.5:1	76	100	[98]
25%Ni/Al$_2$O$_3$	Impregnation	350	3.5:1	74	99	[98]

9.8%Ni/Al$_2$O$_3$	Impregnation	516	11:1	98	100	[99]
15%Ni-2%Ce/Al$_2$O$_3$	Impregnation	300	4:1	71	99	[32]
15%Ni/Al$_2$O$_3$	Impregnation	300	4:1	45	99	[32]
15%Ni/SiO$_2$-Al$_2$O$_3$	Impregnation	600	4:1	63	29	[100]
15%Ni/RHA-Al$_2$O$_3$ (RHA=rice husk ash)	Impregnation	500	4:1	63	90	[100]
4.29%Ni/RHA-Al$_2$O$_3$	Ion exchange	500	4:1	34	56	[101]
4.09%Ni/SiO$_2$-gel	Ion exchange	500	4:1	25	45	[101]

CHARPTER III

PAPER I

Highly active and stable Ni-incorporated spherical silica catalysts for CO$_2$ methanation

Sasithorn Kuhaudomlap[1], Piyasan Praserthdam[1], Masayuki Shirai[2], and Joongjai Panpranot[1,]*

[1]Center of Excellence on Catalysis and Catalytic Reaction, Department of Chemical Engineering, Faculty of Engineering, Chulalongkorn University, Bangkok, 10330 Thailand

[2]Department of Chemistry and Biological Sciences, Faculty of Science and Engineering, Iwate University, Morioka, Iwate, 020-8551 Japan

_____

[*] To whom correspondence should be addressed.

Tel. 66-22186869 Fax. 66-2218-6877 E-mail: joongjai.p@chula.ac.th (J. Panpranot)

3.1 Abstract

Nickel-doped spherical silica (SSP) catalysts with ca. 10 wt% Ni were prepared via a sol-gel method using cetyltrimethyl ammonium bromide as the structure directing agent with different loading sequences of Ni and Si sources (Si1_Ni2, Ni1_Si2, and Ni_Alt_Si). For comparison purposes, the SSP supported Ni catalysts were also prepared by impregnation method (Ni/SSP (Imp)). All the prepared catalysts showed spherical shape with high specific surface area (357-868 m2/g). The X-ray diffraction and H_2-temperature programmed reduction results revealed the stronger interaction between Ni and SiO_2 in the form of nickel silicate for all the Ni-doped SSP catalysts except Ni/SSP (imp), in which only NiO species were detected. For the reaction temperature 350 $°$C, the CO_2 conversion was in the order: Ni_Alt_Si (51%) > Ni1_Si2 (49%) > Si1_Ni2 (28%) > Ni/SSP (Imp) (10%) with methane selectivity 80-95%. The superior performances of the Ni_Alt_Si catalyst were correlated well to the higher electron density of Ni on the surface and higher CO_2 adsorption ability as revealed by the X-ray photoelectron spectroscopy and CO_2-temperature program desorption results.

Keywords: CO_2 methanation; Ni/SiO$_2$ catalysts; Spherical silica; Nickel silicate.

3.2 Introduction

Reduction of carbon dioxide (CO_2) emission, one of the main greenhouse gases to global warming, is the globally concerned topic [31]. This has been done by many routes including reduction of the consumption of fossil fuels, carbon capture, separation and storage, and transformation of CO_2 to value added chemicals or fuel [32, 33]. CO_2 methanation is a simple reaction widely used to produce the substitute natural gas. Production of biomethane from carbon dioxide is considered a significant process to increase the value of natural gas (natural gas upgrade) and biogas derived from biomass fermentation. The CO_2 methanation is highly exothermic reaction and there are kinetic limitations [32, 34]. Therefore, the development of catalysts for this reaction is important and the performances of different metals such as Ru [31], Rh [102], Pd [103], Ni [31, 36], Co [92], and Fe [36] supported on various oxide supports including TiO_2 [38], Al_2O_3 [31, 36], SiO_2 [34, 36], CeO_2 [37, 38, 92], and ZrO_2 [37, 92] have been studied. Nickel-based catalysts are the most widely studied because of their high catalytic activity and relatively low price but they usually suffered from deactivation because of the sintering of nickel particles and carbon deposition [32]. Many attempts have been conducted to improve the catalytic performances of Ni-based catalysts, in order to possess both high activity and resistance to coke deposition.

In a number of studies, formation of nickel silicate species have shown an advantage synergistic effect of both metal and support [104] high dispersion of nickel metal after reduction, high surface area of catalyst, excellent reactivity and stability for hydrogenation reaction. The stronger metal support interaction compared to NiO can also prevent particle agglomeration, [105], which are key parameters for high CO_2 methanation activity. Nickel silicate has been used as catalysts in various reactions such as deoxygenation of methyl palmitate to alkanes [106], carbon dioxide reforming of methane [107], partial oxidation of methane to syngas [105], hydrogenolysis of 5-

hydroxylmethyl-2-furrylaldehyde to yield furanic fuels [108], and waste plastics-derived syngas catalytic reaction [109]. Moreover, Le et al. [34] prepared Ni/SiO_2 catalysts by deposition-precipitation methods and studied in CO and CO_2 methanation. The catalyst exhibited stronger interaction between the nickel species and support than those prepared by a wet impregnation and showed high Ni dispersion due to the availability of nickel silicate species, which resulted in high catalytic activity for both reactions. Lu et al. [110] synthesized a Ni-grafted SBA-15 catalyst with Ni phyllosilicate existing on the SBA-15 surface. The catalysts exhibited higher CO_2 conversion and CH_4 selectivity than the ones containing only NiO species and had high thermal stability for CO_2 methanation.

In the present work, nickel-doped spherical silica (SSP) catalysts were synthesized by modified-sol gel method with cetyltrimethyl ammonium bromide (CTAB) as the structural-directing agent and different loading sequences of Ni and Si source. The sol-gel-derived SSP usually has high surface area with tunable pore size and a narrow pore size distribution [111, 112]. The properties of Ni/SiO_2 catalysts were investigated by X-ray diffraction (XRD), N_2 physisorption, atomic absorption spectrophotometer (AAS), H_2-temperature-programed reduction (H_2-TPR), X-ray photoelectron spectroscopy (XPS), temperature-programmed desorption of CO_2 (CO_2-TPD), transmission electron microscopy (TEM), and their catalytic activities were evaluated in CO_2 methanation.

3.3 Materials and Methods

3.3.1 Preparation of SiO_2 support

SSP supports were prepared according to the procedure given in Ref. [111]. Tetraethoxysilane (TEOS) was used as silica source and CTAB as the structure-directing agent. The SiO_2 support was prepared by gel synthesis with the following molar ratio:

1TEOS: 0.3CTAB: 11NH3: 58ethanol: 114H$_2$O. At first, ethanol and aqueous ammonia were added to distilled water (DI) with continuous stirring at room temperature and CTAB was dissolved in this solution. A mixture solution was then stirred for 15 min followed by slow addition of TEOS and the solution was further stirred for 2 h. After that, the white precipitate was separated by filtration, washed with distilled water, dried at 110°C overnight and calcined in air at 550°C for 6 h with a heating rate of 2°C/min.

3.3.2 Preparation of Ni/SiO$_2$ catalysts by modified sol gel and impregnation method.

Incorporation of 10wt% Ni in SSP were prepared using the modified sol gel method with three different loading sequences during the SSP synthesis. The Ni-doped spherical silica were synthesized using the previous procedure except that nickel nitrate hexahydrate as Ni precursor was added into the solution with sequences as following: adding Ni previous to TEOS, adding Ni and TEOS altogether, and adding TEOS previous to Ni. The obtained catalysts are referred to Ni1_Si2, Ni_Alt_Si and Si1_Ni2, respectively. Ni/SSP (Imp) was also prepared by a incipient wetness impregnation for comparison as follows, the SSP support was impregnated with an aqueous solution of nickel nitrate, following to drying at 110°C overnight and calcination at 550 °C for 6 h in air.

3.3.4 Catalysts characterization

The X-ray diffraction (XRD) was tested by using a Bruker D8 advance with CuK$_\alpha$ Radiation in the 2θ scanning range of 10-90°. Ni loading was determined by atomic absorption spectrophotometer (AAS). The specific surface area, pore volume and pore diameter were determined by N$_2$ adsorption-desorption measurements with a

Micrometrics ASAP 2020 instrument. H_2-temperature program reduction (H_2-TPR) was used to measure the reduction temperature and reducibility of prepared catalysts. The catalyst samples (0.1g) were pretreated with 30 cm^3/min of N_2 flow at 300°C for 1.5 h and then cooled to room temperature. Subsequently, gas mixture of 10%H_2/Ar (30 cm^3/min) was introduced to the catalyst while the sample was heated from 30°C to 800°C. After that, TPR profiles were recorded as a function of temperatures. Transmission electron microscopy (TEM) images were obtained with JEOL (JEM-2010) at 200 kV to observe the morphology of the catalysts. X-ray photoelectron spectroscopy (XPS) analysis was employed to investigate the binding energy and surface properties of catalysts with using an AMICUS photoelectron spectrum spectrometer equipped with an MgK$_\alpha$ X-ray as primary excitation and KRATOS VISION2 software. Temperature-programmed desorption of CO_2 (CO_2-TPD) was carried out in a quartz u-tube. 50 mg of the catalysts were reduced at 500°C under H_2 flow for 3 h and then purged with He for 10 min. After that, the catalysts were cooled down to 40 °C with He flow. The CO_2 was introduced to the catalyst samples for 1 h at 40°C to achieve saturation. The samples was then heated from 40°C to 800°C at heating rate of 10°C/min with He flow. Finally, the CO_2-TPD profiles were recorded during increase of temperature. The morphological properties of the support and the prepared catalysts were observed using *scanning electron microscope (SEM).*

3.3.5 Catalytic activity

The CO_2 methanation reaction was carried out in a fixed-bed quartz reactor under atmospheric pressure. Prior to the reaction test, the catalysts were reduced under H_2 flow with flow rate 30 cm^3/min at 500°C for 3 h. The reactant feed were introduced into reactor at H_2/CO_2 ratio of 10/1 with weight hourly space velocity (WHSV) of 36000 cm^3/(g_{cat}h) and N_2 was added as an internal standard. The reaction

was performed at the temperature range of 350-500°C in steps of 50°C and then kept constant for 1 h at each temperature. The effluent gases were analyzed by a gas chromatograph with a thermal conductivity detector to separate CO_2, CH_4 and CO.

The catalytic performance was presented as CO_2 conversion and CH_4 selectivity, which were defined as following:

$$XCO_2 (\%) = \frac{CO2.in - CO2,out}{CO2,in} \times 100,$$

$$SCH_4 (\%) = \frac{CH4}{CH4+CO} \times 100,$$

where XCO_2 and SCH_4 were CO_2 conversion and CH_4 selectivity, respectively.

3.4 Results and Discussion

3.4.1 Characteristics of the Ni/SiO$_2$ catalysts

The XRD patterns of Ni/SiO$_2$ catalysts prepared by the modified sol-gel and impregnation methods are shown in **Fig. 3.1**. The SSP support exhibtied only a broad peak, corresponding to amorphous silica. The diffraction peaks at 2θ = 33.8-36.1°, 60.8°, which were assigned to nickel phyllosilicate [106], are shown in all the XRD patterns for all the Ni incorporated SSP catalysts. On the other hand, the sharp peaks at 2θ = 37.2°, 43.3°, 62.9°, 75.4° and 79.4°, which indicated the characteristic peaks of nickel oxides [32], were found for the Ni/SSP (Imp) catalyst. The formation of the nickel phyllosilicate with low crystallinity were observed on Ni1_Si2, Ni_Alt_Si and Si1_Ni2 catalysts, suggesting that nickel particles were directly incorporated in the SSP during the synthesis to form nickel phyllosilicate. However, the nickel phyllosilicate phases were not detected in the Ni/SSP (imp) due possibly to the higher intensities of the nickel oxide species as compared to nickel phyllosilicate, thus the diffraction peaks of nickel oxide was keen.
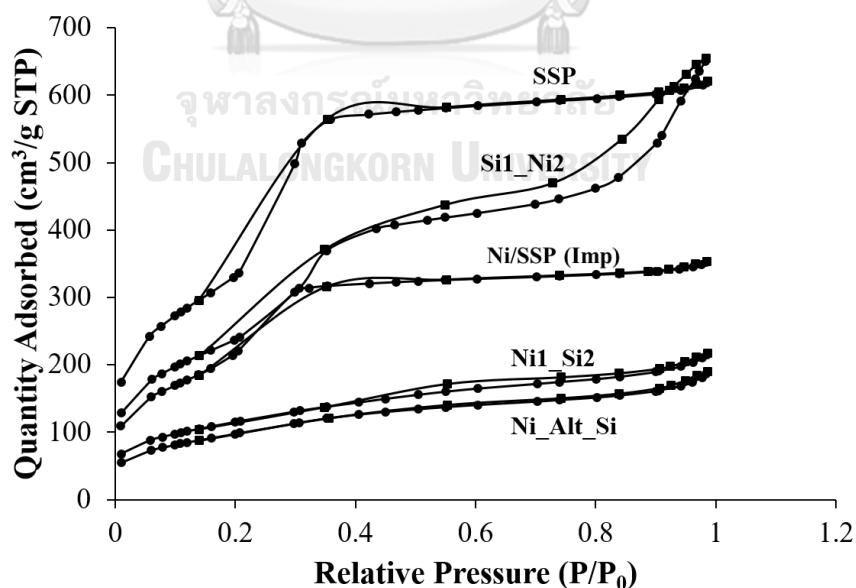

Figure 3. 1 XRD patterns of Ni/SiO$_2$ catalysts after calcined at 550 $^\circ$C for 6 h.

The N$_2$ adsorption-desorption isotherms of all the catalysts are shown in **Fig. 3.2**. All the samples exhibited the characteristic type IV isotherms in the IUPAC classification with H1 and H4 type hysteresis loop. The H1 type hysteresis loop describes a cylindrical-shape pore structure [113-115], indicating that the agglomerates or spherical particles arranged in a fairly uniform way. The H4 type loops shows the existence of slit-like pores, indicating that hollow spheres with walls composed of ordered mesoporous silica [114, 115]. The BET surface area, pore diameter, and pore volume of the bare SSP support and the Ni/SiO$_2$ catalysts are presented in **Table 2.1**. The specific surface area of the catalysts was ranging in the order: SSP (1214 m^2/g) > Si1_Ni2 (868 m^2/g) > Ni/SSP (Imp) (801 m^2/g) > Ni1_Si2 (417 m^2/g) > Ni_Alt_Si (357 m^2/g). It can be noted that deposition of Ni metal on the SSP support caused a decrease in the surface area and pore volume of the catalysts while pore diameter was not obviously changed. In addition, Si1_Ni2 and Ni/SSP (Imp) showed larger surface area than Ni1_Si2 and Ni_Alt_Si. It is suggested that most of the Ni particles were formed inside the pores of Ni1_Si2 and Ni_Alt_Si samples, resulting in pore blockage and lower pore volume and surface area.
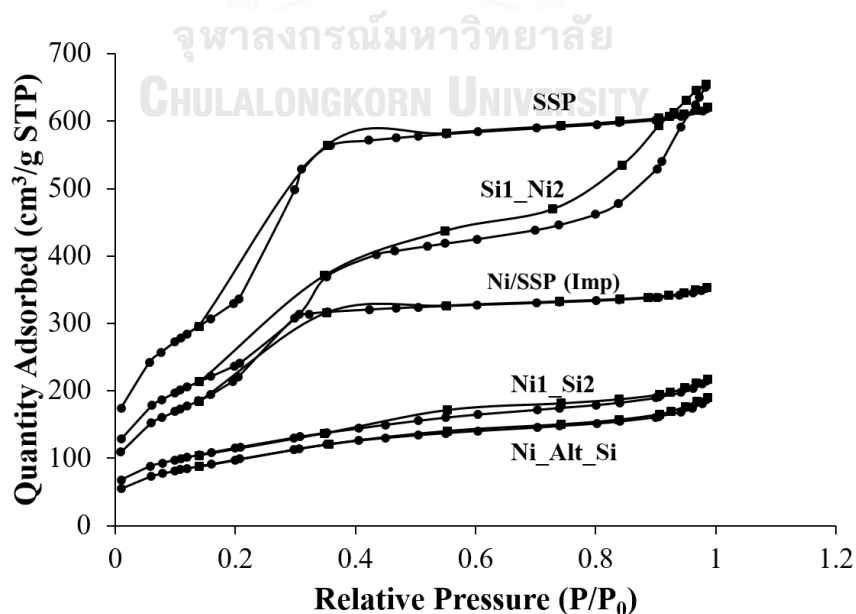

Figure 3. 2 N$_2$ adsorption isotherms of Ni/SiO$_2$ catalysts.

Table 3. 1 Physical properties of the Ni/SiO$_2$ catalysts

catalysts	BET surface area (m^2/g)	Pore volume (cm^3/g)	Pore diameter (nm)
SSP	1214	1.08	2.01
Ni1_Si2	417	0.33	3.38
Si1_Ni2	868	1.08	3.02
Ni_Alt_Si	357	0.35	3.55
Ni/SSP (Imp)	802	0.64	2.23

*Pore volume and pore diameter determined from the Barret-Joyner-Halenda (BJH) desorption method.

The H$_2$-TPR was carried out to investigate the reducibility of the catalysts and the interaction between metal and the support. **Fig. 3.3** shows the TPR profiles of the nickel-doped spherical silica catalysts prepared by different loading sequences of Ni and impregnation methods. The peak below 500°C was assigned to the reduction of NiO on a silica support [105], while the high temperature peak (500-800°C) was due to the reduction of Ni^{2+} located in nickel phyllosilicates [17, 105, 108, 116]. For the Ni/SSP (Imp) catalyst, two reduction peaks were observed in the TPR profile. The first peak appears at low temperature (380°C), which can be attributed to the reduction of nickel oxide and a small reduction peak appeared at higher temperature around 580°C. On the other hand, the modified sol gel catalysts showed a board reduction peak in a range of 350-800°C, corresponding to the reduction of nickel phyllosilicates. It can be observed that most of the nickel species on Ni1_Si2, Si1_Ni2 and Ni_Alt_Si were in the form of nickel phyllosilicates, which are in good agreement with the XRD results of the calcined catalysts. In addition, the reduction peak of the modified sol-gel catalysts

were shifted to higher temperatures compared to the impregnation catalyst. Such results indicated that the interaction between the Ni particles and the SiO_2 support were stronger than that of the impregnation catalyst.
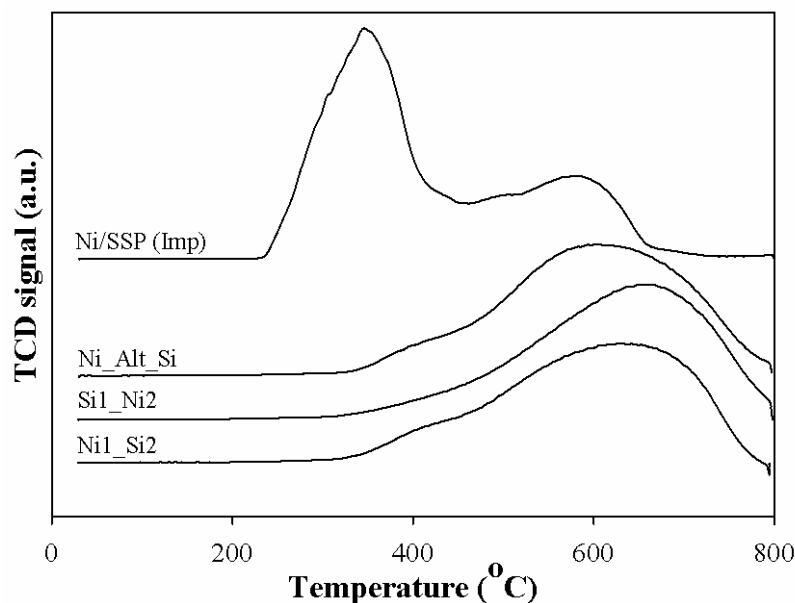

Figure 3. 3 H_2-TPR profiles of the Ni/SiO_2 catalysts.

The actual amount of nickel content on the prepared catalysts were determined by using AAS technique to be ca. 10.5-13.9 wt. %. The Ni contents from AAS were close to the amounts of nickel determined by the TEM-EDX. The percentages of metal dispersion as obtained from the hydrogen chemisorption experiments of the Ni-containing spherical silica catalysts are shown in **Table 3.2**. It was found that all the Ni loading by the modified sol gel method led to higher metal dispersion than the Ni/SiO_2 catalyst prepared by the conventional impregnation method.

Table 3. 2 Nickel loading and chemisorption results of the prepared catalysts.

Catalysts	AAS (Ni, wt. %)	TEM (Ni, wt. %)	Ni dispersion (%)[a]
Ni1_Si2	12.1	12.40	8.30
Si1_Ni2	10.5	13.55	7.03
Ni_Alt_Si	11.2	10.59	9.76
Ni/SSP (Imp)	13.9	14.91	5.10

[a] Determined by hydrogen chemisorption.
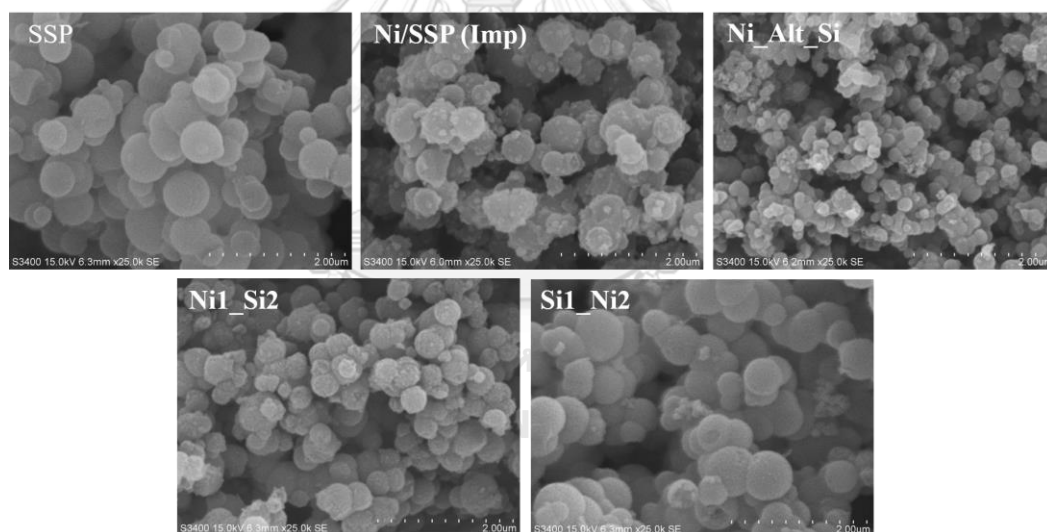
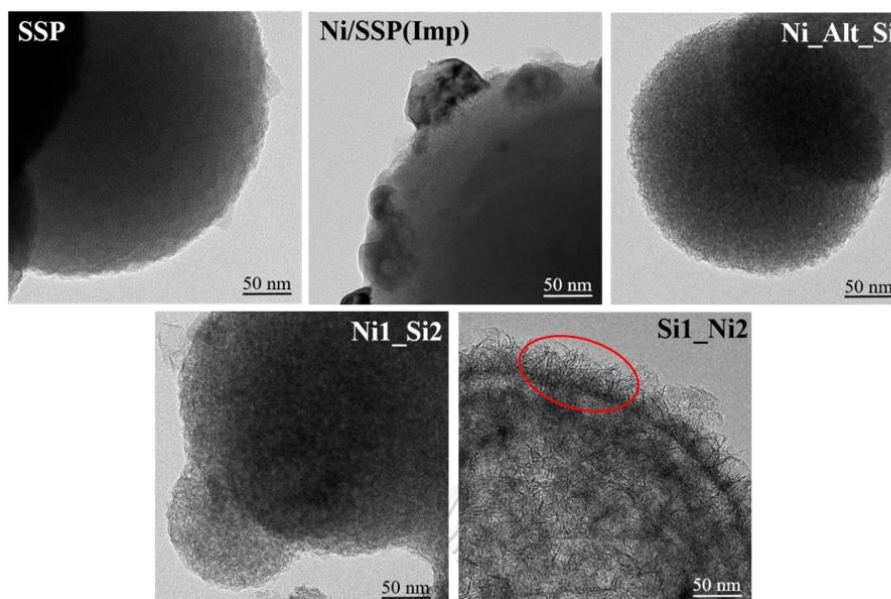**Figure 3. 4** SEM images of Ni/SiO_2 catalysts after calcination.

Figure 3. 5 TEM images of Ni/SiO$_2$ catalysts after calcination.

The SEM and TEM analysis of the Ni-doped SSP catalysts are shown in **Fig. 3.4** and **3.5**, respectively. The SEM images show that the SSP support and the Ni-doped SSP catalysts exhibited spherical shape with 350-600 nm. The surface of the spherical silica particles was relatively smooth and became roughly spherical after nickel loading. The TEM analysis confirmed the results obtained by SEM analysis that the SSP particles had a spherical shape. After Ni loading, the TEM micrographs showed that the SSP supports were covered by nickel phyllosilicate layer, as shown by fibrous morphology [108], which are in good agreement with the XRD results for all Ni catalysts prepared by the modified sol gel method. According to the BET results, most of Ni species were formed on the surface of Si1_Ni2 thus the layer of nickel silicate was more apparent, compared to the Ni1_Si2 and Ni_Alt_Si catalysts. In the case of the impregnation catalyst, larger nickel particles agglomerated on outer surface of SiO$_2$ was presented with lower pore volume compared to the bare SSP. In addition, Si1_Ni2 exhibited higher surface area and pore volume than the impregnation catalysts because of the presence of the layered structure of nickel phyllosilicate [17, 108].

XPS analysis was conducted to investigate the chemical state and surface composition on the catalysts. **Fig. 3.6** shows the XPS spectra for Ni-doped spherical silica catalysts after calcination. For the XPS spectra of the Ni/SSP (Imp) catalyst, the binding energy of Ni2p$_{3/2}$was centered at about 857 eV, which can be attributed to nickel oxide [105, 117]. For Ni1_Si2, Ni_Alt_Si, and Si1_Ni2 catalysts, the Ni2p$_{3/2}$ peak was shown at 858.7 eV, which was assigned to Ni^{2+} species in nickel phyllosilicate [106, 118]. In addition, XPS analysis of the Ni/SiO$_2$ catalysts, which were reduced using H$_2$ at 500℃ was also carried out. For all the modified sol-gel catalysts, a broad main peak of the Ni2p$_{3/2}$ at around 852-859 eV assigned to nickel metal was observed along with nickel phyllosilicate. According to the TPR results, strong interaction between Ni and SSP in the form of nickel silicate resulted in partial reduction of nickel phyllosilicate to nickel metal at the reduction temperature of 500°C. However, the XPS results showed that the peak corresponding to the binding energy of Ni 2p for Ni1_Si2 and Ni_Alt_Si shifted to lower binding energy than Si1_Ni2 catalysts, indicating the electron density of nickel species in Ni1_Si2 and Ni_Alt_Si were higher than Si1_Ni2 catalysts. It is noted that higher values of binding energy of the Ni species in this work as compared to the literature may be due to a bias in the calibration using C 1s peak position of the adventitious carbon[119].
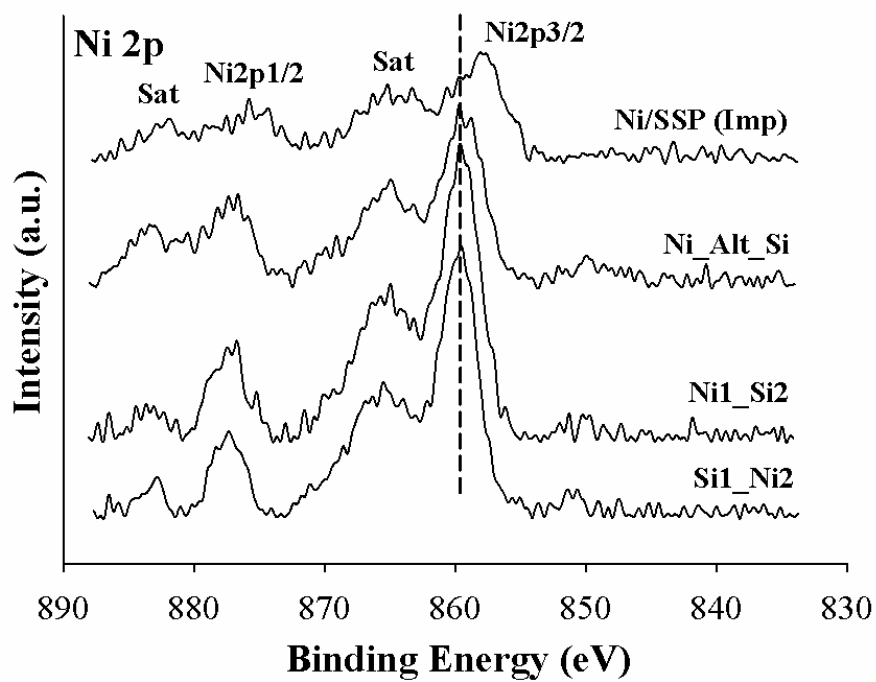
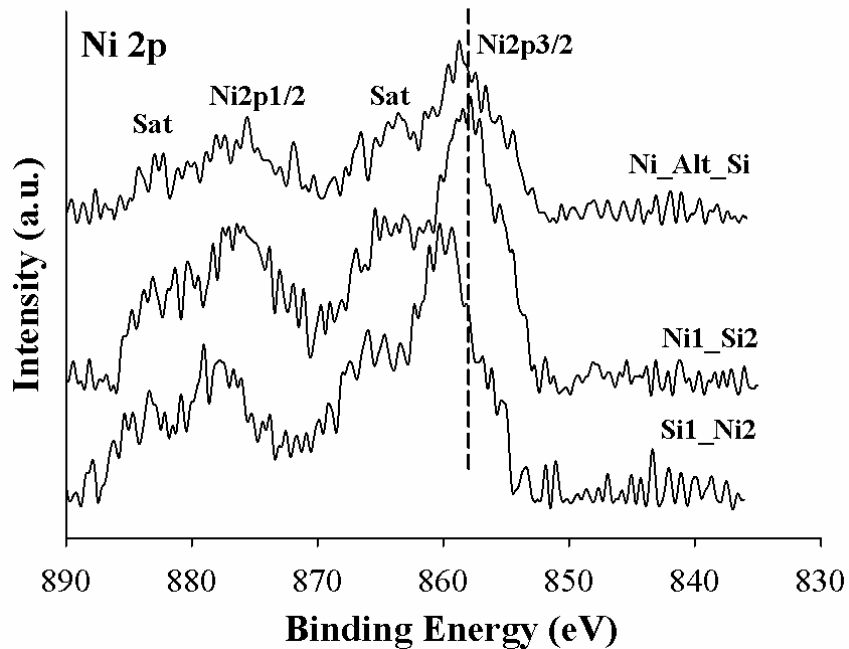**Figure 3. 6** XPS spectra of Ni/SiO$_2$ catalysts after calcination.

Figure 3. 7 XPS spectra of Ni/SiO$_2$ catalysts after reduction.

Temperature-programmed desorption of CO_2 was carried out to obtain the CO_2 adsorption ability over the catalysts. The CO_2 TPD results are shown in **Fig. 3.8**. All the prepared catalysts showed only a desorption peak at low temperature in the range of 90 to 200°C. The amount of CO_2 adsorbed on the modified sol gel catalysts was larger than on the impregnation catalyst. This indicated a larger number of active centers on the surface of modified sol gel catalysts, which facilitated the CO_2 dissociation, and as a consequence improved the CO_2 conversion. In addition, oxygenated species may be created by the dissociation of CO_2, which resulted in the elimination of coke deposited and improved stability of the catalysts [34, 120].
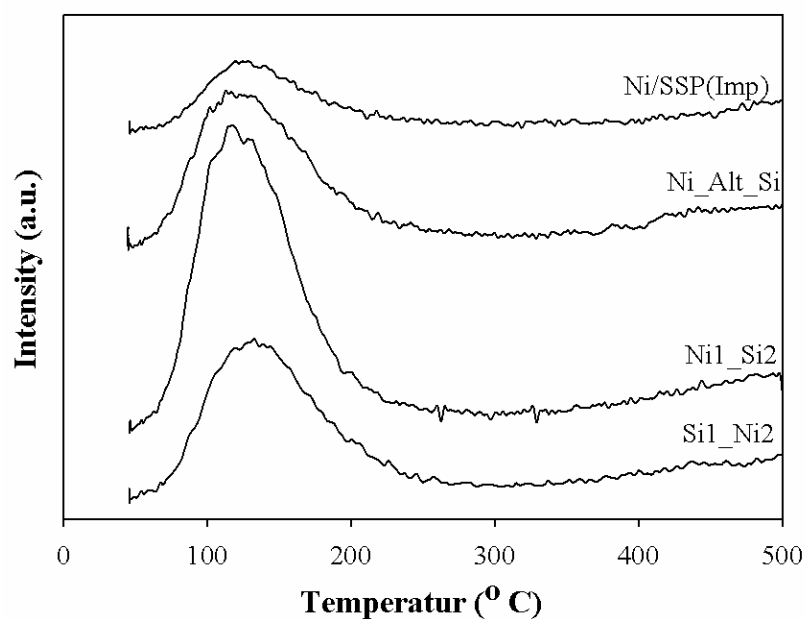

Figure 3. 8 CO_2-TPD of Ni/SiO$_2$ catalysts.

3.4.2 Reaction results

The catalytic performances of the prepared catalysts were tested in the CO_2 methanation. **Fig. 3.9** presents the CO_2 conversion and CH_4 selectivity over the Ni-doped spherical silica catalysts at a WHSV of 36000 $cm^3/(g_{cat}.h)$ at the temperature range of 350-500°C as a function of reaction temperature. The catalysts were reduced in the H_2 flowing at 500°C for 3 h prior to the reaction. The CO_2 conversion over all the catalysts increased with increasing reaction temperature and reached a plateau at the reaction temperature at around 500°C. At 350°C, the CO_2 conversion increased in the order: Ni_Alt_Si (∼51 %) > Ni1_Si2 (∼ 49%) > Si1_Ni2 (∼30 %) >Ni/SSP (Imp) (∼ 10%) with methane selectivity of 80-95%. Despite their lower surface area than the impregnation-catalysts, all the nickel silicate catalysts exhibited superior performances in CO_2 methanation. Prior to the reaction, the catalysts were reduced at 500°C with H_2 flow, which led to partly reduction of nickel phyllosilicate to nickel metal as confirmed by the TPR and XPS results. The existence of both nickel metal and nickel silicate on the catalyst surface appeared to be responsible for the high catalytic performance. Meanwhile, the nickel silicate catalysts may produce metallic nickel with high dispersion after reduction and improved the catalyst stability [17, 105]. Among the silicate catalysts, Ni1_Si2 and Ni_Alt_Si showed high CO_2 conversion at all reaction temperatures with high methane selectivity (90-95%) and the best CO_2 methanation performance was obtained on the Ni_Alt_Si catalyst. It is suggested that the higher electron density of Ni on the surface and the high metal dispersion as well as higher CO_2 adsorption ability over Ni1_Si2 and Ni_Alt_Si catalysts were essential for catalytic activity in CO_2 methanation. In addition, energy of CO_2 desorption from differential scanning calorimetry (DSC) on Ni/SSP (Imp) (1.229 J/g_{cat}) was larger than both of Si1_Ni2 (0.586 J/g_{cat}) and Ni_Alt_Si (0.983 J/g_{cat}), suggesting that too strong interactions between the CO_2 and the catalysts surface resulted to low CH_4 production. Consequently, it can be concluded that the modified sol gel method by Ni and Si source added

alternately during SSP synthesis is a useful method for preparing a highly active and stable Ni-incorporated SSP catalysts for CO_2 methanation.
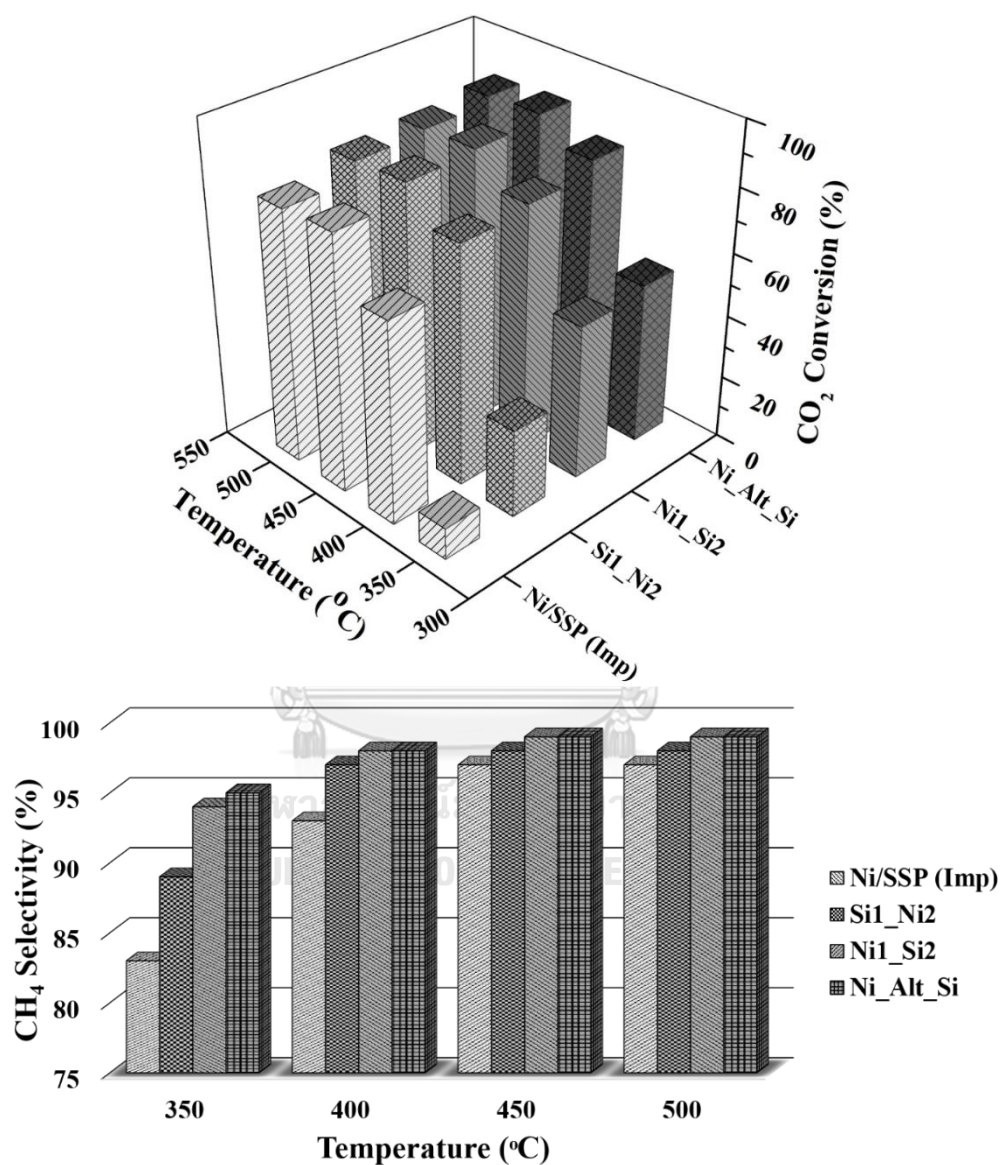

Figure 3. 9 CO_2 conversion and CH_4 selectivity of Ni/SiO_2 catalysts: Reduced under H_2 at 500°C 3 h, Catalyst = 0.05 g, WHSV = 36000 $cm^3/g_{cat}h$, H_2:CO_2 = 10:1
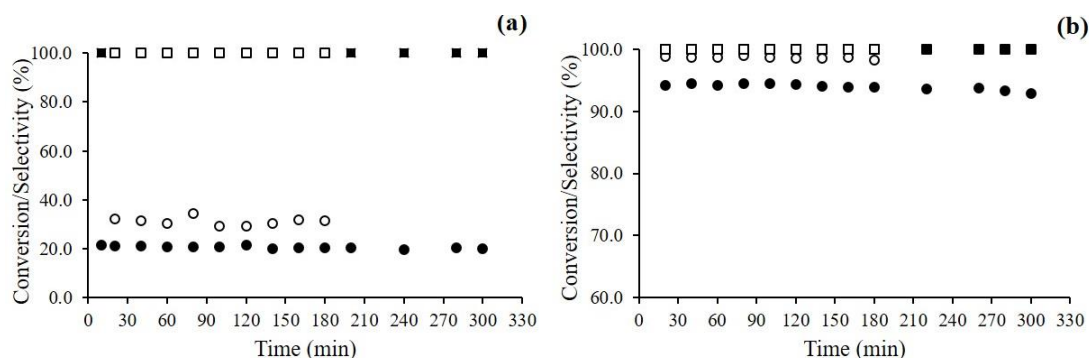
Figure 3. 10 Catalytic stability and recyclability of the Ni_Alt_Si catalyst. Reaction

temperature (a) 300 °C (b) 450 °C. Reduced under H_2 at 500°C 3 h. Reaction

condition: Catalyst = 0.1 g, WHSV = 24000 $cm^3/g_{cat}h$, $H_2:CO_2$ = 10:1. Cycle I: ● CO_2

conversion, ■ CH_4 selectivity Cycle II: ○ CO_2 conversion, □ CH_4 selectivity.

The catalyst stability test was carried out for the Ni_Alt_Si catalyst for 5 h time

on stream at 300 °C and 450 °C, WHSV = 24000 $cm^3/(g_{cat}.h)$ and the results are shown in

Fig 3.10. CO was not produced at these temperatures and CO_2 conversion experienced

a stable trend with 100% selectivity to CH_4. Comparison of the performances of the

Ni-containing spherical silica in this study and the other reported Ni-based catalysts in

the CO_2 methanation is shown in **Table 3.3**. Under similar reaction temperature, the

performances of catalysts prepared in this study in the form of nickel silicate were

comparable to the other supported Ni/NiO catalysts, however, the other reaction

conditions such as space velocity, $H_2:CO_2$, and catalyst weight were varied among the

various studies as indicated in the Table. The recyclability of Ni_Alt_Si catalyst was

investigated for two reaction-regeneration cycles at a WHSV of 24000 $cm^3/(g_{cat}.h)$ and

reaction temperature of 300°C and 450°C. At temperature of 300 °C, CO_2 conversion

increased slightly from 20% in the first cycle to 30% in the second cycle with 100%

selectivity of CH_4. Similarly, there was a slight increase of CO_2 conversion from 94% in

the first cycle to 98% in the second cycle at reaction temperature of 450°C. After the

catalytic test, TGA was conducted to examine the formation of coke after reaction test. Very small amount of coke was detected on these catalysts (< 4%).
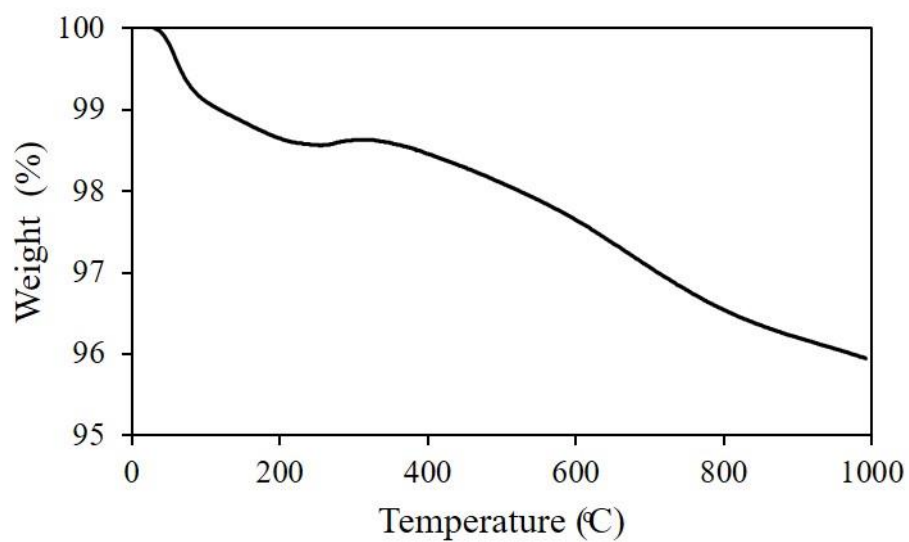

Figure 3. 11 TGA result of Ni_Alt_Si catalyst conducted in air-containing atmosphere.

Table 3. 3 Review of catalytic performances of Ni-based catalysts in CO_2 methanation.

Catalysts	Preparation method	Reaction temp (°C)	Reaction condition	CO_2 conv. (%)	CH_4 selec. (%)	Ref.
10%Ni/SiO$_2$ (Ni_Alt_Si))	Modified sol gel	350	H_2:CO_2 = 10:1, WHSV = 36000 cm^3/(g$_{cat}$h), Cat. = 50 mg	51	95	This work
15%Ni/SiC	Impregnation	360	H_2:CO_2 = 4:1, space velocity = 12000 h^{-1}, Cat. = 200 mg	79	100	[86]
15%Ni-La/SiC	Co-impregnation	360	H_2:CO_2 = 4:1, space velocity = 12000 h^{-1}, Cat. = 200 mg	85	100	
5%Ni-CZ$_{sol-gel}$	Pseudo sol–gel	350	H_2:CO_2 = 4:1, space velocity = 43000 h^{-1}, Cat. = 150 mg, Total flow = 55 cm^3/min	67.9	98.4	[87]
5%Ni-CZ$_{imp}$	Wet impregnation			25.4	84.7	
5%Ni-SiO$_2$	Wet impregnation	350	H_2:CO_2 = 4:1, space velocity = 11000 h^{-1}, Cat. = 150 mg, total flow = 55 cm^3/min	27.6	85.5	
15%Ni/Al$_2$O$_3$	Impregnation	350	H_2:CO_2 = 4:1, GHSV = 15000 cm^3/(g$_{cat}$h), Cat. = 200 mg,	78.5	99	[32]
15%Ni-2CeO$_2$/Al$_2$O$_3$	Co-impregnation			85	99	
10%Ni/CeO$_2$	Wet impregnation	350	H_2:CO_2 = 4:1, space velocity = 10000 h^{-1}, Cat. = 300 mg,	90	100	[88]
10%Ni/MgO		450		70	97	
10%Ni/TiO$_2$		450		76	98	
10%Ni/α-Al$_2$O$_3$		450		80	99	
35Ni5Fe0.6Ru/ alumina xerogel	sol–gel	220 (10 bar)	H_2:CO_2 = 4:1, WHSV = 9600 cm^3/(g$_{cat}$h), Cat. = 50 mg	68.2	98.9	[89]
5NiC4Z	impregnation	350	H_2:CO_2 = 4:1, GHSV = 35,400 h^{-1}, Cat. = 500 mg	68.9	90.2	[90]
30Ni/Al$_2$O$_3$.0.5SiO$_2$	sol–gel	350	H_2:CO_2 = 3.5:1, GHSV = 9000 cm^3/(g$_{cat}$ h), Cat. = 200 mg	82.38	98.19	[91]
10%Ni/ZSM-5	impregnation	400	H_2:CO_2 = 4:1, GHSV = 2400 h^{-1}, total flow = 40 cm^3/min	76	75	[92]
10%Ni/SiO2				66	65	
10%Ni/SBA-15				71	69	
10%Ni/MCM-41				64	63	
10%Ni–1Mg/Si	co-impregnation	400	H_2:CO_2 = 4:1, GHSV = 15,000 cm^3 h^{-1} g^{-1}, Cat. = 200 mg,	73	97	[93]

3.5 Conclusions

The hydrogenation of CO_2 was studied over Ni-containing spherical silica catalysts prepared with different Ni loading sequences. The prepared catalysts exhibited outstanding textural properties with spherical shape and high specific surface area. Nickel catalysts prepared by the direct incorporation of Ni during SSP synthesis exhibited a stronger interaction between Ni and SiO_2 in the form of nickel silicate, which led to better performances in CO_2 methanation than the SSP supported NiO prepared by conventional impregnation. Alternate loading between Ni and Si (Ni_Alt_Si) resulted in the highest CO_2 methanation activity and methane selectivity due to high electron density of Ni on the surface, high metal dispersion, and high CO_2 adsorption ability.

CHARPTER IV

PAPER II

Influence of highly stable Ni^{2+} species in Ni phyllosilicate catalysts in selective hydrogenation of furfural to furfuryl alcohol

Sasithorn Kuhaudomlap[a,e], Okorn Mekasuwandumrong[b], Piyasan Praserthdam[a], Kiat Moon Lee[c], Christopher W. Jones[**e] and Joongjai Panpranot[*a,c,d]

[a]Center of Excellence on Catalysis and Catalytic Reaction Engineering, Department of Chemical Engineering, Faculty of Engineering, Chulalongkorn University, Bangkok 10330, Thailand

[b]Department of Chemical Engineering, Faculty of Engineering and Industrial Technology, Silpakorn University, Nakhon Pathom 73000, Thailand

[c]Department of Chemical & Petroleum Engineering, Faculty of Engineering, Technology and Built Environment, UCSI University, 56000 Kuala Lumpur, Malaysia

[d]Bio-Circular-Green-economy Technology & Engineering Center, BCGeTEC, Department of Chemical Engineering, Faculty of Engineering, Chulalongkorn University, Bangkok, Thailand 10330

[e]School of Chemical & Biomolecular Engineering, Georgia Institute of Technology, Atlanta, Georgia 30332, United States

[*,**] To whom correspondence should be addressed. Email: joongjai.p@chula.ac.th

Email: cjones@chbe.gatech.edu

4.1 Abstract

Enhancing catalytic performance of non-noble Ni catalysts in the selective hydrogenation of furfural to furfuryl alcohol (FA) in terms of furfural conversion, selectivity, and good recyclability is challenging. Here, spherical nickel phyllosilicate catalysts (Ni_PS) with fibrous-like structures, are prepared via a modified sol-gel method with Ni loadings of 2 – 30 wt%. Upon exposure to air, all the reduced Ni_PS catalysts exhibit more than 80% $Ni^0/Ni_{phyllosilicate}$ species on the surface, whereas a large portion of Ni oxide species (> 55%) is presented on the impregnated catalyst. The Ni^{2+} species in nickel phyllosilicate catalysts are active and highly stable during reduction, reaction, and regeneration, yielding stable catalytic performance for multiple recycle tests in furfural hydrogenation to FA. Furfural conversion over the Ni_PS catalysts increased monotonically with increasing Ni loading without FA selectivity drop. The presence of both metallic Ni^0 and $Ni_{phyllosilicate}$ also produces a synergistic promotional effect for FA formation.

4.2 Introduction

Nickel is one of the most frequently used metals in a wide variety of industrial manufacturing. Silica supported nickel catalysts (Ni/SiO$_2$) are used extensively in catalytic reactions due to their low cost, high specific surface area, easy functionalization, and controllable morphology/adjustable pore structures.[1-3] However, Ni/SiO$_2$ usually suffers from a weak interaction between nickel species and silica supports, which is a significant drawback that can cause leaching of nickel species during liquid phase reaction, as well as agglomeration and sintering of nickel under high thermal treatment and reaction process leading to low catalytic activity, deactivation of catalyst, and poor stability. Several efficient strategies have been reported to improve nickel dispersion and enhance the metal-support interaction such as the addition of various promoters such as La$_2$O$_3$ [7] and V$_2$O$_5$,[6] the formation perovskite and hydrotalcite structures,[11, 12] the modification of the support and develop preparation method to enhance metal-support interaction and inhibit the catalyst agglomeration such as molecular layer deposition (MLD),[10] the construction of nickel-based catalysts with a confinement effect like mesostructured cellular foam (MCF).[11] However, there are still some limitation for these methods such as high cost, complicate procedure, requires multiple steps and unique instruments for preparation.

Metal phyllosilicates have received considerable attention in recent catalysis research because of their unique layered structure that can offer outstanding properties such as strong metal-support interaction, small metal domain size and high dispersion of active metal species, rich porous structures, excellent adsorption properties, high thermal stability, and simple preparation procedures. Ni phyllosilicates typically possess a lamellar structure, consisting of tetrahedral layers of SiO$_4$ (Si-O-Si) and octahedral layers of Ni (II) (Ni coordinated to oxygen atoms or hydroxyl groups, Si-O-Ni-O(OH)).[121] It has been reported that metallic nickel derived from the reduction

of nickel phyllosilicate can provide nickel particles with fine size at high nickel content and high dispersion. The Ni phyllosilicates show good performances in a number of reactions including CO_2 and CO methanation,[16] hydrogenation of levulinic acid to **γ**-valerolactone,[28] xylose hydrogenation to xylitol,[24] hydrogenation of maleic anhydride,[15] hydrogenation of polycyclic aromatic hydrocarbons,[29] and carbon dioxide reforming of methane.[30]

Generally, nickel phyllosilicates with different crystal structures can be synthesized via various methods including hydrothermal methods,[1, 5, 14, 19] the ammonia evaporation method,[20-22] deposition-precipitation methods [23, 24] and sol-gel method [25] though the reaction between nickel precursor and silica materials. Among which, the hydrothermal method has been employed for preparation of nickel phyllosilicate catalysts due to high crystallinity, handy experimental operation, environmentally friendly, and uniform dispersed of nickel phyllosilicate. However, conventional hydrothermal reaction is carried out in an autoclave under harsh hydrothermal conditions at high temperature (>180 °C) with long reaction time (> 24 h), resulting in the loss of surface silanol group, limited nickel loading (even though there are excess nickel and silica amount),[7, 19, 26, 27] small amount of nickel phyllosilicate being formed, and large particles at relatively low hydrothermal temperatures (e.g. 120 and 160 °C).[16] Thus, it is a great challenge to improve and synthesize Ni phyllosilicates with high nickel contents under mild conditions and remain the superiority properties of nickel phyllosilicate. Chen et al. [5] synthesized nickel phyllosilicate with high nickel contents (22.4 wt%) using urea-assisted hydrothermal method under mild hydrothermal temperature and reaction time (180 °C, 24 h). The quick formation of nickel phyllosilicate was obtained because urea facilitate the formation of $Ni(OH)_2$ and leaching of SiO_2. Then, they [4] synthesized nickel phyllosilicate via the hydrothermal method assisted by NH_4F and urea, which optimal

nickel phyllosilicate (N/D-120-12) exhibited high catalytic performance for CO_2 methanation and excellent anti-sintering property. They reported that ammonium fluoride and urea can be efficient accelerator of the formation of H_4SiO_4 and $Ni(OH)_2$, respectively which is essential intermediates for the formation of nickel phyllosilicate. Nickel phyllosilicate could be formed under mild hydrothermal conditions at 100 °C for 12 h by double accelerators of ammonium fluoride and urea [1] which has similar morphology and nickel content with conventional hydrothermal method at 220 °C for 48 h. Although, these modified hydrothermal method can improve hydrothermal condition, there are still some limited of complicated operation procedure and too low hydrothermal condition provides low nickel content and small amount of nickel phyllosilicate formation.[4]

Moreover, the preparation of nickel phyllosilicate usually consists of two major steps: step (1) silica material synthesis and step (2) nickel phyllosilicate formation via the reaction of silica material and nickel precursor. It consumes large amounts of the reagent and energy and requires long operation time. One-pot synthesis of Ni phyllosilicates has recently been reported, for example, Chen et al. [26] prepared 3D-SBA-15 derived Ni phyllosilicate via a one-pot and two-pot hydrothermal methods at 180 °C. One-pot synthesis exhibited small size nickel particles and showed high anti-sintering due to strong metal-support interaction derived from nickel phyllosilicate. Many advantages of one-pot synthesized nickel phyllosilicate catalyst (Ni/S-O) were achieved including low cost, monolithic appearance, fine nickel particle size, high nickel phyllosilicate content, high convenience and elimination of the separation, drying and calcination process. In addition, it was found that hydrothermal conditions were significant factor for the formation of nickel phyllosilicate via one-pot synthesis, which sectional hydrothermal at 100 °C, 24 h and 180 °C, 24 h affected to the formation of nickel phyllosilicate in their work.

In this study, spherical silica derived nickel phyllosilicate (Ni_PS) was successfully prepared via one-step modified spherical silica synthesis with alternate addition of nickel and silica precursor under room temperature. The one step synthesized Ni_PS catalysts with various nickel loadings (2 – 30 wt% Ni) were characterized by H_2-TPR, STEM, EDS, and XPS and their catalytic properties were evaluated in the liquid phase selective hydrogenation of furfural to furfuryl alcohol (FA) under mild reaction conditions in order to simultaneously obtain excellent anti-leaching property and improve catalytic activity. Furfural, synthesized via catalytic dehydration of xylose in hemicellulose, is a versatile platform molecule that can be further converted into many high value derivatives and downstream fine chemicals and biofuels. Among the non-noble metal catalysts for furfural hydrogenation, Ni has been demonstrated to be a good furfural hydrogenation catalyst due to its excellent H_2 dissociation and relatively low cost.

4.3 Results and discussion

4.3.1 Characterization of the calcined catalysts

The presence of nickel phyllosilicate and nickel oxide on the prepared catalysts was probed by XRD and the results are shown in **Figure 4.1**. A broad peak located at $2\theta=23°$, which is a characteristic peak of amorphous oxide, was observed for all the samples. The catalysts prepared by one-step modified spherical silica synthesis display the major diffraction peaks at 2θ degrees = 34.1 and 60.8, which are attributed to the nickel phyllosilicate structure.[30] The intensity of the characteristic diffraction peaks of nickel phyllosilicate increased with increasing nickel loading from 10-30 wt% and was not observed with low nickel loading (2-5wt%) may be due to small amount /low crystallinity of nickel phyllosilcate (**Figure 4.1A**). On the other hand, the sharp diffraction peaks assigned to nickel oxides were clearly evident as expected at 2θ =

37.3°, 43.3°, 62.8°, 75.5° and 79.3° [32] in the XRD patterns of the 20Ni_Imp catalyst. The oxidation states of nickel species on the catalyst surface before reduction/passivation were analyzed by XPS and the results are shown in **Figure 4.1**. As shown in **Figure 4.1B**, the Ni $2p_{3/2}$ peaks of the calcined 20Ni_Imp were deconvoluted into two peaks at the binding energy 854.2 eV and 856.2 eV, which were assigned to aggregated NiO and highly dispersed Ni^{2+}, respectively.[22, 122] For all the calcined Ni_PS catalysts, the observed strong peaks at around 857-859 eV were assigned to Ni^{2+} species that strongly interact with silica in the nickel phyllosilicate structure.[30] The XPS peak intensity can be used to indicate the different levels of nickel dispersed on catalyst surface.[105] The results demonstrate that nickel phyllosilicate phase was successfully obtained by one-step modified spherical silica synthesis even for relatively low nickel content (2 wt%) under mild conditions (room temperature and short time).
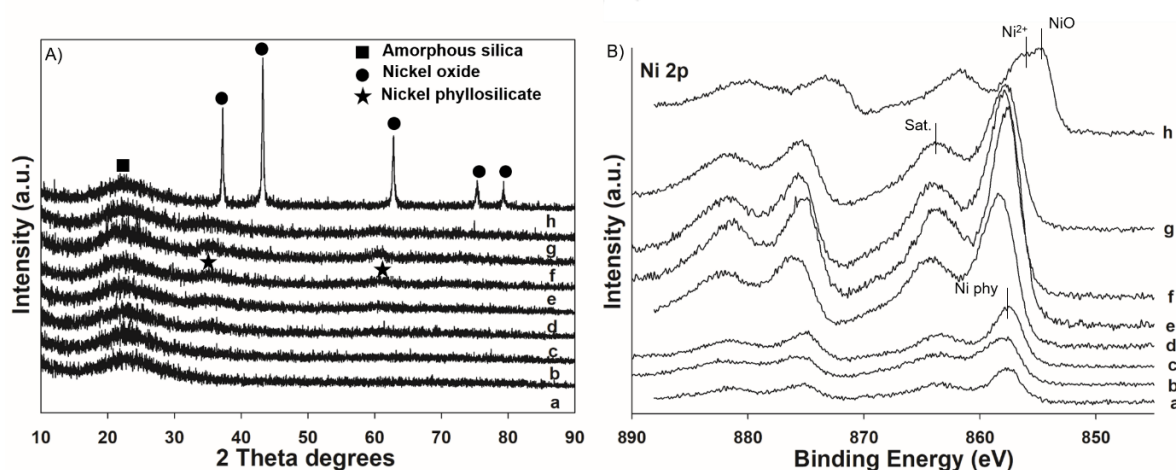

Figure 4. 1 A) XRD patterns and B) Ni 2p XPS spectra of the calcined catalysts (a) 2Ni_PS, (b) 5Ni_PS, (c) 10Ni_PS, (d) 15Ni_PS, (e) 20Ni_PS, (f) 25Ni_PS, (g) 30Ni_PS, (h) 20Ni_Imp

The structures and morphology of the calcined catalysts are shown in the TEM images in **Figure 4.2**. All the prepared catalysts displayed a spherical particle shape, with average size ca. 0.30 μm for the series of Ni_PS. The average particle size was

slightly decreased with increasing nickel loading (∼0.2 μm for 30Ni_PS) and was ca. 0.5 μm for the 20Ni_Imp catalyst. Owing to simultaneous loading of nickel and silica precursors during one-step modified spherical silica synthesis, nickel can form within the structure and on the surface, and nickel density were increased from the unique structure of nickel phyllosilicate that interfere with each other, resulting in smaller particle size with increasing nickel loading. According to the literature, the decrease of particle size of mesostructured silica nanoparticles (MSN) resulted to the improved formation of nickel phyllosilicate due to the increase of surface silanol group concentration.[123] A fibrous-like structure was observed on the nickel phyllosilicate catalysts, whereas on the impregnated catalysts, large metal oxide particles (d_p ∼ 60 nm) were formed on the spherical silica support. It is confirmed that nickel phyllosilicate was successfully formed under relatively mild conditions. The N_2 physisorption results and the corresponding nitrogen adsorption-desorption isotherms are shown in **Table 4.1** and **Figure S4.1**. The specific surface area, pore volume, and pore size diameter of the bare spherical silica support are 1084 m^2/g, 0.79 cm^3/g, and 2.6 nm, respectively. Compared to the bare SiO_2, all the Ni_PS catalysts with 2 – 30 wt% Ni loading possessed lower BET surface areas and smaller pore volumes with slightly larger average pore diameters. The BET surface area and pore volume decreased from 977 to 168 m^2/g and 0.77 to 0.06 cm^3/g with increasing Ni loading from 2 wt% to 10 wt% and then were slightly increased to reach 260 m^2/g surface area and 0.15 cm^3/g pore volume for the 30Ni_PS sample. Typically, the formation of the fibrous-like structure of nickel phyllosilicates can result in an increased specific surface area and pore volume, compared to the silica support and impregnation based catalysts.[15, 108, 121] This correlates with a unique porous structure for the lamellar nickel phyllosilicate. However, a different trend was observed in the present work. Here, nickel phyllosilicate was formed by simultaneous loading of nickel and silica

precursors during the one-step modified spherical silica synthesis with CTAB as the structure directing agent, followed by calcination at 550 $^{\circ}$C for 6 h. For Ni loadings ≤ 10 wt% on the spherical silica, the higher surface area could be attributed to the mesostructured SiO_2 being formed in addition to the nickel phyllosilicate phase, as confirmed by the presence of mesopores in the adsorption isotherm. Samples with larger nickel loadings lacked mesopores according to the nitrogen physisorption isotherms. Further increases of Ni loading to 15, 20, 25, and 30 wt% led to increasing BET surface area, as a result of the formation of fibrous-like structure of the nickel phyllosilicate domains. The specific surface area and pore volume of the 20Ni_Imp catalyst were 828 m^2/g and 0.55 cm^3/g, respectively, which were comparable to those of the Ni_PS samples with Ni loadings between 2 to 5 wt%.
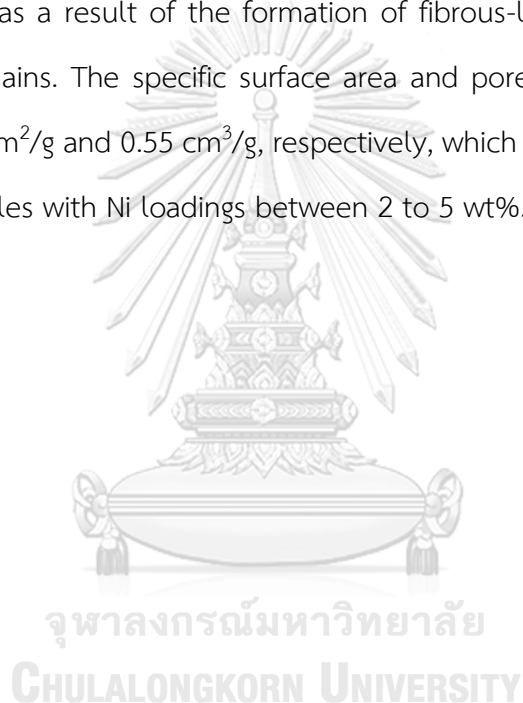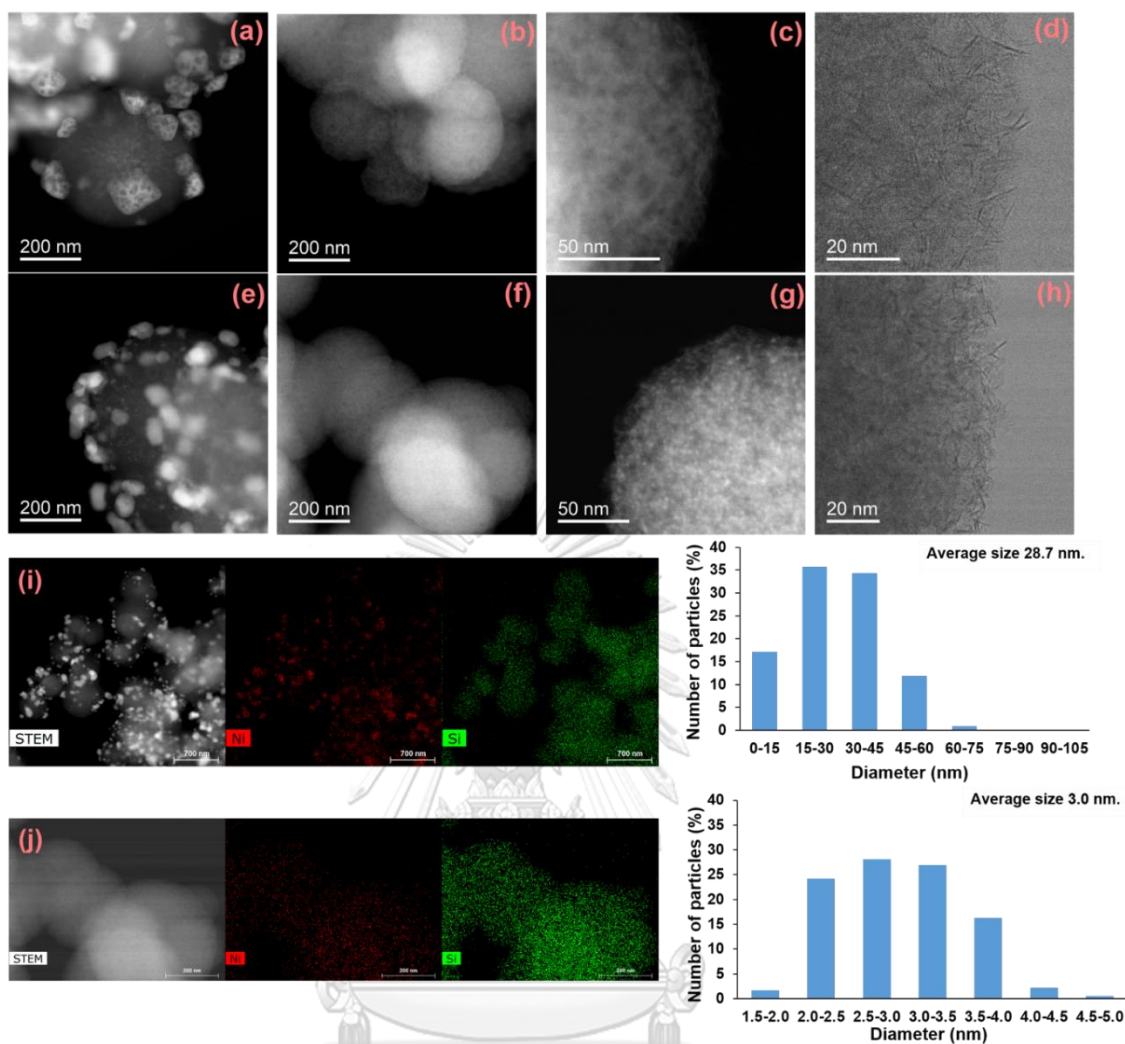
Figure 4. 2 TEM images of the nickel catalysts (a) calcined-20Ni_Imp, (b, c, d) calcined-20Ni_PS, (e) reduced-20Ni_Imp, (f, g, h) reduced-20Ni_PS, EDS mapping images and the Ni particle size distribution histogram of the (i) reduced-20Ni_Imp, (j) reduced-20Ni_PS

Table 4. 1 Physical properties of the calcined catalysts and CO pulse chemisorption results

Catalysts	BET Surface area (m²/g)	Pore volume (cm³/g)	Pore diameter (nm)	CO Adsorption (μmol/g$_{cat}$)[a]
SSP	1084	0.79	2.6	-
2Ni_PS	977	0.77	2.9	10.3
5Ni_PS	491	0.47	3.5	10.4
10Ni_PS	168	0.06	3.8	9.8
15Ni_PS	185	0.11	4.2	10.8
20Ni_PS	234	0.19	4.0	37.6 [b]
				35.8
25Ni_PS	219	0.20	4.9	26.5
30Ni_PS	260	0.15	4.4	19.3
20Ni_Imp	828	0.55	2.5	1.9 [b]
				11.4

*Pore volume and pore diameter determined from the Barret-Joyner-Halenda (BJH) desorption method.

[a] Determined by CO-pulse chemisorption: catalysts were reduced at 500 °C for 3 h

[b] Calcined catalysts

The reducibility of both Ni_PS and 20Ni_Imp catalysts was further investigated by H$_2$-TPR and the results are shown in **Figure 4.3**. The impregnation catalyst exhibited two reduction peaks, a strong reduction peak at 342 °C and a weak shoulder peak at around 489 °C, which are attributed to reduction of the nickel oxide species and the weak interaction between isolated nickel ions (Ni^{2+}) and SiO$_2$, respectively.[22] Interestingly, all the Ni_PS catalysts exhibited only broad reduction peaks in the high temperature ranges from 500 °C to 800 °C, which are assigned to the reduction of Ni^{2+} located in the nickel phyllosilicate with strong interaction between nickel species and

silica.[22] These nickel species existed mostly in the form of strong, chemically bonded Ni-O-Si species in the nickel phyllosilicate structure. Additionally, the reduction peak tended to shift to higher temperature and larger area with increasing nickel loading from 2 to 30 wt% indicating the more nickel phyllosilicate and more difficult to be reduced. The H_2-TPR results suggest the incomplete reduction of nickel species to metallic metal for all catalysts during the reduction process at 500 °C for 3 h prior to the reaction tests.
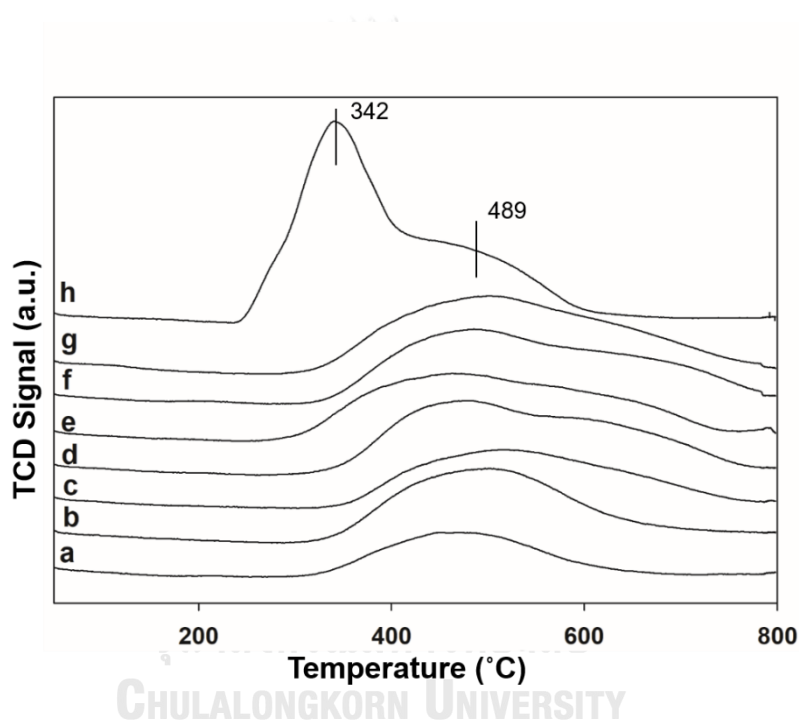

Figure 4. 3 H_2-TPR profiles of the calcined catalysts (a) 2Ni_PS, (b) 5Ni_PS, (c) 10Ni_PS, (d) 15Ni_PS, (e) 20Ni_PS, (f) 25Ni_PS, (g) 30Ni_PS, (h) 20Ni_Imp

4.3.2 Characterization of the reduced catalysts

After reduction with H_2 at 500 °C for 3 h (**Figure 4.4**), the distinct XRD peaks at 2θ = 44.6°, 51.8° and 76.2° observed on the 20Ni_Imp are ascribed to metallic nickel,[50] indicating that the crystalline nickel oxides on the impregnation catalyst were primarily reduced to nickel metal. On the series of reduced/passivated Ni_PS

catalysts, the diffraction peaks of nickel phyllosilicate were moderately weakened and disappeared for the Ni_PS with nickel loadings ≤ 10wt%. Small diffraction peaks corresponding to metallic nickel were additionally detected on the reduced Ni_PS with relatively high Ni loading (e.g., ≥ 15 wt% Ni). Such results indicate the co-existence of nickel phyllosilicate and nickel metal on the reduced Ni_PS, whereas the crystalline nickel oxide species appeared totally reduced into metallic nickel on the 20Ni_Imp. In addition, the morphology of the reduced/passivated catalysts are shown in the TEM images in **Figure 4.2** along with the elemental mapping of Ni and Si species on the catalysts. Small bright sports representing nickel metal domains were well distributed on both types of reduced samples. As shown in **Figure 4.2f-h**, high dispersion of small nickel particles on the catalyst surface without any large aggregation was observed over 20Ni_PS, in addition to the fibrous-like structure of the nickel phyllosilicate, which remained after reduction. The TEM results are consistent with the XRD and H_2-TPR results, showing that the nickel phyllosilicate species were not completely reduced under the reduction conditions used in this work. The average diameters of the nickel particles on the reduced catalysts as well as their size distribution histograms are shown in **Figure 4.2i** and **j**. The average nickel particles after reduction at 500 °C for the reduced 20Ni_PS and 20Ni_Imp are 3 nm and 29 nm, respectively. It can be implied that the remaining of nickel phyllosilicate layer after reduction process act as the support on metallic nickel which resulted in the highly dispersed nickel particles with small size of homogeneous nickel particle at high loading.[108] The nickel phyllosilicate catalyst is highly resistant to sintering and high stability because of the enhanced interaction of Ni and SiO_2 in the nickel phyllosilicate layers, preventing agglomeration under high temperature reduction processes such as the method deployed here.[19, 22, 30]
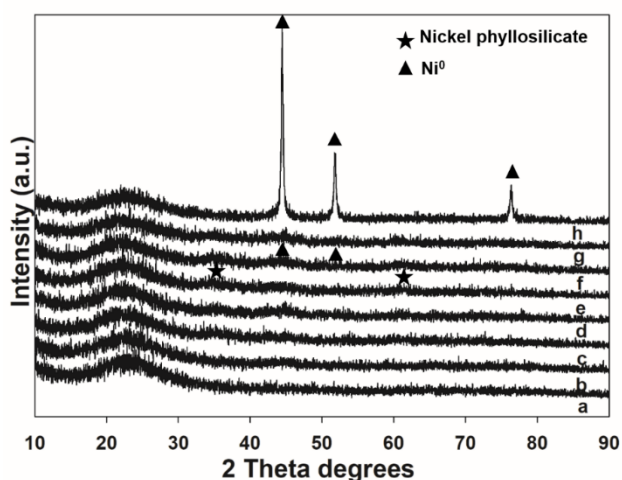
Figure 4. 4 XRD patterns of the reduced catalysts (a) 2Ni_PS, (b) 5Ni_PS, (c) 10Ni_PS, (d) 15Ni_PS, (e) 20Ni_PS, (f) 25Ni_PS, (g) 30Ni_PS, (h) 20Ni_Imp

The Ni 2p XPS spectra of the reduced/passivated catalysts were deconvoluted into five peaks as shown in **Figure 4.5**. The first peak at 853.3 eV is assigned to Ni^0 species. The binding energy at 855.8 eV belongs to highly dispersed of Ni^{2+} and the strong peak at around 857.6 eV and 859.0 eV were ascribed to Ni^{2+} species with strong interactions with SiO_2 in nickel phyllosilicate structure. The last peak centered at 862 eV is attributed to the Ni 2p satellite peak due to electron shake-up.[15] As also revealed by H_2-TPR results, the nickel phyllosilicate species could not be totally reduced at 500 °C, thus, the XPS peaks corresponding to nickel phyllosilicate domains were still apparent on the catalysts after reduction/passivation. For the reduced/passivated 20Ni_Imp, the Ni $2p_{3/2}$ peaks were deconvoluted into three typical nickel species at binding energies of 852.8, 854.5, 855.9-856.9 eV, which corresponded to metallic nickel Ni^0, NiO, and highly dispersed Ni^{2+}, respectively.[7, 22] Comparing to the metallic Ni^0 peaks of the 20Ni_Imp at 852.8 eV, the Ni^0 peaks of the Ni_PS catalyst were shifted to a higher binding energy at 853.3 eV, indicating a stronger interaction between nickel metal and the silica support of the nickel phyllosilicate catalysts. Such results are in good agreement to the well-established trend in the literature.[124] The

surface atomic ratios of $Ni_{(total)}/Si$, Ni^0/Si, $(NiO+Ni^{2+})/Si$), and $Ni_{Phyllosilicate}/Si$ of the various catalysts are provided in **Table 4.2**. The surface atomic ratios of $Ni_{(total)}/Si$ on the Ni_PS catalysts increased with increasing Ni loading and appeared to reach a threshold limit at around 20-25 wt% Ni. For a similar Ni loading (20 wt% Ni), the surface atomic ratio of Ni^0/Si on the reduced/passivated 20Ni_PS catalysts is lower compared to the reduced/passivated impregnation catalyst (20Ni_Imp), which is consistent with the H_2-TPR results showing that the impregnation catalyst was easier to reduce than the nickel phyllosilicate materials. However, the surface atomic ratios of $Ni_{(total)}/Si$ on 20Ni_PS was twice that of 20Ni_Imp, indicating a large amount of Ni phyllosilicate species on the catalyst surface. Moreover, all the reduced Ni_PS catalysts still exhibit more than 80% $Ni^0+Ni_{phyllosilicate}/Ni_{total}$ species on the surface, whereas a large portion of Ni oxide species (> 55%) is presented on the impregnated catalyst. CO pulse chemisorption was performed to evaluate the number of potential Ni active sites on the catalysts, assuming that one CO molecule adsorbed on one nickel site, and the results are reported in **Table 4.1**. On the calcined catalysts, the amounts of CO adsorbed on the calcined 20Ni_Imp and 20Ni_PS were 1.8 μmol/g and 37.6 μmol/g, respectively. It is suggested that CO cannot adsorb on bulk nickel oxides but can adsorb on nickel phyllosilicate domains. The amounts of CO adsorbed on the reduced catalysts are as follows: 2Ni_PS (10.3 μmol/g), 5Ni_PS (10.4 μmol/g), 10Ni_PS (9.8 μmol/g), 15Ni_PS (10.8 μmol/g), 20Ni_PS (35.8 μmol/g), 25Ni_PS (26.5 μmol/g), 30Ni_PS (19.3 μmol/g). The amounts of CO adsorbed on the Ni_PS catalysts with 2-15 wt% Ni were quite similar, being around 10 μmol/g. The amount of CO adsorbed was maximized on the 20 wt% nickel loading, 20Ni_PS catalyst, at 35.8 μmol/g, which was much higher than the 20Ni_Imp (11.38 μmol/g). Further increase of Ni loading to 25 and 30 wt% resulted in a decline of adsorbed CO to around 20 μmol/g. Nevertheless, the results suggest that both metallic Ni^0 and Ni^{2+} in the phyllosilicate structure were active for CO

chemisorption and may provide high active sites for furfural hydrogenation reaction. It can be seen that this work provides simple one-step strategy for the synthesis of spherical silica derived nickel phyllosilicate at room temperature, which still exhibited unique property of nickel phyllosilicate.
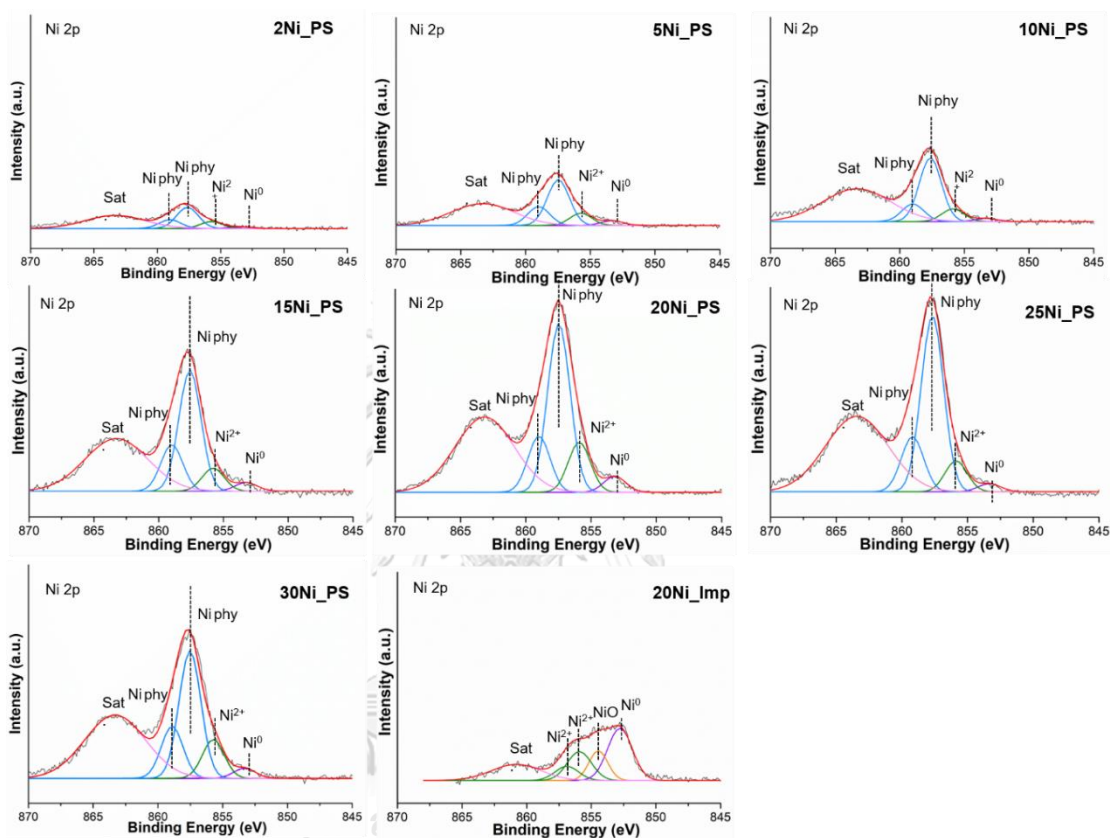

Figure 4. 5 Ni 2p XPS spectra of the reduced/passivated catalysts

Table 4. 2 Ni peak fitting parameters and Ni species proportion over the surface of reduced/passivated catalysts in the Ni 2p

Catalysts	Ni^0		NiO		Ni^{2+} highly dispersed		Ni phyllosilicate		Atomic surface ratio			
	B.E. (eV)	FWHM	B.E. (eV)	FWHM	B.E. (eV)	FWHM	B.E. (eV)	FWHM	Ni/Si	Ni^0/Si	NiO+Ni^{2+}/Si	Ni phy/Si
2Ni_PS	853.4	1.98	-	-	855.7	1.98	857.6 / 859.0	2.02 / 1.98	1.15	0.05	0.21	0.89
5Ni_PS	853.3	1.98	-	-	855.7	1.99	857.5 / 859.0	2.02 / 1.99	2.12	0.12	0.32	1.68
10Ni_PS	853.3	1.99	-	-	855.9	2.00	857.6 / 859.0	2.01 / 2.00	2.30	0.07	0.30	1.93
15Ni_PS	853.2	2.01	-	-	855.9	2.00	857.6 / 859.0	2.01 / 1.98	7.06	0.30	0.81	5.94
20Ni_PS	853.2	1.98	-	-	855.9	1.99	857.5 / 859.0	2.03 / 1.99	9.50	0.51	1.61	7.37
25Ni_PS	853.3	2.02	-	-	855.9	1.99	857.7 / 859.2	2.01 / 2.01	9.89	0.30	1.12	8.47
30Ni_PS	853.3	1.98	-	-	855.7	1.98	857.5 / 858.9	1.99 / 1.98	8.11	0.36	1.37	6.38
20Ni_Imp	852.8	2.25	854.5	1.71	855.9 / 856.9	2.22 / 2.16	-	-	4.78	2.14	2.65	0.00

4.3.3 Catalytic test results

The catalytic performances of the prepared catalysts were evaluated in the selective hydrogenation of furfural to FA at 50 °C under H_2 pressure of 20 bar for 5 h with methanol as the solvent. All the catalysts were reduced at 500 °C under H_2 flow for 3 h and passivated prior to the reactions. Furfural is an interesting biomass platform molecule that contains several functional groups in its structure, which can be hydrogenated to various products. The desired product in this work is FA, while THFA was found as a minor product. The blank test result is shown in **Table S4.1**, 2-furaldehyde dimethyl acetal was the only by-product obtained ($\sim$ 6% conversion) which was produced by the solvent reaction via acetalization mechanism.[44, 125] The influence of nickel loadings in the range of 2-30 wt% Ni in the Ni_PS catalysts on furfural conversion, selectivity, and FA yield as a function of reaction time are shown in **Figure 4.6**.

Typically, furfural conversion and FA selectivity over nickel catalysts increase with increasing nickel loading up to an optimum amount (e.g. 4.6%Ni in the Ni-Cu/ZrO_2 catalyst [126] and 10%Ni/CNT),[46] then decrease with further increases of nickel content, which is possibly due to agglomeration of Ni particles at high Ni loadings resulting in low metal dispersion/low activity.[12] Interestingly, furfural conversion of all the Ni_PS catalysts monotonically increased with increasing nickel loading from 2 to 30 wt% Ni. Although the CO chemisorption and XPS results suggest the largest availability of active sites and the highest Ni^0/Si on the surface at 20 wt% Ni loading, furfural conversion continued to increase on 30Ni_PS comparing to 20Ni_PS and 25Ni_PS. For a similar Ni loading at 20 wt%, 20Ni_Imp exhibited a higher hydrogenation rate than 20Ni_PS. Furfural conversion over 20Ni_Imp and 20Ni_PS after 5 h of reaction time were 58% and 48 %, respectively. However, it can be clearly seen that all the nickel phyllosilicate catalysts exhibited higher FA selectivity (65-75%) than 20Ni_Imp

(∼ 48% FA). The selectivity of THFA on all the Ni_PS catalysts was below 10% (except

for 30Ni_PS, where the THFA selectivity was ∼ 13%) while that of 20Ni_Imp was > 15%.

According to the literature, and as shown in **Figure 4.6**, the selectivity of FA and THFA

did not depend on furfural conversion and reaction time and was rather affected by

the electronic properties of Ni species and/or Ni-support interaction.[61, 70, 127-129]
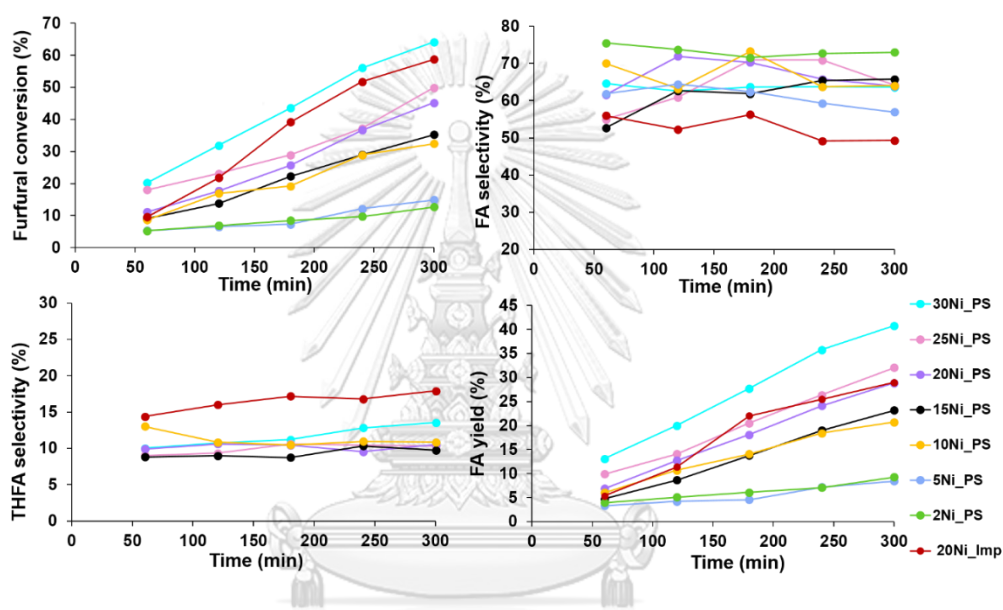

Figure 4. 6 Hydrogenation of furfural to FA over nickel phyllosilicate catalysts with
varying nickel loading and impregnation catalyst (20Ni_Imp) versus reaction time.
Reaction conditions: 250 mg catalyst, 3 mmol furfural, 50 ml methanol solvent, 0.4
mmol dodecane, reaction temperature 50 °C, 20 bar H_2 pressure, reaction time 5 h
and catalysts were reduced at 500 °C

A proposed reaction pathway for furfural hydrogenation over Ni-based catalysts is shown in **Figure S4.2**. Hydrogenation of carbonyl group (C=O) in furfural produces the desired product FA and further hydrogenation of FA (C=C) results in THFA. Other by-products such as furan, tetrahydrofuran, methyl furan, etc. are produced in a small amount (total selectivity ≤ 10%). The carbon balances (**Table S4.1.**) were calculated above 85 % over all samples for each time point. Typically, supported Ni catalysts without modification/addition of a promoter produce higher selectivity towards THFA than FA (76-91% selectivity of THFA).[46, 47] The use of high surface area spherical silica in this study can enhance FA selectivity of the impregnated Ni/SiO_2 catalysts since significant amounts of highly dispersed Ni^{2+} species were formed on the 20Ni_Imp catalyst, as revealed by the XPS results. Based on the catalyst characterization and reaction results, nickel phyllosilicate species were active for both CO chemisorption and also for furfural hydrogenation under mild reaction condition. Synergistic of highly dispersed nickel particles and Lewis acid sites of the remaining nickel phyllosilicate contributes to the low-temperature hydrogenolysis/hydrogenation in biomass conversion.[108, 121] For the same Ni loading (20 wt% Ni), the amount of CO adsorbed on 20Ni_PS was much higher than 20Ni_Imp, despite its lower hydrogenation activity. The larger amounts of CO chemisorption on the Ni_PS catalysts were correlated to the larger amounts of Ni phyllosilicate being formed, and not the higher hydrogenation activity. In other words, the Ni_PS exhibited higher CO chemisorption ability but the hydrogenation activity of Ni phyllosilicate species was lower than metallic Ni^0. It is widely accepted that metallic Ni^0 function as active sites for H_2 dissociation [15, 29, 66] while Ni^{2+} in NiO is inactive. However, Ni^{2+} species that are strongly interacting with SiO_2 can play an important role in binding and activating the C=O group in the furfural structure, as suggested by CO chemisorption results. The electron-deficiency of some Ni^{2+} atoms may allow them to act as Lewis acid sites for the adsorption of the C=O bond through oxygen atoms, which likely enhances the adsorption and conversion of

furfural.[80] The presence of both metallic Ni^0 and highly dispersed Ni^{2+} that strongly interact with SiO_2 is suggested to be necessary for high furfural conversion and high FA selectivity under mild reaction condition.

Loading of 20 wt% Ni by impregnation on high surface area spherical silica resulted in about 50:50 metallic Ni^0 species: (NiO/highly dispersed Ni^{2+}) as revealed by XPS results. As a result, the 20Ni_Imp catalyst exhibited relatively high conversion of furfural but the selectivity of FA was lowest among the catalysts studied, producing the highest %THFA. The 20Ni_PS (78% Ni phyllosilicate species, 5% Ni^0) showed lower activity with higher FA selectivity and as a consequence the FA yield was essentially similar to that of 20Ni_Imp. This is because the hydrogenation activity of Ni phyllosilicate is lower than metallic Ni^0. However, increasing the Ni loading on Ni_PS to 30 wt% can further increase the furfural conversion without any change in FA selectivity, resulting in much higher FA yield on the 30Ni_PS.

4.3.4 Catalyst Recyclability Tests

The recyclability of the catalysts was investigated on the 30Ni_PS and 20Ni_Imp catalysts by conducting three cycles run under identical conditions at 50 °C under 20 bar H_2 pressure for 5 h. After use, the spent catalysts were washed with methanol solvent several times and were subjected to H_2 reduction at 500 °C for 3 h before being reused for furfural hydrogenation. The recyclability results are shown in **Figure 4.7**. It is clear that the 30Ni_PS exhibited excellent recyclability for furfural hydrogenation with enhanced FA selectivity. The conversion decreased slightly (by ~10%) while FA selectivity increased from 64% to 74% in the third cycle. On the other hand, the 20Ni/_Imp catalyst showed poor reusability. Furfural conversion drastically declined from 58% for the fresh catalyst to 29% in the third cycle (~ 50% change) with a significantly drop of FA selectivity from 48% to 32% in the third run.
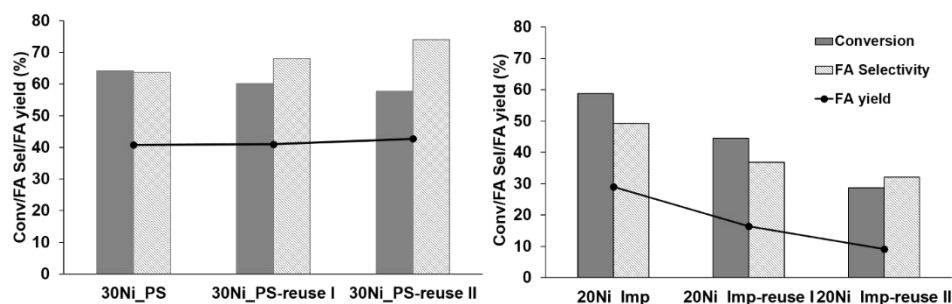
Figure 4. 7 The recycle test for the hydrogenation of furfural to FA over 30Ni_PS and 20Ni_Imp catalysts with three repeated runs. Reaction conditions: 250 mg catalyst, 3 mmol furfural, 50 ml methanol solvent, 0.4 mmol dodecane, reaction temperature 50 °C, 20 bar H_2 pressure, reaction time 5 h and catalysts were reduced at 500 °C.

The spent catalysts after three runs were further characterized by TEM and XPS to examine the changes in the characteristics of the catalysts after reaction and the results are shown in **Figure S4.3, Figure S4.4** and **Table S4.2**. TEM images confirm that there were no significant changes in the morphology of the spent 30Ni_PS catalyst, in which spherical particles of 0.19 μm covered by nickel phyllosilicate layers were evidently observed. The average nickel particle size was slightly increased from 2.9 to 3.1 nm after the third cycle of reaction tests. It has been suggested that the fibrous nickel phyllosilicate structure can inhibit the growth of nickel particles and prevent the sintering/leaching of nickel particles during CO_2 methanation [19] and hydrogenation of maleic anhydride.[15] In contrast, the average Ni particle sizes on 20Ni_Imp increased from 29 nm to 35 nm, indicating that agglomeration of Ni particles on the silica support occurred under reaction conditions as a result from weaker interaction between nickel and the silica support, which led to a decline in the catalytic performance for each run. The XPS spectra of the used 30Ni_PS catalyst confirmed the presence of nickel metal and nickel phyllosilicate domains after the third run. There was no obvious

change in the XPS spectra before and after the reaction tests. The high stability of Ni_PS catalysts was ascribed to strong metal-support interaction and unique properties of Ni phyllosilicate that the unreduced Ni^{2+} could serve as a good support for the Ni^0 species, resulting in the active metallic nickel highly dispersed with small size nickel particle.[108] However, the atomic surface ratio of Ni^0/Si species increased from 0.36 to 0.57 on the 30Ni_PS whereas that of 20Ni_Imp decreased from 2.1 to 1.4. It is suggested a lower Ni dispersion on the spent 20Ni_Imp. Such results also suggest that nickel phyllosilicate species could be reduced into metallic Ni^0 during reaction on the 30Ni_PS, which was still beneficial for reaction. The good recyclability of the Ni_PS catalysts was attributed to the strong interaction between nickel and the silica support and the high stability of the nickel phyllosilicate species that can prevent agglomeration of Ni particles during reaction and re-reduction.[7, 15, 24]

4.3.5 Effects of reduction temperature and reaction temperature

The effects of reduction temperature and reaction temperature in the selective hydrogenation of furfural to FA were further investigated on the 30Ni_PS catalyst. Prior to the reactions, the 30Ni_PS catalyst was reduced under H_2 at 400—700 °C. The catalyst reduced at 400 °C yielded low furfural conversion. The highest furfural conversion and FA selectivity were obtained after 5 h of reaction time on the catalysts reduced at temperatures between 500—600 °C. Further increasing the reduction temperature to 700 °C led to a drop of furfural conversion, despite the larger amount of metallic Ni^0 formed (from TPR and XPS results). Interestingly, the catalysts reduced at relatively high reduction temperatures (500, 600, and 700 °C) maintained their high selectivity to FA, varying from 60-70% during the 5 h reaction time with negligible amounts of THFA and undesired products.
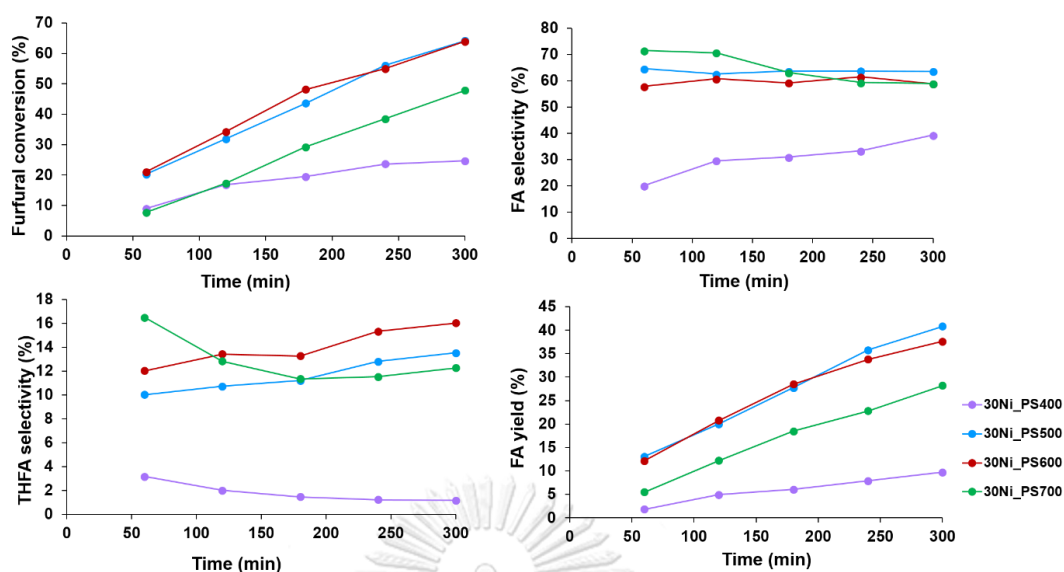
Figure 4. 8 Hydrogenation of furfural to FA at different reduction temperatures over 30Ni_PS catalysts. Reaction conditions: 250 mg catalyst, 3 mmol furfural, 50 ml methanol solvent, 0.4 mmol dodecane, reaction temperature 50 °C, 20 bar H_2 pressure, reaction time 5 h

The reduced catalysts were characterized by TEM, BET, and XPS analyses to correlate their characteristics with the catalytic performances. From the TEM results, the nickel phyllosilicate layers still existed on the surface of the 30Ni_PS catalysts. The average nickel particle sizes were slightly increased from 2.9 nm to 3.2 nm with increasing reduction temperature from 500 °C to 700 °C (**Figure S4.5**), but were still much smaller than the reduced 20Ni_Imp catalyst, as shown in **Figure 4.2**. Such results suggest that the reduction temperature has little effect on the particle size of metallic nickel being formed. The BET surface area, pore volume, and pore diameter of the reduced catalysts are presented in **Table S4.3**. There were no major differences in the structural properties of the reduced catalysts. They had similar average nickel particle sizes of ca. 3 nm with BET surface areas 236-257 m^2/g, pore volumes 0.11-0.13 cm^3/g, and pore diameters 4.3-4.4 nm. It confirms that Ni_PS catalyst presented a high anti-

sintering and prevented the agglomeration of nickel particles at high temperature. However, as revealed by XPS results, the main peak, assigned to nickel phyllosilicate at around 857.6-859 eV disappeared on the catalyst reduced at 700 °C and the peak corresponding to metallic Ni^0 species was observed at the binding energy 853.1 eV instead. The results suggest that a suitable proportion of metallic nickel and nickel phyllosilicate can enhance the catalytic performances of Ni_PS catalysts in the furfural hydrogenation to FA.

The influence of reaction temperature on the catalytic performances of 30Ni_PS on furfural conversion, FA selectivity, and FA yield are shown in **Figure 4.9**. Furfural conversion significantly increased with increasing reaction temperature and with increasing reaction time. The complete conversion of furfural (100%) was achieved at 100 °C. At 3 h reaction time, the furfural conversion was enhanced from 44% to 66% and reached 100% when the reaction temperature rose from 50 °C to 80 °C and 100 °C, respectively. The reaction temperature also had a significant impact on the product distribution. From the results, it is obviously seen that higher temperature and longer reaction times promoted deeper hydrogenation of the furan ring in furfural, resulting in higher selectivity towards THFA and lower FA selectivity. The optimum reaction temperature and reaction time to produce the highest yield of FA over the 30Ni-PS catalyst were 80°C and 4 h reaction time, which gave 82% conversion and 42% yield of FA.
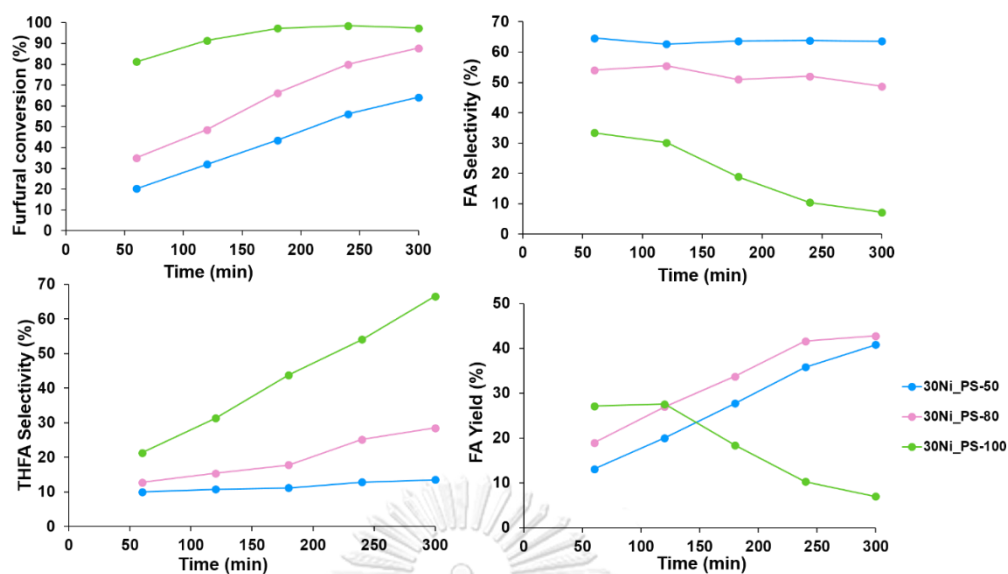
Figure 4. 9 Hydrogenation of furfural to FA under different reaction temperature over 30Ni_PS catalysts. Reaction conditions: 250 mg catalyst, 3 mmol furfural, 50 ml methanol solvent, 0.4 mmol dodecane, 20 bar H_2 pressure, reaction time 5 h and catalysts were reduced at 500 °C

4.4 Conclusions

Spherical silica supported nickel phyllosilicate catalysts were synthesized by the one-step modified spherical silica synthesis at room temperature with nickel loadings of 2-30 wt% and evaluated in the liquid-phase selective hydrogenation of furfural to FA at 50 °C and 2 MPa H_2. The unique properties of nickel phyllosilicate were successfully obtained via a simple one-step synthesis strategy by an alternate addition of the nickel and silica sources during the spherical silica synthesis, yielding a high dispersion of small Ni particles (< 3 nm) in the silica matrix, as well as nickel phyllosilicate species throughout the spherical particles, as revealed by TEM and XPS results. The strong interaction between nickel and the silica support and the unique structure of nickel phyllosilicate not only prevent Ni agglomeration during reaction and re-reduction but also facilitate furfural adsorption via the C=O bond through oxygen atoms, resulting in higher FA yield and good recyclability. The nickel phyllosilicate catalysts were superior to the impregnated Ni on spherical silica, which suffered from agglomeration of nickel particles and a large portion of inactive NiO. Moreover, there appeared to be a synergistic effect due to the presence of both metallic nickel and nickel phyllosilicate that promoted FA formation under the reaction conditions used. The optimum reduction temperature, reaction temperature, and reaction time to produce the highest yield of FA (42%) over the nickel phyllosilicate catalyst with 30 wt% Ni were 500 °C, 80 °C, and 4 h reaction time, respectively. The attractive properties of Ni_PS catalysts could be a great potential for mild reaction condition of furfural hydrogenation to FA.

4.5 Materials and methods

4.5.1 Preparation of spherical silica

The spherical silica supports were prepared by using tetraethoxysilane (TEOS) as the silica source and hexadecyltrimethylammonium bromide (CTAB) as the structure-directing agent. The molar ratio of TEOS: CTAB: NH_3: ethanol: H_2O was 1:0.3:11:58:114. First, a mixture of ethanol and distilled water was stirred at room temperature followed by the addition of aqueous ammonia. After that CTAB was dissolved the mixed solution under continuous stirring for 15 min, TEOS was added and the mixed solution was further stirred for 2 h. Then, the obtained white precipitate was collected by filtration and washed with distilled water. Finally, the resulting powder was dried overnight at 110 °C and calcined at 550 °C for 6 h in air with a heating rate of 2 °C/min

4.5.2 Loading of nickel on spherical silica

Nickel nitrate hexahydrate was chosen as the nickel precursor and was incorporated into the spherical silica support by a one-step modified spherical silica synthesis method with different nickel loadings in the range of 2-30 wt%. After a solution of ethanol, aqueous ammonia, distilled water and CTAB was continuously stirred for 15 min, the nickel precursor and TEOS were simultaneously loaded into the solution and further stirred for 2 h. The precipitate was separated by filtration, washed with distilled water, dried at 110 °C, and calcined at 550 °C for 6 h in air. The obtained catalysts are referred to xNi_PS catalysts, where x indicates the percent nickel loading.

For comparison proposes, 20 wt% Ni on spherical silica was prepared by incipient wetness impregnation and is denoted as the 20Ni_Imp catalyst. The spherical silica support was impregnated with an aqueous solution of nickel precursor followed by drying at 110 °C overnight and calcination in air at 550 °C for 6 h.

4.5.3 Catalytic Reactions

The obtained catalysts were used in the liquid phase hydrogenation of furfural in a 160 mL stainless steel Parr autoclave reactor with a Teflon liner. Prior to the reaction, the catalysts were reduced under H_2 flow at 500 °C for 3 h, then cooled to room temperature, followed by passivation with $1\%O_2/N_2$ for 1 h. This passivation step was performed to protect and control the reduced catalysts from oxidation in air by creating an oxide layer over the metallic surface. In a typical experiment, 3 mmol of furfural, 50 mL of methanol solvent, 0.25 g of the reduced/passivated catalysts, and 0.4 mmol of dodecane (internal standard) were charged into the autoclave. After that, it was purged with N_2 (300 psig, 2 min) five times and heated to reaction temperature (50-100 °C) under N_2 to ensure minimal reaction during heat up. When the reaction reached the target temperature, the autoclave reactor was purged with H_2 (500 psig, 2 min) five times and the reaction was carried out under 800 rpm stirring with 20 bar of H_2 for 5 h. Samples were collected through a sampling port with a sample volume less than 300 μL for each sample (every 60 min), to minimize reaction volume losses. The liquid products were filtered and analyzed by a Shimadzu GC-2010 chromatograph using an auto sampler with a CP-Wax 58 FFAP CB column and a flame ionization detector. Furfural conversion, selectivity, and FA yield were calculated using dodecane as an internal standard. For the recyclability study, the catalysts were washed with methanol solvent several times and recycled for three cycles under the same reaction conditions.

4.5.4 Catalyst Characterization

X-ray diffraction (XRD) was conducted by using PaNalytical X'Pert Pro Alpha-1 diffractometer with Cu K_α radiation. XRD patterns of the calcined and reduced/passivated catalysts were measured in a range from 10° to 90° at room

temperature. Nitrogen physisorption was carried out by a Micromeritics Tristar II 3020 at -196 °C. The samples (about 0.1 g) were pretreated at 180 °C for 10 h under vacuum prior to the nitrogen physisorption measurement. The average pore diameter and pore volume were determined using desorption isotherm by the BJH method. X-ray photoelectron spectroscopy (XPS) analysis was performed on the calcined and reduced/passivated catalysts in a Thermo K-Alpha spectrometer with a monochromatic Al Kα radiation source. H_2-temperature programmed reduction (H_2-TPR) and CO- pulse chemisorption were carried out on a Micromeritics AutoChem II 2920 equipped with a TCD to measure the reducibility and chemisorption uptake of the catalysts. For TPR experiments, the sample (0.03 g) was loaded on a bed of quartz wool in a quartz u-tube. First, the sample was pretreated under He flow at 200 °C for 1 h and was then cooled to 50 °C. The gas was switched to 10%H_2/Ar flowing at 20 mL/min and the sample was heated to 800 °C at a ramp rate of 10 °C/min. For CO-pulse chemisorption analysis, approximately 0.03 g of the catalyst was introduced into a quartz u-tube like the TPR experiment. Prior to the chemisorption, the catalyst was reduced under H_2 flow at 500 °C for 3 h and was then cooled to 400 °C with He flow for 30 min to remove weakly adsorbed species. After that, the sample was cooled to 40 °C followed by CO-pulse chemisorption testing. Doses of 10%CO/He were passed over the reduced catalyst until saturation was obtained, as analyzed in the TCD. Finally, He was passed over the sample for 60 min. Scanning transmission electron microscopy (STEM) images and EDS element mapping were obtained on a Hitachi HD 2700. TEM samples were dispersed in ethanol and then the suspension was dropped on a TEM grid.

Acknowledgements
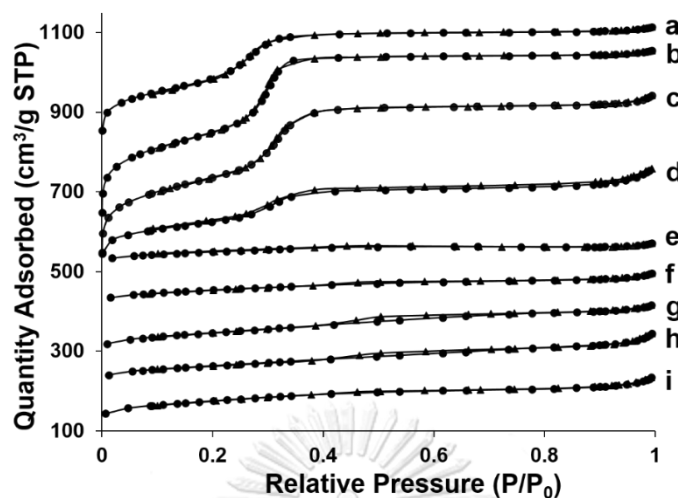
4.6 Support information

Figure S4. 1 N$_2$ adsorption-desorption isotherm results of the calcined catalysts (a) 20Ni_Imp, (b) SSP, (c) 2Ni_PS, (d) 5Ni_PS, (e) 10Ni_PS, (f) 15Ni_PS, (g) 20Ni_PS, (h) 25Ni_PS, (i) 30Ni_PS

Table S4. 1 Carbon balance over nickel phyllosilicate catalysts with varying nickel loading and impregnation catalyst for hydrogenation of furfural to FA

Time (min)	2Ni_PS	5Ni_PS	10Ni_PS	15Ni_PS	20Ni_PS	25Ni_PS	30Ni_PS	20Ni_Imp
60	0.99	0.95	0.97	0.97	0.97	0.95	0.96	0.92
120	0.98	0.96	0.96	0.96	0.97	0.95	0.93	0.91
180	0.98	0.95	0.97	0.94	0.95	0.96	0.91	0.9
240	0.97	0.96	0.92	0.93	0.91	0.95	0.88	0.89
300	0.97	0.94	0.92	0.91	0.90	0.89	0.87	0.89
120			6/100*					

Reaction conditions: 250 mg catalyst, 3 mmol furfural, 50 ml methanol solvent, 0.4 mmol dodecane, reaction temperature 50 °C, 20 bar H$_2$ pressure, reaction time 5 h and catalysts were reduced at 500 °C.

*Reaction conditions without catalyst: 50 μl furfural in 10 ml methanol at 50 ℃ with a 50 mg catalyst under 20 bar H$_2$ for 2 h (% furfural conversion/% selectivity of solvent product (SP) = 2-furaldehyde dimethyl acetal)
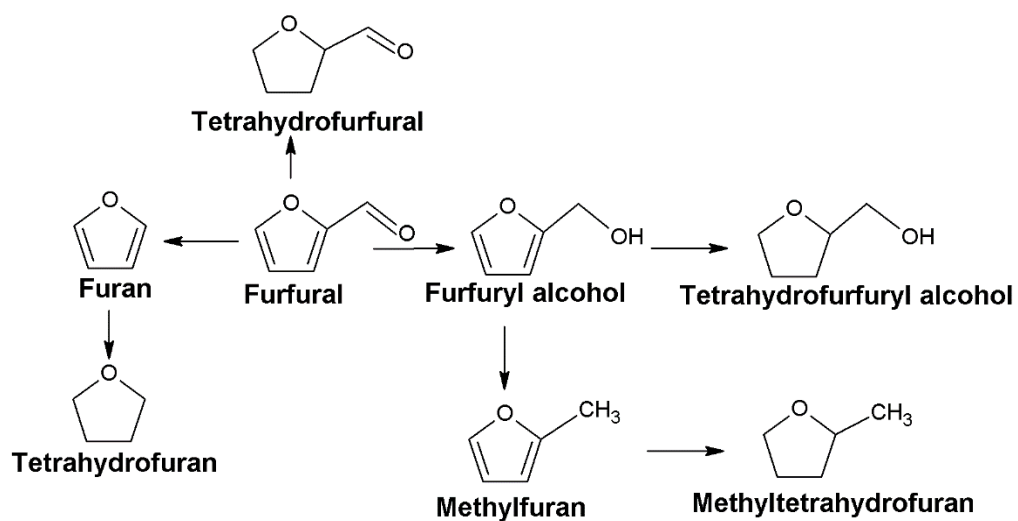
Figure S4. 2 A proposed reaction pathway for the hydrogenation of furfural
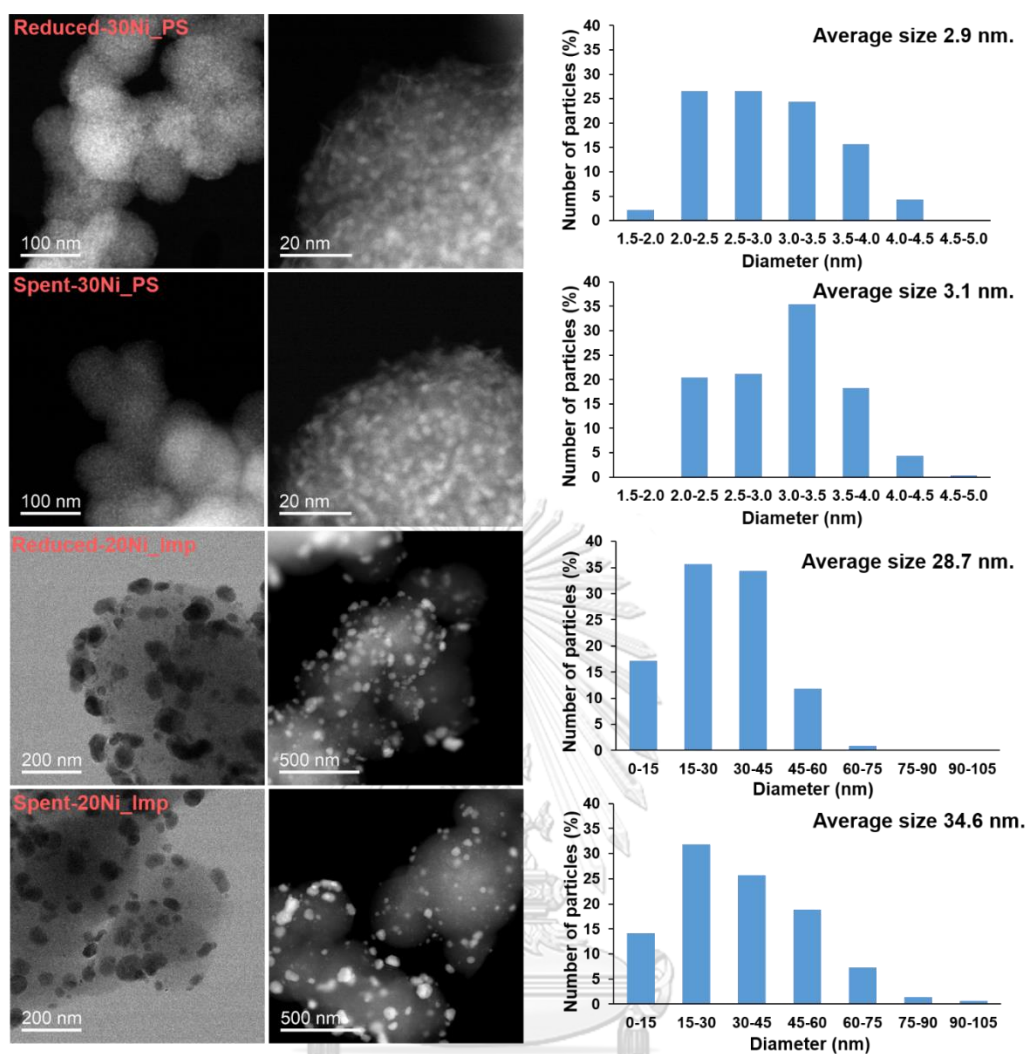
Figure S4. 3 TEM images of the freshly reduced and the spent catalysts of 30Ni_PS and 20Ni_Imp catalysts and the Ni particle size distribution histogram
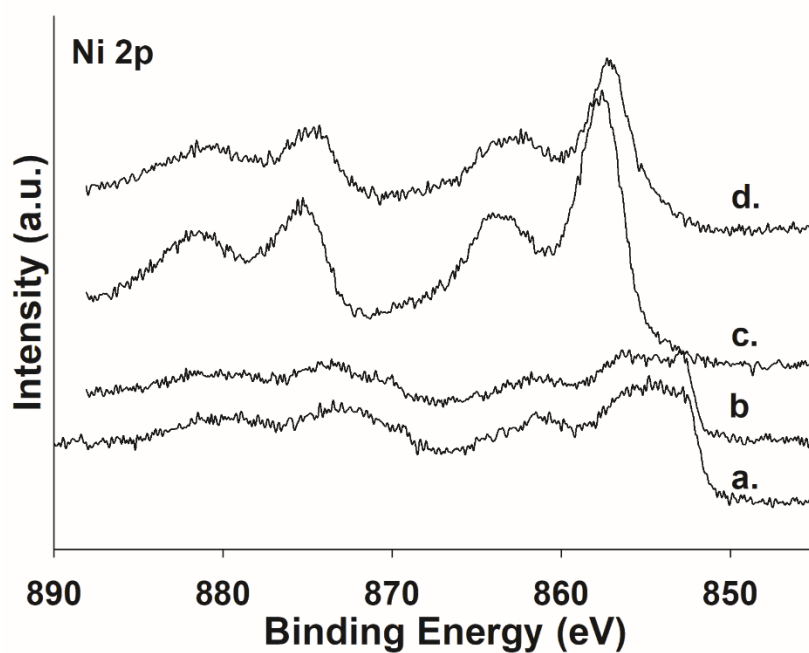
Figure S4. 4 Ni 2p XPS spectra of the freshly reduced and the spent catalysts a) Reduced-20Ni_Imp, b) 3cycles-20Ni_Imp, c) Reduced-30Ni_PS, d) 3cycles-30Ni_PS

Table S4. 2 Ni species proportion over the surface of freshly reduced and the spent catalysts in the Ni 2p binding energy region

Catalysts	Atomic surface ratio			
	Ni/Si	Ni^0/Si	$NiO+Ni^{2+}$/Si	Ni phy/Si
Reduced-20Ni_Imp	4.8	2.1	2.7	0
3cycles-20Ni_Imp	4.3	1.4	2.9	0
Reduced-30Ni_PS	8.1	0.4	1.4	6.4
3cycles-30Ni_PS	7.8	0.6	1.7	5.5
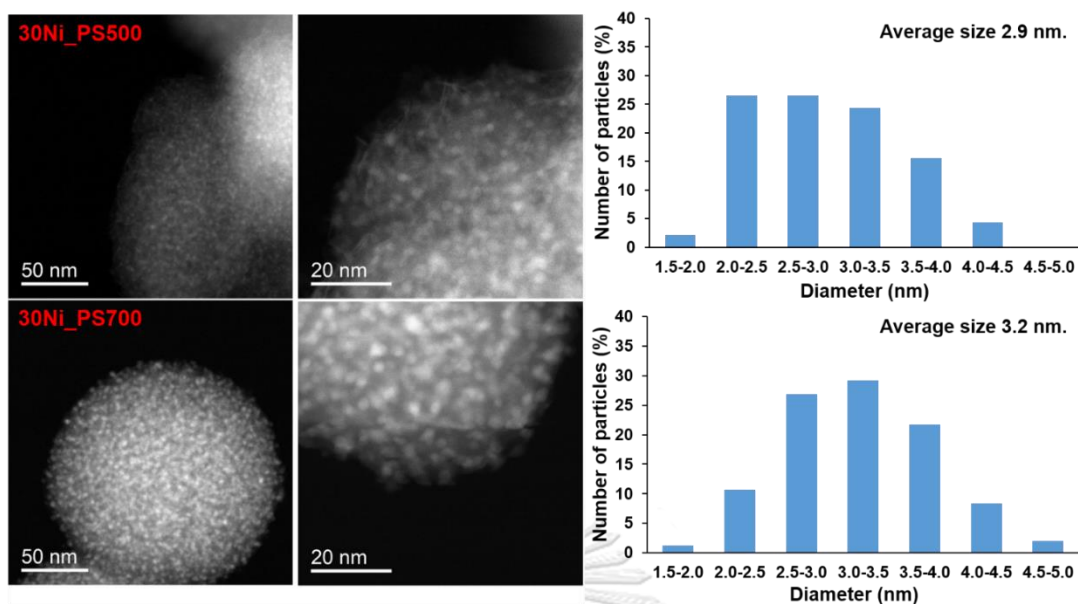
Figure S4. 5 TEM images of the reduced 30Ni_PS catalysts with varying reduction temperature (500 °C and 700 °C) and the Ni particle size distribution histogram

Table S4. 3 Physical properties of reduced 30Ni_PS catalyst at different reduction temperatures

Catalysts	BET Surface area (m²/g)	Pore volume (cm³/g)	Avg. pore diameter (nm)
30Ni_PS400	253	0.13	4.4
30Ni_PS500	257	0.13	4.4
30Ni_PS700	236	0.11	4.3
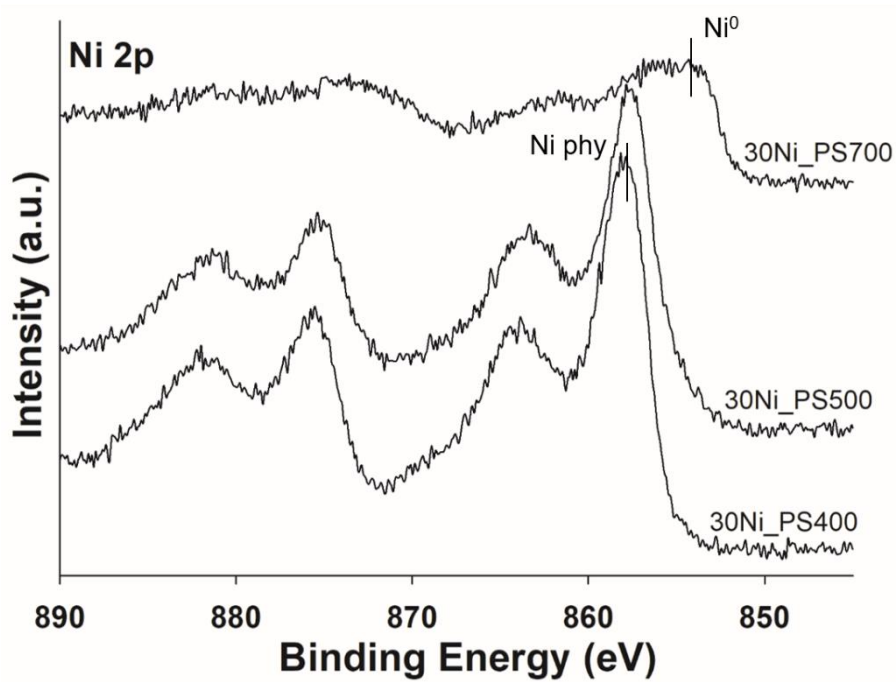
Figure S4. 6 Ni 2p XPS spectra of the 30Ni_PS catalysts with varying reduction temperature

CHARPTER V

CONCLUSIONS

5.1 Conclusions

The spherical silica derived nickel phyllosilicate catalysts were successfully synthesized via a simple one-step modified spherical silica synthesis at room temperature by the direct incorporation of nickel precursor during spherical silica synthesis. The prepared catalysts exhibited a stronger interaction between nickel and silica in the form of nickel phyllosilicate than the silica supported NiO prepared by two step conventional impregnation method. The presence of unique layer structure of nickel phyllosilicate not only solved the main problem of conventional Ni/SiO_2 catalysts during reduction, reaction and regeneration but also can improve the catalytic performances in both gas phase and liquid phase reactions.

**Paper I: Highly active and stable Ni-incorporated spherical silica catalysts for CO_2 methanation**

Spherical silica supported nickel phyllosilicate catalysts (10 wt%) were synthesized by the one step modified spherical silica synthesis with different loading sequenced of nickel and silica source (Si1_Ni2, Ni1_Si2, and Ni_Alt_Si) and evaluated in gas phase hydrogenation of carbon dioxide. All the nickel loading by one step strategy exhibited nickel phyllosilicate species with a strong interaction between nickel species and silica material and high specific surface area. Ni-doped spherical silica had a spherical silica shape with 350-600 nm and were cover by nickel phyllosilicate layer with the fibrous morphology. The loading sequence of Si and Ni source affect to the formation of nickel phyllosilicate. The layer of nickel phyllosilicate was more apparent on Si1_Ni2 catalyst and showed larger surface area than Ni1_Si2 and Ni_Alt_Si catalysts because the most of nickel species were formed on the surface for Si1_Ni2 and can form inside the pored for Ni1_Si2 and Ni_Alt_Si. For the impregnation catalyst, the

nickel oxide species were observed and the agglomeration of large nickel particle were found on the outer surface.

The amount of CO_2 adsorbed on the nickel phyllosilicate was larger than on the impregnation catalyst, indicating a larger number of active center on the surface. Thus, all the spherical silica derived nickel phyllosilicate exhibited superior performance than spherical supported NiO prepared by conventional impregnation method in the order: Ni_Alt_Si (∼51 %) > Ni1_Si2 (∼ 49%) > Si1_Ni2 (∼30 %) >Ni/SSP (Imp) (∼ 10%) with methane selectivity of 80-95% at 350°C. The best CO_2 methanation performances were obtained on the Ni_Alt_Si catalyst (highest CO_2 methanation activity and methane selectivity) due to high electron density of Ni on the surface, high metal dispersion, and high CO_2 adsorption ability. The Ni_Alt_Si catalyst was stable during the regeneration and recyclability tests.

Paper II: Highly stable nickel phyllosilicate prepared by modified spherical silica synthesis in selective hydrogenation of furfural to furfuryl alcohol

Nickel phyllosilicate supported on spherical silica prepared via one-step strategy with various nickel loadings in the 2-30wt% range by an alternate addition of the nickel and silica sources during the spherical silica synthesis and evaluated in liquid phase selective hydrogenation of furfural to furfuryl alcohol. A fibrous-like structure of nickel phyllosilicate was obtained for all the prepared catalysts. After reduction at 500°C, the co-existence of nickel phyllosilicate and nickel metal were observed on the reduced Ni_PS and small nickel particles was highly dispersed without any large aggregation. The crystalline nickel oxide species appeared to be totally reduced into metallic nickel on the 20Ni_Imp. Moreover, all the reduced Ni_PS catalysts still exhibit more than 80% Ni^0+$Ni_{phyllosilicate}$/Ni_{total} species on the surface, whereas a large portion of Ni oxide species (> 55%) is presented on the impregnated catalyst.

All the nickel phyllosilicate catalysts exhibited higher FA selectivity (65-75%) than 20Ni_Imp ($\sim$ 48% FA, producing the highest %THFA). Increasing the Ni loading on Ni_PS to 30 wt% can further increase the furfural conversion without any change in FA selectivity. For similar nickel loading, 20Ni_PS (78% Ni phyllosilicate species, 5% Ni^0) showed lower activity with higher FA selectivity than 20Ni_Imp because the hydrogenation activity of Ni phyllosilicate is lower than metallic Ni^0. Thus, Ni^{2+} species that are strongly interacting with SiO_2 can play an important role in binding and activating the C=O group in the furfural structure. The presence of both metallic Ni^0 and $Ni_{phyllosilicate}$ also produced a synergistic promotional effect for FA formation under mild reaction condition.

The 30Ni_PS exhibited excellent recyclability for furfural hydrogenation with enhanced FA selectivity (from 64% to 74% in the third cycle). The Ni^{2+} species in nickel phyllosilicate catalysts are active and highly stable during reduction, reaction, and regeneration, yielding stable catalytic performances for multiple recycle runs in the furfural hydrogenation to furfuryl alcohol. The 20Ni_Imp catalyst showed poor reusability because the agglomeration of Ni particles on the silica support occurred on 20Ni_Imp as a result from weaker interaction between nickel and the silica support. It can conclude that the fibrous nickel phyllosilicate structure can inhibit the growth of nickel particles and prevent the sintering/leaching of nickel particles because there were no significant changes in the morphology and average nickel particle size of the spent 30Ni_PS catalyst. Thus, the excellence of stability/recyclability of Ni_PS catalysts was ascribed to a unique properties of Ni phyllosilicate that the unreduced Ni^{2+} could serve as a good support for the Ni^0 species, resulting in the active metallic nickel highly dispersed with strong metal-support interaction.

The highest furfural conversion and FA selectivity were obtained on the reduction temperatures between 500─600 °C. The high reduction temperatures (500,

600, and 700 °C) maintained their high selectivity to FA, varying from 60-70%. Combined reaction results with characterization, the reduction temperature has little effect on the particle size of metallic nickel (3 nm) and there were no major differences in the structural properties of the reduced catalysts. Thus, one step strategy derived nickel phyllosilicate catalyst presented a high anti-sintering and prevented the agglomeration of nickel particles at high temperature. The best catalytic performance was obtained on reduction temperature at 500°C.

The reaction temperature also had a significant impact on the product distribution. The higher temperature and longer reaction times promoted deeper hydrogenation of the furan ring in furfural, resulting in higher selectivity towards THFA and lower FA selectivity. The optimum reduction temperature, reaction temperature, and reaction time to produce the highest yield of FA (42%) over the nickel phyllosilicate catalyst with 30 wt% Ni were 500 °C, 80 °C, and 4 h reaction time, respectively

5.2 Recommendations

1. The acidity analysis should be carred out in order to study the effect of acidity on nickel phyllosilicate.

2. The catalytic performance of selective hydrogenation of furfural to furfuryl alcohol should be investigated at higher temperature (>100 °C) and high hydrogen pressure comparable to the other reports.

APPENDIX A

Table A1 Hydrogenation of furfural to FA over 10wt% Ni by one-step modified spherical silica synthesis with difference loading sequence of Ni and Si source and impregnation catalysts

catalysts	Reduction condition	Rxn time (min)	Conv. (%)	Selectivity (%)			FA Yield
				FA	THFA	Other	
Ni_Alt_Si	500 °C, 3h	120	81	73	14	13	59
Ni_Alt_Si	600 °C, 3h	60	50	66	9	25	33
Ni_Alt_Si	600 °C, 3h	120	73	68	8	24	50
Si1Ni2	500 °C, 3h	120	90	63	26	11	57
Si1Ni2	600 °C, 3h	60	51	63	14	23	32
Si1Ni2	600 °C, 3h	120	72	63	18	19	45
Ni1Si2	500 °C, 3h	120	94	61	26	13	57
Ni1Si2	600 °C, 3h	60	52	64	13	23	33
Ni1Si2	600 °C, 3h	120	70	60	21	19	42
Ni1Si2	600 °C, 3h	180	90	57	30	13	51
Ni/SSP(imp)	500 °C, 3h	120	95	49	39	12	47
Ni/SSP(imp)	500 °C, 3h	180	91	48	36	16	44
Ni/SSP(imp)	500 °C, 3h	240	90	50	36	14	45
Ni/SSP(imp)	600 °C, 3h	60	22			100(SP)	0
Ni/SSP(imp)	600 °C, 3h	120	19			100(SP)	0

*Reaction conditions: 50 μl FA in 10 ml methanol at 50 °C with a 50 mg catalyst under 20 bar H_2

*solvent product (SP) = 2-furaldehyde dimethyl acetal

Table A2 Hydrogenation of furfural to FA under water solvent over 10wt% Ni by one-step modified spherical silica synthesis with alternate addition of the nickel and silica sources during the spherical silica synthesis and impregnation catalysts.

catalysts	Reduction condition	Rxn time (min)	Conv. (%)	Selectivity (%)		FA Yield
				FA	Other	
Ni_Alt_Si	500 °C, 3h	10	53	62	38	33
Ni_Alt_Si	500 °C, 3h	60	100	52	48	52
Ni/SSP(imp)	500 °C, 3h	10	89	48	52	43
Ni/SSP(imp)	500 °C, 3h	30	100	42	58	42
Ni/SSP(imp)	500 °C, 3h	120	100	10	90	10
1%Pt_Alt_Si	200 °C, 2h	60	18	91	9	16
1%Pt/SSP(imp)	200 °C, 2h	60	18	98	2	18

*Reaction conditions: 50 μl FA in 10 ml water at 50 °C with a 50 mg catalyst under 20 bar H_2

APPENDIX B

Table B1 Hydrogenation of furfural to FA under methanol solvent over 10wt% Ni by one-step modified spherical silica synthesis with alternate addition of the nickel and silica sources during the spherical silica synthesis modified with second metal.

Catalysts	conversion	Selectivity (%)					FA Yield (%)
		FA	THFA	SP	Furun	Others	
No cat	36			100			0
NiAltSi	81	73	14			13	59
Fe-NiAltSi	64	70	8			22	45
Mn-NiAltSi	79	48	12			40	38
Pd-NiAltSi	76	7	83		3	7	5
Co-NiAltSi	91	34			55	11	31

*Reaction conditions: 50 μl FA in 10 ml methanol at 50 °C with a 50 mg catalyst under 20 bar H_2 for 2 h, Catalysts: 10wt%Ni and Ni : 2nd metal mole ratio = 15:1

*solvent product (SP) = 2-furaldehyde dimethyl acetal

Table B2 and figure B1 CO_2 conversion and CH_4 selectivity over 10wt% Ni by one-step modified spherical silica synthesis with alternate addition of the nickel and silica sources during the spherical silica synthesis modified with second metal.

Catalysts	Temp (°C)	Time (min)	CO_2 conversion	CH_4 selectivity
Ni_Alt_Si	300	60	20.8	100
	450	60	94.1	100
Fe-Ni_Alt_Si	300	60	23.78	100
	450	60	97.16	100
Mn-Ni_Alt_Si	300	60	23.72	100
	450	60	92.73	100
Co-Ni_Alt_Si	300	60	28.02	100
	450	60	97.92	100
Pd-Ni_Alt_Si	300	60	24.5	100
	450	60	96.29	100

**Reaction conditions: reduced under H_2 at 500°C 3 h, Catalyst = 0.1 g, WHSV = 24000 cm^3/g_{cat}h, H_2:CO_2 = 10:1, Catalysts: 10wt%Ni and Ni : 2nd metal mole ratio = 15:1
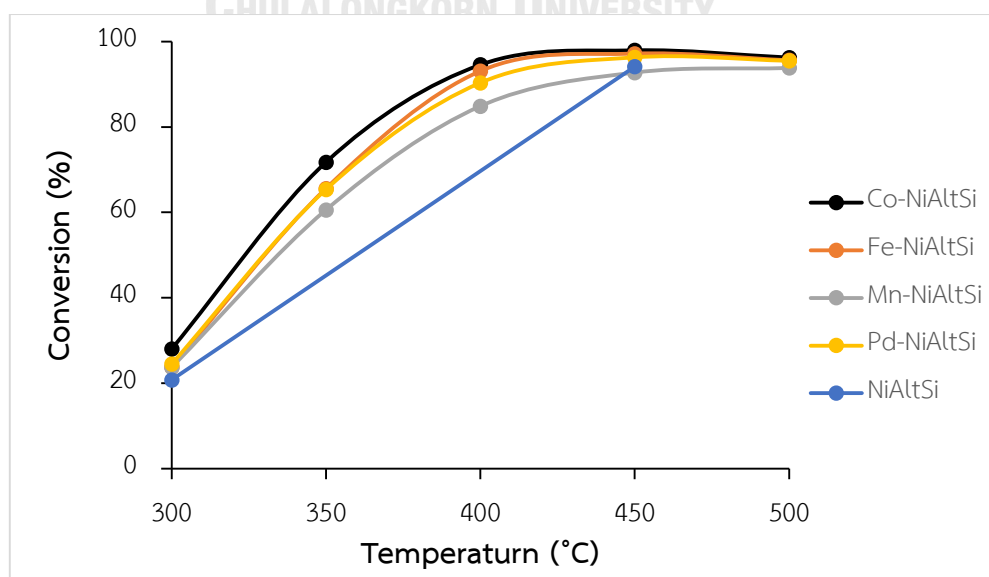
APPENDIX C

The effect of second metal, preparation method and loading sequence of Ni, Si, and second metal were investigated in hydrogenation of furfural to FA

Catalysts: 20wt%Ni loading, Ni:Fe mole ratio 10:1, Ni:Cu mole ratio 10:1 and 5:1

NiAltSi = One-step modified spherical silica synthesis with alternate addition of the nickel and silica sources during the spherical silica synthesis

(2CuNiSi)Alt = One-step modified spherical silica synthesis with alternate addition of the nickel, copper and silica sources during the spherical silica synthesis (Ni:Cu mole ratio 10:1)

(4CuNiSi)Alt = One-step modified spherical silica synthesis with alternate addition of the nickel, copper and silica sources during the spherical silica synthesis (Ni:Cu mole ratio 5:1)

(NiAltSi)-4Cu = One-step modified spherical silica synthesis with alternate addition of the nickel and silica sources during the spherical silica synthesis and then addition of copper (Ni:Cu mole ratio 5:1)

(NiCu)-Imp/SSP = Impregnation co-precursor between nickel and copper source onto spherical silica (Ni:Cu mole ratio 10:1)

NiFeSi = One-step modified spherical silica synthesis with alternate addition of the nickel, iron and silica sources during the spherical silica synthesis (Ni:Cu mole ratio 10:1)

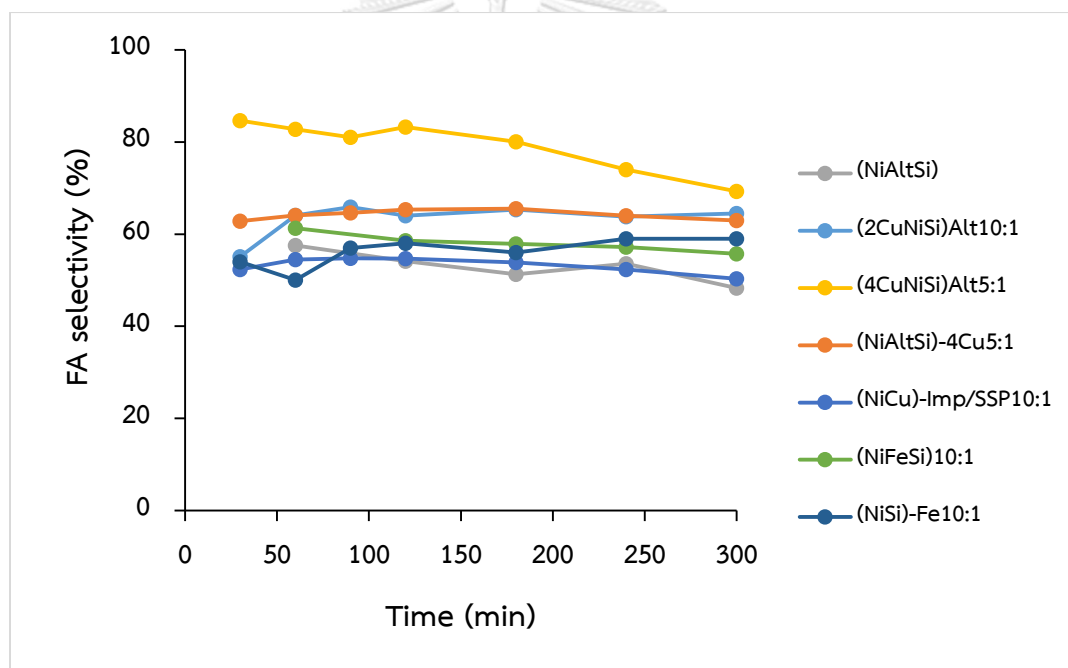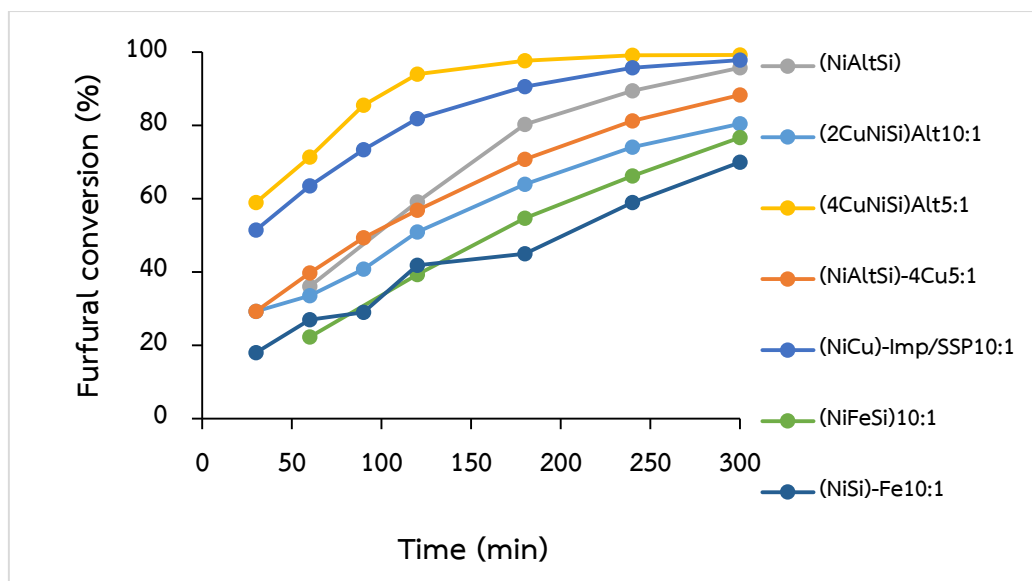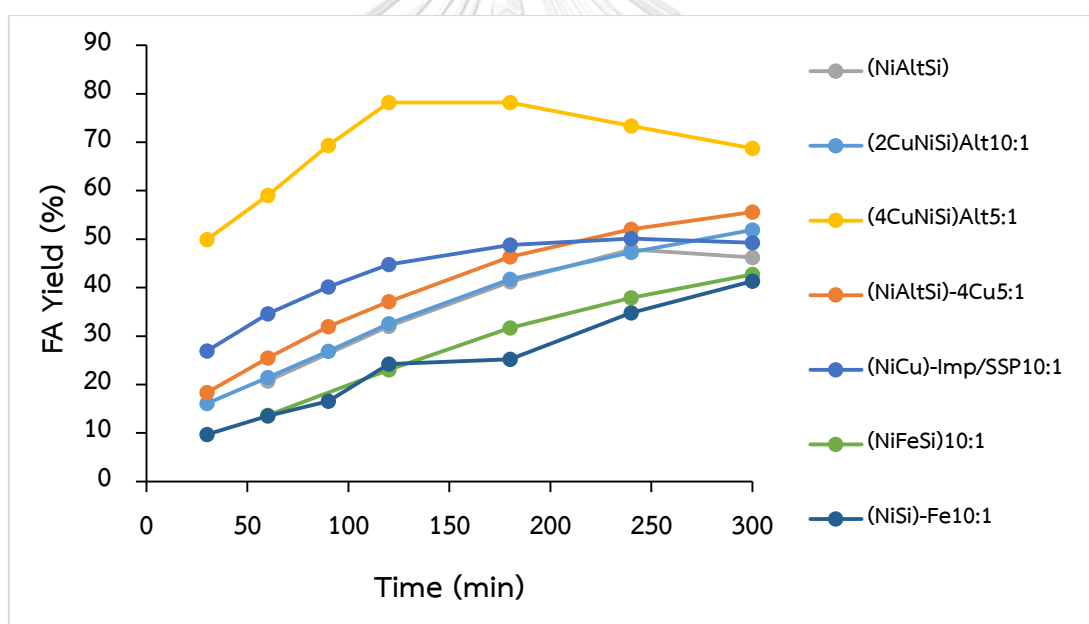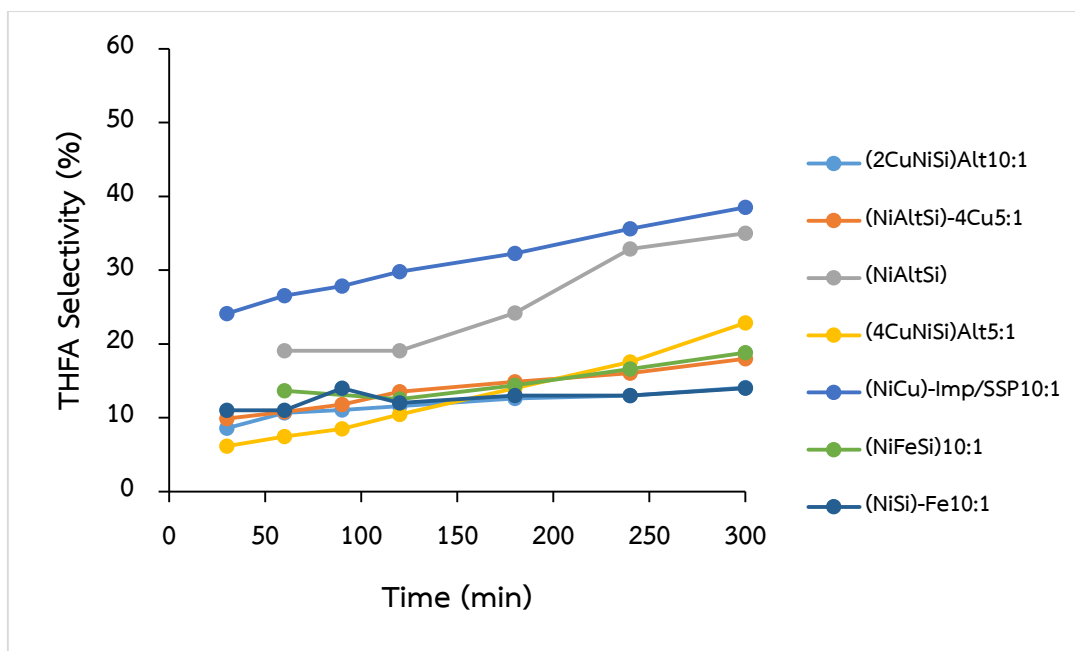(NiSi)-Fe = One-step modified spherical silica synthesis with alternate addition of the nickel and silica sources during the spherical silica synthesis and then addition of iron (Ni:Cu mole ratio 10:1)

*Reaction conditions: 250 mg catalyst, 3 mmol furfural, 50 ml methanol solvent, 0.4 mmol dodecane, reaction temperature 80 °C, 20 bar H_2 pressure, reaction time 5 h and catalysts were reduced at 500 °C

REFERENCES

[1]   Li, H., Chen, Y., Liu, S., and Liu, Q. Enhancement of hydrothermal synthesis of FDU-12-derived nickel phyllosilicate using double accelerators of ammonium fluoride and urea for CO2 methanation. <u>Journal of CO2 Utilization</u> 52 (2021): 101677.

[2]   Mallesham, B., Sudarsanam, P., Venkata Shiva Reddy, B., Govinda Rao, B., and Reddy, B.M. Nanostructured Nickel/Silica Catalysts for Continuous Flow Conversion of Levulinic Acid to γ-Valerolactone. <u>ACS omega</u> 3(12) (2018): 16839-16849.

[3]   Wu, X., et al. Recent Progresses in the Design and Fabrication of Highly Efficient Ni-Based Catalysts With Advanced Catalytic Activity and Enhanced Anti-coke Performance Toward CO2 Reforming of Methane. <u>Frontiers in Chemistry</u> 8 (2020).

[4]   Chen, Y. and Liu, Q. Synthesis and Regeneration of Ni-Phyllosilicate Catalysts Using a Versatile Double-Accelerator Method: A Comprehensive Study. <u>ACS Catalysis</u> 11(20) (2021): 12570-12584.

[5]   Chen, Y., Bi, W., Chen, L., and Liu, Q. Urea-assisted synthesis towards a renewable rice husk silica-derived Ni-phyllosilicate catalyst for CO2 methanation. <u>International Journal of Hydrogen Energy</u> 46(54) (2021): 27567-27575.

[6]   Zhang, Y., Chen, Y., and Liu, Q. Green synthesis of MCM-41 derived from renewable biomass and construction of VOx-Modified nickel phyllosilicate catalyst for CO2 methanation. <u>International Journal of Hydrogen Energy</u> 46(63) (2021): 32003-32016.

[7]   Zhang, T. and Liu, Q. Lanthanum-Modified MCF-Derived Nickel Phyllosilicate Catalyst for Enhanced CO2 Methanation: A Comprehensive Study. <u>ACS Applied Materials & Interfaces</u> 12(17) (2020): 19587-19600.

[8]   Bukhari, S.N., Chong, C.C., Setiabudi, H.D., Cheng, Y.W., Teh, L.P., and Jalil, A.A. Ni/Fibrous type SBA-15: Highly active and coke resistant catalyst for CO2 methanation. <u>Chemical Engineering Science</u> 229 (2021): 116141.

[9]   Vrijburg, W.L., et al. Tunable colloidal Ni nanoparticles confined and redistributed in mesoporous silica for CO2 methanation. <u>Catalysis Science & Technology</u> 9(10) (2019): 2578-2591.

[10]   Ingale, P., Guan, C., Kraehnert, R., Naumann d'Alnoncourt, R., Thomas, A., and Rosowski, F. Design of an active and stable catalyst for dry reforming of methane via molecular layer deposition. <u>Catalysis Today</u> 362 (2021): 47-54.

[11]   Zhang, T. and Liu, Q. Perovskite LaNiO 3 Nanocrystals inside Mesostructured Cellular Foam Silica: High Catalytic Activity and Stability for CO 2 Methanation. <u>Energy technology</u> 8 (2020): 1901164.

[12]   Manikandan, M., Venugopal, A.K., Prabu, K., Jha, R.K., and Thirumalaiswamy, R. Role of surface synergistic effect on the performance of Ni-based hydrotalcite catalyst for highly efficient hydrogenation of furfural. <u>Journal of Molecular Catalysis A: Chemical</u> 417 (2016): 153-162.

[13]   Liu, Q. and Dong, H. In Situ Immobilizing Ni Nanoparticles to FDU-12 via Trehalose with Fine Size and Location Control for CO2 Methanation. <u>ACS Sustainable Chemistry & Engineering</u> 8(4) (2020): 2093-2105.

[14]   Sivaiah, M.V., et al. Nickel based catalysts derived from hydrothermally synthesized 1:1 and 2:1 phyllosilicates as precursors for carbon dioxide reforming of methane. <u>Microporous and Mesoporous Materials</u> 140(1-3) (2011): 69-80.

[15]   Tan, J., Xia, X., Cui, J., Yan, W., Jiang, Z., and Zhao, Y. Efficient Tuning of Surface Nickel Species of the Ni-Phyllosilicate Catalyst for the Hydrogenation of Maleic Anhydride. <u>The Journal of Physical Chemistry C</u> 123(15) (2019): 9779-9787.

[16]   Yang, H., Zhang, Y., and Liu, Q. Highly Efficient Ni-Phyllosilicate Catalyst with Surface and Interface Confinement for CO2 and CO Methanation. <u>Industrial & Engineering Chemistry Research</u> 60(19) (2021): 6981-6992.

[17]   Zhang, C., et al. Hydrogen Production via Steam Reforming of Ethanol on Phyllosilicate-Derived Ni/SiO2: Enhanced Metal–Support Interaction and Catalytic Stability. <u>ACS Sustainable Chemistry & Engineering</u> 1(1) (2013): 161-173.

[18]   Bian, Z. and Kawi, S. Preparation, characterization and catalytic application of phyllosilicate: A review. <u>Catalysis Today</u> 339 (2020): 3-23.

[19]   Dong, H. and Liu, Q. Three-Dimensional Networked Ni-Phyllosilicate Catalyst for CO2 Methanation: Achieving High Dispersion and Enhanced Stability at High Ni Loadings. ACS Sustainable Chemistry & Engineering 8(17) (2020): 6753-6766.

[20]   Wang, Y.-w., Zhang, Y.-j., Wang, K.-j., Tan, L.-m., and Chen, S.-y. Preparation of Ni/SiO2 by ammonia evaporation method for synthesis of 2-MTHF from 2-MF hydrogenation. Journal of Fuel Chemistry and Technology 49(1) (2021): 97-103.

[21]   Yang, F., Wang, H., Han, J., Ge, Q., and Zhu, X. Enhanced selective deoxygenation of m-cresol to toluene on Ni/SiO2 catalysts derived from nickel phyllosilicate. Catalysis Today 330 (2019): 149-156.

[22]   Ye, R.-P., et al. Enhanced stability of Ni/SiO2 catalyst for CO2 methanation: Derived from nickel phyllosilicate with strong metal-support interactions. Energy 188 (2019): 116059.

[23]   Ciotonea, C., et al. Phyllosilicate-derived Nickel-cobalt Bimetallic Nanoparticles for the Catalytic Hydrogenation of Imines, Oximes and N-heteroarenes. ChemCatChem 12(18) (2020): 4652-4663.

[24]   Du, H., Ma, X., Jiang, M., Yan, P., Zhao, Y., and Conrad Zhang, Z. Efficient Ni/SiO2 catalyst derived from nickel phyllosilicate for xylose hydrogenation to xylitol. Catalysis Today 365 (2021): 265-273.

[25]   Alencar, J.M., Oliveira, F.J.V.E., Airoldi, C., and Silva Filho, E.C. Organophilic nickel phyllosilicate for reactive blue dye removal. Chemical Engineering Journal 236 (2014): 332-340.

[26]   Chen, Y., Zhang, T., and Liu, Q. One-pot or two-pot synthesis? Using a more facile and efficient method to synthesize Ni-phyllosilicate catalyst derived from 3D-SBA-15. International Journal of Hydrogen Energy 46(59) (2021): 30373-30381.

[27]   Zhang, T., Tian, Z., and Liu, Q. Three-dimensional flower-like nickel phyllosilicates for CO2 methanation: enhanced catalytic activity and high stability. Sustainable Energy & Fuels 4(7) (2020): 3438-3449.

[28]   Li, C.-C., Hsieh, C.-H., and Lin, Y.-C. Ni/SiO2 catalysts derived from carbothermal reduction of nickel phyllosilicate in the hydrogenation of levulinic acid to γ-valerolactone: The efficacy of nitrogen decoration. Molecular Catalysis (2021): 111720.

[29]   Wang, M., et al. Synthesis of a Ni Phyllosilicate with Controlled Morphology for Deep Hydrogenation of Polycyclic Aromatic Hydrocarbons. ACS Sustainable Chemistry & Engineering 7(2) (2018): 1989-1997.

[30]   Wei, Y., Horlyck, J., Song, M., Scott, J., Amal, R., and Cao, Q. Inducing Ni phyllosilicate formation over a carbon fiber support as a catalyst for the CO_2 reforming of methane. Applied Catalysis A: General 592 (2020): 117418.

[31]   Zhen, W., Li, B., Lu, G., and Ma, J. Enhancing catalytic activity and stability for CO_2 methanation on Ni–Ru/γ-Al_2O_3 via modulating impregnation sequence and controlling surface active species. RSC Advances 4(32) (2014): 16472-16479.

[32]   Liu, H., Zou, X., Wang, X., Lu, X., and Ding, W. Effect of CeO_2 addition on Ni/Al_2O_3 catalysts for methanation of carbon dioxide with hydrogen. Journal of Natural Gas Chemistry 21(6) (2012): 703-707.

[33]   Díez-Ramírez, J., et al. Effect of support nature on the cobalt-catalyzed CO_2 hydrogenation. Journal of CO2 Utilization 21(Supplement C) (2017): 562-571.

[34]   Le, T.A., Kang, J.K., and Park, E.D. CO and CO_2 Methanation Over Ni/SiC and Ni/SiO_2 Catalysts. Topics in Catalysis 61(15) (2018): 1537-1544.

[35]   Panagiotopoulou, P., Kondarides, D.I., and Verykios, X.E. Mechanistic aspects of the selective methanation of CO over Ru/TiO_2 catalyst. Catalysis Today 181(1) (2012): 138-147.

[36]   Pandey, D. and Deo, G. Promotional effects in alumina and silica supported bimetallic Ni–Fe catalysts during CO_2 hydrogenation. Journal of Molecular Catalysis A: Chemical 382 (2014): 23-30.

[37]   Ashok, J., Ang, M.L., and Kawi, S. Enhanced activity of CO_2 methanation over Ni/CeO_2-ZrO_2 catalysts: Influence of preparation methods. Catalysis Today 281 (2017): 304-311.

[38]   Le, T.A., Kim, M.S., Lee, S.H., Kim, T.W., and Park, E.D. CO and CO_2 methanation over supported Ni catalysts. Catalysis Today 293-294 (2017): 89-96.

[39]   Li, Z., Li, B., Li, Z., and Rong, X. The promoter action of CeO_2 for the Ni/Al_2O_3-catalyzed methanation of CO_2. Kinetics and Catalysis 56(3) (2015): 329-334.

[40]   Ge, X., et al. Conversion of Lignocellulosic Biomass Into Platform Chemicals for Biobased Polyurethane Application. Advances in Bioenergy 3 (2018): 161-213.

[41]   Takkellapati, S., Li, T., and Gonzalez, M.A. An Overview of Biorefinery Derived
        Platform Chemicals from a Cellulose and Hemicellulose Biorefinery. <u>Clean
        Technol Environ Policy</u> 20(7) (2018): 1615-1630.

[42]   Jia, P., Lan, X., Li, X., and Wang, T. Highly Active and Selective NiFe/SiO2
        Bimetallic Catalyst with Optimized Solvent Effect for the Liquid-Phase
        Hydrogenation of Furfural to Furfuryl Alcohol. <u>ACS Sustainable Chemistry &
        Engineering</u> 6(10) (2018): 13287-13295.

[43]   Kotbagi, T.V., Gurav, H.R., Nagpure, A.S., Chilukuri, S.V., and Bakker, M.G. Highly
        efficient nitrogen-doped hierarchically porous carbon supported Ni
        nanoparticles for the selective hydrogenation of furfural to furfuryl alcohol. <u>RSC
        Advances</u> 6(72) (2016): 67662-67668.

[44]   Taylor, M.J., et al. Highly selective hydrogenation of furfural over supported Pt
        nanoparticles under mild conditions. <u>Applied Catalysis B: Environmental</u> 180
        (2016): 580-585.

[45]   Yuan, Q., et al. Selective liquid phase hydrogenation of furfural to furfuryl
        alcohol by Ru/Zr-MOFs. <u>Journal of Molecular Catalysis A: Chemical</u> 406 (2015): 58-
        64.

[46]   Liu, L., Lou, H., and Chen, M. Selective hydrogenation of furfural to
        tetrahydrofurfuryl alcohol over Ni/CNTs and bimetallic Cu Ni/CNTs catalysts.
        <u>International Journal of Hydrogen Energy</u> 41(33) (2016): 14721-14731.

[47]   Gong, W., et al. Highly selective liquid-phase hydrogenation of furfural over N-
        doped carbon supported metallic nickel catalyst under mild conditions.
        <u>Molecular Catalysis</u> 429 (2017): 51-59.

[48]   Nakagawa, Y., Nakazawa, H., Watanabe, H., and Tomishige, K. Total
        Hydrogenation of Furfural over a Silica-Supported Nickel Catalyst Prepared by
        the Reduction of a Nickel Nitrate Precursor. <u>ChemCatChem</u> 4(11) (2012): 1791-1797.

[49]   Sitthisa, S., An, W., and Resasco, D.E. Selective conversion of furfural to
        methylfuran over silica-supported NiFe bimetallic catalysts. <u>Journal of Catalysis</u>
        284(1) (2011): 90-101.

[50]   Moogi, S., Lee, I.-G., and Park, J.-Y. Effect of La2O3 and CeO2 loadings on
        formation of nickel-phyllosilicate precursor during preparation of Ni/SBA-15 for

hydrogen-rich gas production from ethanol steam reforming. <u>International Journal of Hydrogen Energy</u> 44(56) (2019): 29537-29546.

[51] Wei, S., et al. Preparation and activity evaluation of NiMoB/γ-Al2O3 catalyst by liquid-phase furfural hydrogenation. <u>Particuology</u> 9(1) (2011): 69-74.

[52] Xu, C., Zheng, L., Jianying, L., and Huang, Z. Furfural Hydrogenation on Nickel-promoted Cu-containing Catalysts Prepared from Hydrotalcite-Like Precursors. <u>Chinese Journal of Chemistry</u> 29 (2011).

[53] Zhang, C., Lai, Q., and Holles, J.H. Bimetallic overlayer catalysts with high selectivity and reactivity for furfural hydrogenation. <u>Catalysis Communications</u> 89 (2017): 77-80.

[54] Chen, B., Li, F., Huang, Z., and Yuan, G. Tuning catalytic selectivity of liquid-phase hydrogenation of furfural via synergistic effects of supported bimetallic catalysts. <u>Applied Catalysis A: General</u> 500 (2015): 23-29.

[55] Liu, L., Lou, H., and Chen, M. Selective hydrogenation of furfural to tetrahydrofurfuryl alcohol over Ni/CNTs and bimetallic CuNi/CNTs catalysts. <u>International Journal of Hydrogen Energy</u> 41(33) (2016): 14721-14731.

[56] Yang, Y., Ma, J., Jia, X., Du, Z., Duan, Y., and Xu, J. Aqueous phase hydrogenation of furfural to tetrahydrofurfuryl alcohol on alkaline earth metal modified Ni/Al2O3. <u>RSC Advances</u> 6(56) (2016): 51221-51228.

[57] Khromova, S.A., et al. Furfural Hydrogenation to Furfuryl Alcohol over Bimetallic Ni–Cu Sol–Gel Catalyst: A Model Reaction for Conversion of Oxygenates in Pyrolysis Liquids. <u>Topics in Catalysis</u> 59(15) (2016): 1413-1423.

[58] Wu, J., Gao, G., Li, J., Sun, P., Long, X., and Li, F. Efficient and versatile CuNi alloy nanocatalysts for the highly selective hydrogenation of furfural. <u>Applied Catalysis B: Environmental</u> 203 (2017): 227-236.

[59] Srivastava, S., Jadeja, G.C., and Parikh, J. Synergism studies on alumina-supported copper-nickel catalysts towards furfural and 5-hydroxymethylfurfural hydrogenation. <u>Journal of Molecular Catalysis A: Chemical</u> 426 (2017): 244-256.

[60] Putro, W.S., Kojima, T., Hara, T., Ichikuni, N., and Shimazu, S. Selective hydrogenation of unsaturated carbonyls by Ni–Fe-based alloy catalysts. <u>Catalysis Science & Technology</u> 7(16) (2017): 3637-3646.

[61]   Sang, S., Wang, Y., Zhu, W., and Xiao, G. Selective hydrogenation of furfuryl alcohol to tetrahydrofurfuryl alcohol over Ni/γ-Al2O3 catalysts. Research on Chemical Intermediates 43(2) (2017): 1179-1195.

[62]   Li, S., et al. Short channeled Ni-Co/SBA-15 catalysts for highly selective hydrogenation of biomass-derived furfural to tetrahydrofurfuryl alcohol. Microporous and Mesoporous Materials 262 (2018): 154-165.

[63]   Guo, H., et al. Selective Hydrogenation of Furfural to Furfuryl Alcohol over Acid-Activated Attapulgite-Supported NiCoB Amorphous Alloy Catalyst. Industrial & Engineering Chemistry Research 57(2) (2018): 498-511.

[64]   Rodiansono, Astuti, M.D., Mujiyanti, D.R., Santoso, U.T., and Shimazu, S. Novel preparation method of bimetallic Ni-In alloy catalysts supported on amorphous alumina for the highly selective hydrogenation of furfural. Molecular Catalysis 445 (2018): 52-60.

[65]   Liu, L., Lou, H., and Chen, M. Selective hydrogenation of furfural over Pt based and Pd based bimetallic catalysts supported on modified multiwalled carbon nanotubes (MWNT). Applied Catalysis A: General 550 (2018): 1-10.

[66]   Gong, W., et al. Sulfonate group modified Ni catalyst for highly efficient liquid-phase selective hydrogenation of bio-derived furfural. Chinese Chemical Letters 29(11) (2018): 1617-1620.

[67]   Giorgianni, G., et al. Effect of the Solvent in Enhancing the Selectivity to Furan Derivatives in the Catalytic Hydrogenation of Furfural. ACS Sustainable Chemistry & Engineering 6(12) (2018): 16235-16247.

[68]   Smirnov, A., Shilov, I., Bulavchenko, O., and Yakovlev, V. Study of Bimetallic Ni-Mo Carbides in Catalytic Hydrogenation of Furfural to Value-Added Chemicals. 2018.

[69]   Chen, C., Fan, R., Gong, W., Zhang, H., Wang, G., and Zhao, H. The catalytic behaviour in aqueous-phase hydrogenation over a renewable Ni catalyst derived from a perovskite-type oxide. Dalton Transactions 47(48) (2018): 17276-17284.

[70]   Meng, X., Yang, Y., Chen, L., Xu, M., Zhang, X., and Wei, M. A Control over Hydrogenation Selectivity of Furfural via Tuning Exposed Facet of Ni Catalysts. ACS Catalysis 9(5) (2019): 4226-4235.

[71]   Hu, F., et al. Efficient and Selective Ni/Al2O3–C Catalyst Derived from Metal–Organic Frameworks for the Hydrogenation of Furfural to Furfuryl Alcohol. Catalysis Letters 149 (2019).

[72]   Shilov, N.I., Smirnov, A.A., Bulavchenko, A.O., and Yakovlev, A.V. Effect of Ni–Mo Carbide Catalyst Formation on Furfural Hydrogenation. Catalysts 8(11) (2018).

[73]   Wang, T., Hu, A., Wang, H., and Xia, Y. Catalytic transfer hydrogenation of furfural into furfuryl alcohol over Ni–Fe‑layered double hydroxide catalysts. Journal of the Chinese Chemical Society (2019).

[74]   Guerrero-Torres, A., et al. Ni supported on sepiolite catalysts for the hydrogenation of furfural to value-added chemicals: influence of the synthesis method on the catalytic performance. Topics in Catalysis 62(5) (2019): 535-550.

[75]   Marakatti, V.S., Arora, N., Rai, S., Sarma, S.C., and Peter, S.C. Understanding the Role of Atomic Ordering in the Crystal Structures of NixSny toward Efficient Vapor Phase Furfural Hydrogenation. ACS Sustainable Chemistry & Engineering 6(6) (2018): 7325-7338.

[76]   Wang, Y., et al. Comparative Study of Supported Monometallic Catalysts in the Liquid-Phase Hydrogenation of Furfural: Batch Versus Continuous Flow. ACS Sustainable Chemistry & Engineering 6(8) (2018): 9831-9844.

[77]   Luo, L., Yuan, F., Zaera, F., and Zhu, Y. Catalytic hydrogenation of furfural to furfuryl alcohol on hydrotalcite-derived CuxNi3–xAlOy mixed-metal oxides. Journal of Catalysis 404 (2021): 420-429.

[78]   Wu, J., Yan, X., Wang, W., Jin, M., Xie, Y., and Wang, C. Highly Dispersed CoNi Alloy Embedded in N‑doped Graphitic Carbon for Catalytic Transfer Hydrogenation of Biomass‑derived Furfural. Chemistry–An Asian Journal 16(20) (2021): 3194-3201.

[79]   Fan, Y., et al. Efficient single-atom Ni for catalytic transfer hydrogenation of furfural to furfuryl alcohol. Journal of Materials Chemistry A 9(2) (2021): 1110-1118.

[80]   Wu, J., et al. Understanding the geometric and electronic factors of PtNi bimetallic surfaces for efficient and selective catalytic hydrogenation of biomass-derived oxygenates. Journal of Energy Chemistry 60 (2021): 16-24.

[81]   Stepanova, L.N., et al. Study of the properties of the catalysts based on Ni(Mg)Al-Layered Hydroxides for the reaction of furfural hydrogenation. Materials Chemistry and Physics 263 (2021): 124091.

[82]   Zhang, J., Mao, D., and Wu, D. Industrially Applicable Aqueous-Phase Selective Hydrogenation of Furfural on an Efficient TiOx-Modified Ni Nanocatalyst. ACS Sustainable Chemistry & Engineering 9(41) (2021): 13902-13914.

[83]   Sreenavya, A., Ganesh, V., Venkatesha, N.J., and Sakthivel, A. Hydrogenation of biomass derived furfural using Ru-Ni-Mg–Al-hydrotalcite material. Biomass Conversion and Biorefinery (2022).

[84]   Wonglekha, K., et al. Effects of TiO2 Support and Cobalt Addition of Ni/TiO2 Catalyst in Selective Hydrogenation of Furfural to Furfuryl Alcohol. Journal of Renewable Materials 10(8) (2022): 2055-2072.

[85]   Abreu, C., Simon, P., Wojcieszak, R., Souza, P., and Toniolo, F. Effect of Rhenium on the Catalytic Activity of Activated Carbon-Supported Nickel Applied in the Hydrogenation of Furfural and Levulinic Acid. Topics in Catalysis (2022): 1-13.

[86]   Zhi, G., Guo, X., Wang, Y., Jin, G., and Guo, X. Effect of La2O3 modification on the catalytic performance of Ni/SiC for methanation of carbon dioxide. Catalysis Communications 16(1) (2011): 56-59.

[87]   Aldana, P.A.U., et al. Catalytic CO2 valorization into CH4 on Ni-based ceria-zirconia. Reaction mechanism by operando IR spectroscopy. Catalysis Today 215 (2013): 201-207.

[88]   Tada, S., Shimizu, T., Kameyama, H., Haneda, T., and Kikuchi, R. Ni/CeO2 catalysts with high CO2 methanation activity and high CH4 selectivity at low temperatures. International Journal of Hydrogen Energy 37(7) (2012): 5527-5531.

[89]   Hwang, S., et al. Methanation of carbon dioxide over mesoporous Ni–Fe–Ru–Al2O3 xerogel catalysts: Effect of ruthenium content. Journal of Industrial and Engineering Chemistry 19(2) (2013): 698-703.

[90]   Cai, W., Zhong, Q., and Zhao, Y. Fractional-hydrolysis-driven formation of non-uniform dopant concentration catalyst nanoparticles of Ni/CexZr1−xO2 and its catalysis in methanation of CO2. Catalysis Communications 39 (2013): 30-34.

[91]   Moghaddam, S.V., Rezaei, M., Meshkani, F., and Daroughegi, R. Synthesis of nanocrystalline mesoporous Ni/Al2O3SiO2 catalysts for CO2 methanation reaction. International Journal of Hydrogen Energy 43(41) (2018): 19038-19046.

[92]   Guo, X., et al. Carbon Dioxide Methanation over Nickel-Based Catalysts Supported on Various Mesoporous Material. Energy & Fuels 32(3) (2018): 3681-3689.

[93]   Guo, M. and Lu, G. The effect of impregnation strategy on structural characters and CO2 methanation properties over MgO modified Ni/SiO2 catalysts. Catalysis Communications 54 (2014): 55-60.

[94]   Graça, I., et al. CO2 hydrogenation into CH4 on NiHNaUSY zeolites. Applied Catalysis B: Environmental 147 (2014): 101-110.

[95]   Du, G., Lim, S., Yang, Y., Wang, C., Pfefferle, L., and Haller, G. Methanation of carbon dioxide on Ni-incorporated MCM-41 catalysts: The influence of catalyst pretreatment and study of steady-state reaction. Journal of Catalysis 249(2) (2007): 370-379.

[96]   Song, H., Yang, J., Zhao, J., and Chou, L. Methanation of Carbon Dioxide over a Highly Dispersed Ni/La2O3 Catalyst. Chinese Journal of Catalysis 31(1) (2010): 21-23.

[97]   Rahmani, S., Rezaei, M., and Meshkani, F. Preparation of promoted nickel catalysts supported on mesoporous nanocrystalline gamma alumina for carbon dioxide methanation reaction. Journal of Industrial and Engineering Chemistry 20(6) (2014): 4176-4182.

[98]   Rahmani, S., Rezaei, M., and Meshkani, F. Preparation of highly active nickel catalysts supported on mesoporous nanocrystalline γ-Al2O3 for CO2 methanation. Journal of Industrial and Engineering Chemistry 20(4) (2014): 1346-1352.

[99]   Shashidhara, G.M. and Ravindram, M. A kinetic study of the methanation of CO2 over Ni−Al2O3 catalyst. Reaction Kinetics and Catalysis Letters 37(2) (1988): 451-456.

[100]   Chang, F.-W., Kuo, M.-S., Tsay, M.-T., and Hsieh, M.-C. Hydrogenation of CO2 over nickel catalysts on rice husk ash-alumina prepared by incipient wetness impregnation. Applied Catalysis A: General 247(2) (2003): 309-320.

[101]   Chang, F.-W., Tsay, M.-T., and Liang, S.-P. Hydrogenation of CO2 over nickel catalysts supported on rice husk ash prepared by ion exchange. Applied Catalysis A: General 209(1) (2001): 217-227.

[102]   Swalus, C., Jacquemin, M., Poleunis, C., Bertrand, P., and Ruiz, P. CO2 methanation on Rh/γ-Al2O3 catalyst at low temperature: "In situ" supply of hydrogen by Ni/activated carbon catalyst. Applied Catalysis B: Environmental 125 (2012): 41-50.

[103]   Mihet, M. and Lazar, M.D. Methanation of CO2 on Ni/γ-Al2O3: Influence of Pt, Pd or Rh promotion. Catalysis Today 306 (2018): 294-299.

[104]   Ashik, U.P.M. and Daud, W. Nanonickel catalyst reinforced with silicate for methane decomposition to produce hydrogen and nanocarbon: Synthesis by co-precipitation cum modified Stöber method. RSC Advances 5 (2015).

[105]   Yang, M., et al. Preparation and characterization of a highly dispersed and stable Ni catalyst with a microporous nanosilica support. RSC Advances 6(84) (2016): 81237-81244.

[106]   Yan, L., Liu, X., Deng, J., and Fu, Y. Molybdenum modified nickel phyllosilicates as a high performance bifunctional catalyst for deoxygenation of methyl palmitate to alkanes under mild conditions. Green Chemistry 19(19) (2017): 4600-4609.

[107]   Oemar, U., Kathiraser, Y., Mo, L., Ho, X.K., and Kawi, S. CO2 reforming of methane over highly active La-promoted Ni supported on SBA-15 catalysts: mechanism and kinetic modelling. Catalysis Science & Technology 6(4) (2016): 1173-1186.

[108]   Kong, X., Zhu, Y., Zheng, H., Li, X., Zhu, Y., and Li, Y.-W. Ni Nanoparticles Inlaid Nickel Phyllosilicate as a Metal–Acid Bifunctional Catalyst for Low-Temperature Hydrogenolysis Reactions. ACS Catalysis 5(10) (2015): 5914-5920.

[109] Yang, R.-X., Xu, L.-R., Wu, S.-L., Chuang, K.-H., and Wey, M.-Y. Ni/SiO2 core–shell catalysts for catalytic hydrogen production from waste plastics-derived syngas. International Journal of Hydrogen Energy 42(16) (2017): 11239-11251.

[110] Lu, B., Ju, Y., Abe, T., and Kawamoto, K. Grafting Ni particles onto SBA-15, and their enhanced performance for CO2 methanation. RSC Advances 5(70) (2015): 56444-56454.

[111] Liu, S., et al. The Influence of the Alcohol Concentration on the Structural Ordering of Mesoporous Silica: Cosurfactant versus Cosolvent. The Journal of Physical Chemistry B 107(38) (2003): 10405-10411.

[112] Lv, X., Zhang, L., Xing, F., and Lin, H. Controlled synthesis of monodispersed mesoporous silica nanoparticles: Particle size tuning and formation mechanism investigation. Microporous and Mesoporous Materials 225 (2016): 238-244.

[113] Chen, B.-H., Liu, W., Li, A., Liu, Y.-J., and Chao, Z.-S. A simple and convenient approach for preparing core–shell-like silica@nickel species nanoparticles: highly efficient and stable catalyst for the dehydrogenation of 1,2-cyclohexanediol to catechol. Dalton Transactions 44(3) (2015): 1023-1038.

[114] Sing, K.S.W. Reporting physisorption data for gas/solid systems with special reference to the determination of surface area and porosity (Recommendations 1984). in Pure and Applied Chemistry. 1985. 603.

[115] Zhang, P. Adsorption and Desorption Isotherms (2016).

[116] Majewski, A.J., Wood, J., and Bujalski, W. Nickel–silica core@shell catalyst for methane reforming. International Journal of Hydrogen Energy 38(34) (2013): 14531-14541.

[117] Ando, H. Effect of Metal Additives on the Hydrogenation of Carbon Dioxide over Nickel Catalyst Prepared by Sol-gel Method. Energy Procedia 34 (2013): 517-523.

[118] Wu, Y., Chang, G., Zhao, Y., and Zhang, Y. Preparation of hollow nickel silicate nanospheres for separation of His-tagged proteins. Dalton Transactions 43(2) (2014): 779-783.

[119] Jacquemin, M., Genet, M.J., Gaigneaux, E.M., and Debecker, D.P. Calibration of the X-ray photoelectron spectroscopy binding energy scale for the

characterization of heterogeneous catalysts: is everything really under control? Chemphyschem 14(15) (2013): 3618-26.

[120] Zhang, X., Sun, W.-j., and Chu, W. Effect of glow discharge plasma treatment on the performance of Ni/SiO2 catalyst in CO2 methanation. Journal of Fuel Chemistry and Technology 41(1) (2013): 96-101.

[121] Wang, X., Zhu, S., Wang, S., Wang, J., Fan, W., and Lv, Y. Ni nanoparticles entrapped in nickel phyllosilicate for selective hydrogenation of guaiacol to 2-methoxycyclohexanol. Applied Catalysis A: General 568 (2018): 231-241.

[122] Zhao, B., Chen, Z., Chen, Y., and Ma, X. Syngas methanation over Ni/SiO2 catalyst prepared by ammonia-assisted impregnation. International Journal of Hydrogen Energy 42(44) (2017): 27073-27083.

[123] Zhang, Y. and Liu, Q. Nickel phyllosilicate derived Ni/SiO2 catalysts for CO2 methanation: Identifying effect of silanol group concentration. Journal of CO2 Utilization 50 (2021): 101587.

[124] Wang, C., et al. Bimetallic Synergy Effects of Phyllosilicate-Derived NiCu@SiO

2

Catalysts for 1,4-Butynediol Direct Hydrogenation to 1,4-Butanediol. ChemCatChem 11(19) (2019): 4777-4787.

[125] Bell, J.M., Kubler, D.G., Sartwell, P., and Zepp, R.G. Acetal Formation for Ketones and Aromatic Aldehydes with Methanol1. The Journal of Organic Chemistry 30(12) (1965): 4284-4292.

[126] Şebin, M.E., Akmaz, S., and Koc, S.N. Hydrogenation of furfural to furfuryl alcohol over efficient sol-gel nickel-copper/zirconia catalyst. Journal of Chemical Sciences 132(1) (2020): 157.

[127] MacIntosh, K.L. and Beaumont, S.K. Nickel-Catalysed Vapour-Phase Hydrogenation of Furfural, Insights into Reactivity and Deactivation. Topics in Catalysis 63(15) (2020): 1446-1462.

[128] Xu, J., Cui, Q., Xue, T., Guan, Y., and Wu, P. Total Hydrogenation of Furfural under Mild Conditions over a Durable Ni/TiO(2)-SiO(2) Catalyst with Amorphous TiO(2) Species. ACS omega 5(46) (2020): 30257-30266.

[129]   Halilu, A., Ali, T.H., Atta, A.Y., Sudarsanam, P., Bhargava, S.K., and Abd Hamid, S.B. Highly Selective Hydrogenation of Biomass-Derived Furfural into Furfuryl Alcohol Using a Novel Magnetic Nanoparticles Catalyst. Energy & Fuels 30(3) (2016): 2216-2226.

VITA

NAME	Sasithorn Kuhaudomlap
DATE OF BIRTH	6 April 1991
PLACE OF BIRTH	Kanchanaburi
INSTITUTIONS ATTENDED	Bachelor's Degree: Chemical Engineering from Department of Chemical Engineering, Faculty of Engineering and Industrial Technology, Silpakorn University, Nakhonpathom, Thailand
	Master's Degree: Chemical Engineering at Department of Chemical Engineering, Chulalongkorn University, Bangkok Thailand
	Doctoral Degree: Chemical Engineering at Department of Chemical Engineering, Chulalongkorn University, Bangkok Thailand
HOME ADDRESS	15/3 Moo 3 Tombon Thamai
	Amphoe Thamaka
	Changwat Kanchanaburi
	71120
PUBLICATION	Publications:

- Sasithorn Kuhaudomlap, Okorn Mekasuwandumrong, Piyasan Praserthdam, Shin-Ichiro Fujita, Masahiko Arai and Joongjai Panpranot, "The H2-treated TiO2 supported Pt catalysts prepared by strong electrostatic adsorption for liquid-phase selective hydrogenation", Catalysts 2018, 8, 87.

- Sasithorn Kuhaudomlap, Piyasan Praserthdam, Masayuki Shirai, Joongjai Panpranot. "Highly active and stable Ni-incorporated spherical silica catalysts for

CO2methanation" Catalysis Today. 2020, 358, 30-36.

Conferences:

- Sasithorn Kuhaudomlap, Okorn Mekasuwandumrong, Piyasan Praserthdam and Joongjai Panpranot "Ni-doped high surface area spherical silica catalysts for CO2 methanation" The 8th Tokyo Conference on Advanced Catalytic Science and Technology (TOCAT8), August 5 - 10, 2018 at Yokohama, Japan (Oral presentation).

- Sasithorn Kuhaudomlap, Piyasan Praserthdam, Masayuki Shirai, and Joongjai Panpranot "Highly active and stable Ni-incorporated spherical silica catalysts for CO2 methanation" 3rd International Conference on Catalysis and Chemical Engineering 2019 (CCE-2019), February 25 – 27, 2019 at Houston, TX, United States (Oral presentation).

- Sasithorn Kuhaudomlap and Joongjai Panpranot "Selective hydrogenation of furfural to furfuryl alcohol over nickel phyllosilicate catalyst" The 2021 National RGJ and RRI Conference, 14 June 2021, Online. (Poster Presentation)

Short-term research:

The Georgia Institute of Technology, the school of Chemical & Biomolecular Engineering, Atlanta, Georgia, U.S.A., under supervision of Professor Christopher W. Jones.